Institute of Paper Science and Technology

MODELING OF FLUID FLOW AND HEAT TRANSFER IN A CROWN COMPENSATED IMPULSE DRYING PRESS ROLL

II. The Heat Transfer Problem

Project 3470

Report 12

to the

MEMBER COMPANIES OF THE INSTITUTE OF PAPER SCIENCE AND TECHNOLOGY

February 1995

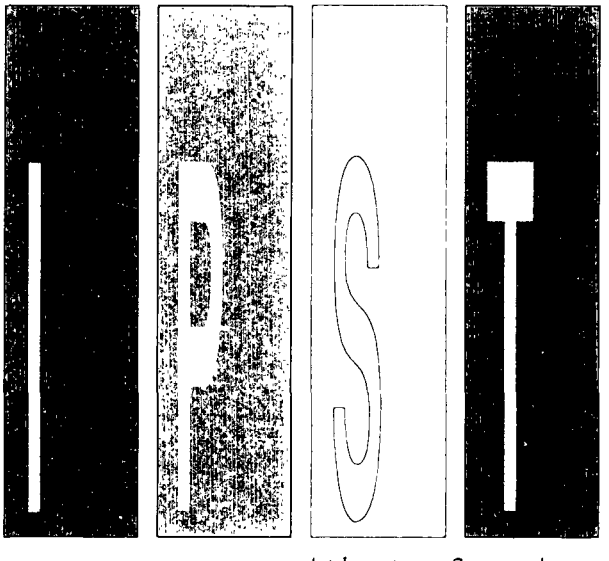

Atlanta, Georgia

INSTITUTE OF PAPER SCIENCE AND TECHNOLOGY
PURPOSE AND MISSION STATEMENT

The Institute of Paper Science and Technology is a unique organization whose charitable, educational, and scientific purpose evolves from the singular relationship between the Institute and the pulp and paper industry which has existed since 1929. The purpose of the Institute is fulfilled through three missions, which are:

- to provide high quality students with a multidisciplinary graduate educational experience which is of the highest standard of excellence recognized by the national academic community and which enables them to perform to their maximum potential in a society with a technological base; and
- to sustain an international position of leadership in dynamic scientific research which is participated in by both students and faculty and which is focused on areas of significance to the pulp and paper industry; and
- to contribute to the economic and technical well-being of the nation through innovative educational, informational, and technical services.

ACCREDITATION

The Institute of Paper Science and Technology is accredited by the Commission on Colleges of the Southern Association of Colleges and Schools to award the Master of Science and Doctor of Philosophy degrees.

NOTICE AND DISCLAIMER

The Institute of Paper Science and Technology (IPST) has provided a high standard of professional service and has put forth its best efforts within the time and funds available for this project. The information and conclusions are advisory and are intended only for internal use by any company who may receive this report. Each company must decide for itself the best approach to solving any problems it may have and how, or whether, this reported information should be considered in its approach.

IPST does not recommend particular products, procedures, materials, or service. These are included only in the interest of completeness within a laboratory context and budgetary constraint. Actual products, procedures, materials, and services used may differ and are peculiar to the operations of each company.

In no event shall IPST or its employees and agents have any obligation or liability for damages including, but not limited to, consequential damages arising out of or in connection with any company's use of or inability to use the reported information. IPST provides no warranty or guaranty of results.

INSTITUTE OF PAPER SCIENCE AND TECHNOLOGY

Atlanta, Georgia

MODELING OF FLUID FLOW AND HEAT TRANSFER IN A CROWN COMPENSATED IMPULSE DRYING PRESS ROLL

II. The Heat Transfer Problem

Project 3470

Report 12

A Progress Report

to the

MEMBER COMPANIES OF THE INSTITUTE OF PAPER SCIENCE AND TECHNOLOGY

By

F. Bloom, B. Hojjatie, and D. Orloff

February 1995

TABLE OF CONTENTS

SUMMARY

Using our earlier work on the lubrication problem which arises in the impulse drying of paper employing a crown-compensated roll [4] (and, in particular, the analytical and numerical results for the pressure fields, mass flow rates, etc., contained in [4]), we derive in this report analytical expressions and numerical results related to the velocity and temperature profiles in each of the five distinct subregions of the lubrication channel, as well as results for the associated values of the corresponding heat fluxes across the bottom surface of the rotating CC roll.

Our main goals in this first analysis of the heat transfer problem for the CC roll/internal shoe configuration were as follows: (i) to produce analytical and numerical results for the variation in the heat flux along the inner surface of the roll which could, in turn, be used as one of the boundary conditions in a finite element code geared towards determining the distribution of thermal stresses in the CC roll, (ii) to determine the relative influence of the contribution of viscous dissipation of heat onto the lubricant on those heat transfer characteristics related to the operation of the roll/shoe configuration, and (iii) to determine the relative influence of the operating parameters, i.e., the speed of the roll and the load on the internal shoe, as well as the influence of the prescribed temperatures on the bottom surface of the shoe and inner surface of the roll on the thermal performance of the system consisting of the shoe, roll, and lubricant.

For this report, calculations were performed for various values of the shoe temperature in the range 100-160°C and an inner roll surface temperature in the range 100-300°C. In general, for the conditions analyzed in this study, the computed net heat flux from the roll to the oil was negative thus indicating that because of the viscous nature of the lubricant, and the large tangential speed of the roll, under steady state conditions, in general the temperature of the lubricant at the regions near the roll is greater than that of the inner surface of the roll so that the direction of heat transfer is actually from the oil to the roll. In the left-hand subchannel, because the lubricant is flowing in a direction opposite to the motion of the roll, viscous heat dissipation was found to be larger than that in the right-hand subchannel; this, in turn, produced a greater temperature increase in the oil flowing in the left-hand subchannel as compared with the oil in the right-hand subchannel. Also, it was noted that the maximum oil temperature at the end of the right-hand subchannel occurs in a region near the bottom surface of the shoe while for the oil in the left-hand subchannel it occurs in a region close to the inner surface of the roll. Throughout this first study it was assumed that, in each district subregion of the channel, the variation of the temperature along the machine direction is much smaller than that along the thickness direction (i.e., the direction normal to the inner surface of the roll). Because of the significant roll played by viscous heat dissipation, significant changes in the temperature profiles in the channel occur as the speed of the roll increases. It was also noted that the net heat flux was inversely proportional to the inner roll surface temperature and directly proportional to the shoe surface temperature, a larger heat transfer from oil to roll occurring for a smaller roll temperature and a larger

shoe temperature. Finally, the analysis shows that those regions under the solid parts of the shoe on either side of the two sets of recesses play the major role in the transfer of heat from the oil to the roll.

Among the problem areas to be addressed in future work we note the following: (i) an effort will be directed at carrying out a finite difference analysis of the heat transfer equation, in each subregion of the channel, retaining in each case the convective term in the equation which was not employed in the first approximation which is reported here, (ii) an iterative procedure, using the initial results generated in this report, will be employed in order to compute higher order approximations which involve the convective term in the heat transfer equation and an averaging technique will be applied in order to compare the magnitude of the convective term, relative to the initial results generated in this report, with the corresponding conductive term in the heat transfer equation, (iii) the influence on the prediction of the thermal characteristics of the system, which results from using different types of boundary conditions along the bottom surface of the shoe and the inner surface of the roll, will be explored, and (iv) the analysis and numerical analysis carried out in [4], and in this initial investigation of the heat transfer problem for the roll/shoe configuration, will be extended so as to incorporate what is expected to be the very realistic and important influence of a temperature dependent viscosity for the lubricating oil.

OVERVIEW AND OBJECTIVES

Ongoing research at the Institute of Paper Science and Technology (IPST) has demonstrated the feasibility of using impulse drying to increase productivity, quality and energy efficiency of Linerboard and other heavy weight grades of paper. Plans are in progress for commercializing the impulse drying technology through a joint venture between the Institute and the Beloit Corporation; that commercialization would be supported in part by the U.S. Department of Energy's Office of Industrial Programs.

Much of the Institute's previous research in impulse drying has focused on understanding the details of the process and in demonstrating the benefits of the process to paper machine productivity, physical property improvement and energy savings [1-3]. With the start of the commercialization phase of the effort, the Institute has additionally focused on mechanical design and materials issues that would increase the likelihood of successful technology transfer.

In 1995 that effort will include the operation of a high speed test stand for the evaluation of the long term durability of various impulse drying press roll coatings. The test stand will be operated at commercial paper machine speeds of 2500 ft/min. It will consist of a roll shell coated with three or more test materials, an induction heating system, and a continuous wet felt that can be loaded against the roll surface to simulate impulse drying. The roll shell will be monitored to detect the onset of roll coating failure. The test stand will be used to evaluate the long term durability of these roll coatings under commercial impulse drying conditions.

In future work, the Institute plans to develop a finite-element model of a crown-compensated impulse drying press roll. The model will be capable of predicting the temperature and state of stress at any location within the roll as a function of impulse drying operating conditions and roll composition. The results of the model may be compared to the experimental results from the high speed test stand and used to optimize roll design for maximum energy efficiency and component durability.

As a first step in the development of the finite element model, work was carried out in 1994 to determine the stress and heat transfer boundary conditions that would be imposed on a crown-controlled impulse drying press roll. In particular, the present research effort was directed to determining the heat flux at the interface between the inside surface of the press roll and the internal hydrostatic shoe. This report is a continuation of our previous report concerning the lubrication part of the problem [4].

1 Introduction

In [4] we analyzed the lubrication problem which arises in modeling impulse drying employing a crown compensated roll; the geometry for the associated steady flow problem was constructed and expressions were derived for the relevant velocity fields, mass flow rates, and normal and tangential forces acting on both the bottom surface of an internal hydrostatic shoe and the inside surface of the CC roll.

The bottom surface of the shoe and the inside surface of the roll form a curvilinear channel and are assumed to lie on circles of either equal or different radii; the coordinates of the center of the circle on which the arc describing the bottom surface of the shoe lies, were used, in [4], in conjunction with the angular deflection ψ of the shoe, to define a base lubrication thickness d_0 for an approximate planar-walled channel (in which the lubrication problem is posed) whose angular deviation from a parallel wall channel is denoted as β.

The parameters d_0 and ψ were then determined by the solution of a set of coupled, nonlinear, transcendental algebraic equilibrium equations. Parameters entering into the equilibrium equations included geometrical design parameters such as the radii of both the shoe and the roll, and the angular opening of the shoe, as well as physical parameters such as the load per unit width on the shoe, exerted along the top surface of the shoe, and the tangential speed of the CC roll (which rotates counterclockwise).

The equilibrium equations in [4] were obtained by balancing horizontal and vertical components of all forces acting on the shoe (including the tangential and normal forces, exerted by the lubricating oil, on the planar-walled surface of the convergent wedge-shaped channel which approximates the actual curvilinear channel in a precise geometric manner) and by imposing, as well, balance of moments for all forces. The lubrication channel in [4] is fed by two sets of capillaries which traverse the shoe and enter the channel through recesses cut out of the bottom of the shoe; lubricating oil is injected through the capillaries on each side of the shoe, to the inside surface of the roll, and the shoe subsequently turns in the clockwise direction as a consequence of the viscosity of the oil, the motion of the roll, and the balance of forces and their moments.

The base thickness d_0 of the approximate channel, and the angular deflection ψ of the shoe, not only serve, in [4], to completely determine the equilibrium position of the shoe, once the load on the shoe and the speed of the CC roll are given, but also determine all pressure and velocity fields in the channel and, therefore, all normal and tangential forces which act on the bottom surface of the shoe.

Numerical solutions of the algebraic equilibrium equations were carried out in [4] both for a "small" shoe/roll configuration in which the shoe radius is smaller than the roll radius, and for a "large" shoe/roll configuration in which the two radii are machined so as to be approximately equal; these numerical studies indicate that the model can be used effectively to study the variation in channel thickness, deflection of the shoe, net mass flow rate, pressure

distributions, and the power required to operate the roll, either in terms of the load F (on the shoe) for a fixed tangential speed s (of the roll) or in terms of s for fixed F.

We now describe, briefly, the construction of the model employed in [4]. In figures 1 and 2 we show a crown-compensated (CC) extended-nip press which is configured with a ceramic coated press roll. The roll revolves at high speed, counterclockwise, and is loaded, in the impulse drying mode, by the internal hydrostatic support element. Oil is injected through the hydrostatic support element, i.e., the shoe, so as to produce an oil film between the bottom of the shoe and the inside surface of the roll which provides lubrication and, also, acts as a heat sink for heat lost to the interior of the roll. In the overall process, wet paper sheets transported on felt enter an extended nip at point A, in figure 1, and leave the nip at point C, while the roll itself is heated in a zone from point D to point E so as to achieve a prescribed roll surface temperature at the entrance to the nip at point A.

Key variables which enter into the analytical model constructed in [4] are the radii R and R_s, of the CC roll and shoe, respectively, p_{sh} (the pressure at the top of the shaft of the shoe), p_{exit} (the pressure at which the lubricating oil exits each of the two subchannels — for our purposes in this report, as well as in [4], $p_{exit} = p_{atm}$, i.e., atmospheric pressure), $\tilde{R}_{eff}$ and $\tilde{\ell}_{eff}$ (respectively, the effective radius and length of each of the capillaries through which the lubrication oil enters the channel formed by the bottom of the shoe and the inside surface of the roll, i.e., see figure 3), Φ (the angular opening of the shoe), s (the linear speed of the roll), and μ and ρ (respectively, the viscosity and density of the lubricating oil). In the model [4] it was assumed that the viscosity μ is constant, but, in future work we will take into account the fact that μ varies with temperature, albeit linearly over the range of temperatures in which it is anticipated that the roll will be operated.

As a consequence of the loading of the internal shoe, the pressure difference $p_{sh} - p_{atm}$ and the counterclockwise motion of the roll, the shoe is forced downward and will deflect clockwise once the shaft of the shoe has been displaced sufficiently far to the right so that the middle rib (figure 4) at the top of this shaft comes into contact with the wall of the confinement shaft. Turning to figure 5, point $(0, R)$ is the location of the center of the circle describing the inside surface of the roll so that $(0, 0)$ is the point of contact (tangency) between the roll and the paper. At a given tangential speed s and load F, on the shoe, the center of the circle describing the bottom of the shoe is located at the point $(a, R+b)$ where a, b are determined by the set of coupled, nonlinear equilibrium equations. The points E and B lie, respectively, at the centers of the top of the shaft of the shoe and the arc describing the bottom surface of the shoe. The line segments from $(a, R+b)$ to A, B and C are radii of the shoe of length $R_s \leq R$, while ψ is always the angle between the center line of the shoe (through E, B) and the radius of the circle describing the roll through (O, R) and (O, O). The lubrication channel is formed by the arcs $\overset{\frown}{ABC}$ and $\overset{\frown}{A'B'C'}$ and a base lubrication thickness may be measured along the segment $\overline{BB'}$. The approximating planar-walled channel (or wedge) is constructed by using the secant lines through the points A, C and A', C'. There is a slight

tapering of the shoe near the endpoints located at A and C which was not taken into account in the model formulated in [4].

When the upper right hand corner of the shaft of the shoe makes contact with the confinement wall (by virtue of the 2nd or middle rib at the top of the shaft of the shoe coming into contact with that wall) the shoe will turn slightly in the clockwise direction (see figure 6) and the point of contact between the rib on the shaft of the shoe and the confinement wall (labeled as point PV in figure 6) will slide up and down that wall without friction. As shown in figure 6, the rib in questions protrudes a distance β_r, from the shaft of the shoe and is located a distance α_r down from the top of the shaft. In [4] we located the position of the pivot point PV and indicated that the parameter α is determined entirely in terms of the angle ψ and geometrical quantities associated with the design of the shoe; the two primary independent variables used, in the model constructed in [4], are the angle ψ and either the base lubrication thickness d_0 (essentially the length of the line segment $\overline{BB'}$ in figure 7) or the parameter b (in the y coordinate $R+b$ of the point which locates the center of the circle on which the arc that describes the bottom surface of the shoe lies).

The variables ψ and b (or d_0) are determined by the physics of the problem, i.e., by enforcing equilibria of forces in both the vertical and horizontal directions as well as balance of moments of forces acting on the internal hydrostatic shoe; the resulting equilibrium equations in [4] are a system of coupled, nonlinear, transcendental algebraic equations which can be solved, numerically, by an iterative procedure. Once ψ and d_0 are determined in [4], for given F, s it is then possible to compute all the geometrical quantities which are needed in order to fix the size of the approximate wedge-shaped channel (figure 8) as well as the pressures $\tilde{p}_R$ and $\tilde{p}_{\mathcal{L}}$ in each of the two sets of recesses, the mass flow rates $\dot{m}_R$ and $\dot{m}_{\mathcal{L}}$ in each subchannel, and the explicit forms of all velocity fields in each of the two subchannels (figures 9, 10). The velocity fields are two-dimensional and are obtained, in [4], by imposing the standard lubrication theory assumption of pseudo-plane Couette flow [5], [6]. The expressions for the tangential and normal forces exerted by the lubricating oil, both on the bottom surface of the shoe, as well as on the inside surface of the roll, were used in [4] to compute the net drag force acting on the roll and, thus, the mechanical horsepower which must be expended to operate the *CC roll*.

Inasmuch as the equilibrium equations in [4] yield implicit relations for ψ and b of the form

$$\begin{cases} \psi = \psi(F, p_{sh} - p_{atm}, s, R, \varphi, R_s, \tilde{R}_{eff}, \tilde{\ell}_{eff}, \mu, \rho) \\ b = b(F, p_{sh} - p_{atm}, s, R, \varphi, R_s, \tilde{R}_{eff}, \tilde{\ell}_{eff}, \mu, \rho) \end{cases} \tag{1.1}$$

one can, in principle, study the effect of holding all variables in the parameter space $\mathcal{P}$,

$$\mathcal{P} = \{F, p_{sh} - P_{atm}, s, R, \varphi, R_s, \tilde{R}_{eff}, \tilde{\ell}_{eff}, \mu, \rho\} \tag{1.2}$$

fixed except for one, say, s in order to study how ψ and b (or d_0) vary with the tangential speed of the CC roll; the same procedure then yields valuable information on how e.g., the

drag on the roll varies with s if all other elements in the parameter space $\mathcal{P}$ are frozen. In this companion report to [4] we will show that having determined ψ and b (or d_0) for a fixed set of values in the parameter space $\mathcal{P}$, so that all velocity fields may be explicitly computed, we are led to well-posed boundary value problems for the steady-state temperature distributions in each distinct part of the channel; the solution of these boundary-value problems then enables us to determine the net heat flow from the CC roll to the lubricating oil, the net heat flow from the oil to the shoe, and the net heat convected away by the fluid, in terms of the variables in the parameter space.

2 The Heat Transfer Boundary Value Problem

Heat transfer in the lubricant is governed by the following partial differential equation for the temperature field $\theta = \theta(x, y, t)$:

$$\frac{\partial \theta}{\partial t} + \underset{\sim}{u} \cdot \nabla\theta = \frac{1}{\rho c}[\kappa \nabla^2 \theta + \Psi] \tag{2.1}$$

with

$$\Psi = \frac{1}{2}\mu \sum_{i,j=1}^{2} \left(\frac{\partial u_i}{\partial x_j} + \frac{\partial u_j}{\partial x_i}\right)^2 \tag{2.2}$$

where $\underset{\sim}{u} = (u_1, u_2)$ is the velocity field, ρ, μ, κ and c are, respectively, the lubricant density, viscosity, thermal conductivity, and heat capacitance, ∇^2 is the Laplacian operator, $\nabla^2 = \frac{\partial^2}{\partial x^2} + \frac{\partial^2}{\partial y^2}, x_1 = x, x_2 = y$, and Ψ is the viscous dissipation function. For steady state heat transfer $\frac{\partial \theta}{\partial t} = 0$ so that $\theta = \theta(x, y)$. With $u(x, y)$ denoting any of the five velocity fields in the channel,

$$\bar{u}_R(x, y), \tilde{u}_R(x, y), u_c(x, y), \tilde{u}_{\mathcal{L}}(x, y), \bar{u}_{\mathcal{L}}(x, y),$$

as given by (V1)-(V5) in Appendix II, and $\theta(x, y)$ denoting any one of the corresponding temperature fields

$$\bar{\theta}_R(x, y), \tilde{\theta}_R(x, y), \theta_c(x, y), \tilde{\theta}_{\mathcal{L}}(x, y), \bar{\theta}_{\mathcal{L}}(x, y),$$

the domains of definition of all velocity and temperature fields being given in Appendix I, we have

$$\begin{cases} \underset{\sim}{u} \cdot \nabla\theta = u(x, y)\dfrac{\partial \theta}{\partial x} \\ \\ \nabla^2\theta = \dfrac{\partial^2 \theta}{\partial x^2} + \dfrac{\partial^2 \theta}{\partial y^2} \\ \\ \Psi = 2\mu \left(\dfrac{\partial u}{\partial x}\right)^2 + \mu \left(\dfrac{\partial u}{\partial y}\right)^2 \end{cases}$$

Thus, each of the five temperature fields in the lubrication channel, and their corresponding velocity fields, will satisfy the equation

$$u\frac{\partial \theta}{\partial x} = \frac{\kappa}{\rho c}\left[\frac{\partial^2 \theta}{\partial x^2} + \frac{\partial^2 \theta}{\partial y^2}\right] + \frac{1}{\rho c}\left[2\mu \left(\frac{\partial u}{\partial x}\right)^2 + \mu \left(\frac{\partial u}{\partial y}\right)^2\right] \tag{2.3}$$

However, it is known from the work in [4] that the angle $\beta \approx 0$ (see Appendix I for the definition of β) and that $\nabla \cdot \underset{\sim}{u} \simeq 0$ on $D = \{(x, y) | 0 \leq y \leq d_R(x), -L_\beta < x < L_\beta\}$; this implies that $\frac{\partial u}{\partial x} \simeq 0$ for each of the five respective velocity fields in the channel, so that (2.3)

reduces to

$$\kappa \nabla^2 \theta(x,y) + b(x,y)\frac{\partial \theta}{\partial x} = f(x,y;\mu) \tag{2.4}$$

with

$$\begin{cases} b(x,y) = -\rho c u(x,y) \\ f(x,y;\mu) = -\mu \left(\dfrac{\partial u}{\partial y}\right)^2 \end{cases} \tag{2.5}$$

We also have boundary data of the form:

$$\begin{cases} \theta(x,0) = T_1 & -L_\beta < x < L_\beta \\ \theta(x,d(x)) = T_0, & -L_\beta < x < L_\beta \end{cases} \tag{2.6}$$

and in the general case would also have to prescribe

$$\begin{cases} \theta(L_\beta, y) \equiv \bar{\theta}_R(L_\beta, y) = \alpha(y), 0 \le y \le d(L_\beta) \\ \theta(-L_\beta, y) \equiv \theta_{\mathcal{L}}(-L_\beta, y) = \gamma(y), 0 \le y \le d(-L_\beta) \end{cases} \tag{2.7}$$

e.g., if we were to impose at $x = L_\beta$ a linear interpolation of T_0 and T_1 then

$$\alpha(y) = \left(\frac{T_0 - T_1}{d(L_\beta)}\right) y + T_1,\ 0 \le y \le d(L_\beta) \tag{2.8}$$

Some remarks regarding the nature of the boundary data (2.6), (2.7) are no order at this point. First of all, because of the discontinuous nature of the temperature field, as one transitions from one subregion in the channel to a different subregion, the boundary value problem (2-4)-(2.7) must actually be posed in each separate subregion, i.e., for $l_\beta < x < L_\beta$, $\theta = \bar{\theta}_R$, and $\bar{\theta}_R(x,y)$ must satisfy (2.4), (2.5) and boundary data of the form

$$\begin{cases} \bar{\theta}_R(x,0) = T_1,\ \bar{\theta}_R(x,d(x)) = T_0, l_\beta < x < L_\beta \\ \bar{\theta}_R(l_\beta, y) = \bar{\gamma}_R(y),\ 0 \le y \le d(l_\beta) \\ \bar{\theta}_R(L_\beta, y) = \bar{\alpha}_R(y),\ 0 \le y \le d(L_\beta) \end{cases}$$

Next, it is important to note that in the idealized problem being considered here, it is assumed that the constant temperatures T_0 and T_1 on the boundaries are maintained by ambient conditions and thus imply a result in which heat conduction from the lubricating oil to the domain walls significantly dominates heat convection in the oil. For a better treatment one should consider both for the boundary at $y = 0$, as well as for the boundary at $y = d(x)$, a modified boundary condition of the form

$$\frac{\partial \theta}{\partial y} = \alpha\theta, \quad \alpha = \text{ const.}$$

where α is to be determined experimentally and $\alpha = 0$ corresponds to perfect insulation at these walls while $\alpha \to \infty$ corresponds to perfect conduction.

We begin with a description of the temperature field $\bar{\theta}_R(x,y), 0 \leq y \leq d(x), l_\beta < x < L_\beta$. Employing (V1) to compute $\dfrac{\partial \bar{u}_R}{\partial y}$ and, then, $\left(\dfrac{\partial \bar{u}_R}{\partial y}\right)^2$ and substituting the result in (2.4), (2.5), with $\theta = \bar{\theta}_R$ and $u = \bar{u}_R$, we find as the governing equation

$$\kappa \bigtriangledown^2 \bar{\theta}_R(x,y) + \bar{b}_R(x,y)\frac{\partial \bar{\theta}_R}{\partial x} = -\mu \bar{\mathcal{A}}^R(x,y) \tag{2.9}$$

for $0 \leq y \leq d(x), l_\beta < x < L_\beta$, where $\bar{b}_R = -\rho c \bar{u}_R$ and

$$\bar{\mathcal{A}}^R(x,y) = \frac{36\dot{m}_R^2}{\rho^2}\bar{\mathcal{A}}_1^R(x,y) - \frac{24\dot{m}_R s}{\rho}\bar{\mathcal{A}}_2^R(x,y) + 4s^2\bar{\mathcal{A}}_3^R(x,y) \tag{2.10}$$

with $\dot{m}_R$ the mass-flow rate in the channel for $x > 0$ and

$$\begin{cases} \bar{\mathcal{A}}_1^R = 4(y^2 d^{-6}(x) - y d^{-5}(x)) + d^{-4}(x) \\ \bar{\mathcal{A}}_2^R = 6y^2 d^{-5}(x) - 7y d^{-4}(x) + 2d^{-3}(x) \\ \bar{\mathcal{A}}_3^R = 9y^2 d^{-4}(x) - 12y d^{-3}(x) + 4d^{-2}(x) \end{cases} \tag{2.11}$$

For $\bar{\theta}_\mathcal{L}(x,y), 0 \leq y \leq d(x), -L_\beta < x < -l_\beta$, we use (V2) and (2.4), (2.5), with $\theta = \bar{\theta}_\mathcal{L}$ and $u = \bar{u}_\mathcal{L}$, and compute that

$$\kappa \bigtriangledown^2 \bar{\theta}_\mathcal{L}(x,y) + \bar{b}_\mathcal{L}(x,y)\frac{\partial \bar{\theta}_\mathcal{L}}{\partial x} = -\mu \bar{\mathcal{A}}^\mathcal{L}(x,y) \tag{2.12}$$

where $\bar{b}_\mathcal{L} = -\rho c \bar{u}_\mathcal{L}$ and

$$\bar{\mathcal{A}}^\mathcal{L}(x,y) = 36\left(\frac{\dot{m}_\mathcal{L}}{\rho}\right)^2 \bar{\mathcal{A}}_1^\mathcal{L}(x,y) + 24\left(\frac{\dot{m}_\mathcal{L}}{\rho}\right) s\bar{\mathcal{A}}_2^\mathcal{L}(x,y) + 4s^2\bar{\mathcal{A}}_3^\mathcal{L}(x,y) \tag{2.13}$$

with $\dot{m}_\mathcal{L}$ the mass-flow rate in the channel for $x < o$ and

$$\begin{cases} \bar{\mathcal{A}}_1^\mathcal{L}(x,y) = & 4(y^2 d^{-6}(x) - y d^{-5}(x)) + d^{-4}(x) \\ \bar{\mathcal{A}}_2^\mathcal{L}(x,y) = & 6y^2 d^{-5}(x) - 7y d^{-4}(x) + 2d^{-3}(x) \\ \bar{\mathcal{A}}_3^\mathcal{L}(x,y) = & 9y^2 d^{-4}(x) - 12y d^{-3}(x) + 4d^{-2}(x) \end{cases} \tag{2.14}$$

From (V3) and (V4) we have, in conjunction with both (2.4) and (2.5)

$$\kappa \bigtriangledown^2 \tilde{\theta}_R(x,y) + \tilde{b}_R(x,y)\frac{\partial \tilde{\theta}_R}{\partial x} = -\mu \tilde{\mathcal{A}}^R(x,y) \tag{2.15}$$

where $\tilde{b}_R = -\rho c \tilde{u}_R, l_c < x < l_\beta$:

$$\tilde{\mathcal{A}}^R(x,y) = s^2 d^{-2}(x), l_c < x < l_\beta \tag{2.16}$$

and

$$\kappa \bigtriangledown^2 \tilde{\theta}_\mathcal{L}(x,y) + \tilde{b}_\mathcal{L}(x,y)\frac{\partial \tilde{\theta}_\mathcal{L}}{\partial x} = -\mu \tilde{\mathcal{A}}^\mathcal{L}(x,y) \tag{2.17}$$

where $\tilde{b}_{\mathcal{L}} = -\rho c \tilde{u}_{\mathcal{L}}, -l_\beta < x < -l_c$,

$$\tilde{\mathcal{A}}^{\mathcal{L}}(x,y) = s^2 d^{-2}(x), -l_\beta < x < -l_c. \tag{2.18}$$

Finally, by virtue of (V5), (2.4), and (2.5)

$$\kappa \nabla^2 \theta_c(x,y) + b_c(x,y)\frac{\partial \theta_c}{\partial x} = -\mu \mathcal{A}^c(x,y) \tag{2.19}$$

where $b_c = -\rho c u_c, -l_c < x < l_c$, and

$$\mathcal{A}^c(x,y) = 4\Gamma_c^2 y^2 - 4\Gamma_c^2 y d(x) + 4\Gamma_c s y d^{-1}(x) + \Gamma_c^2 d^2(x) + s^2 d^{-2}(x) - 2\Gamma_c s \tag{2.20}$$

for $-l_c < x < l_c$, where $\Gamma_c = (\tilde{p}_{\mathcal{L}} - \tilde{p}_R)/4\mu l_c$. In summary, the equations for the temperature fields $\bar{\theta}_R, \tilde{\theta}_R, \theta_c, \tilde{\theta}_{\mathcal{L}}$, and $\bar{\theta}_{\mathcal{L}}$ are, respectively, (2.9), (2.15), (2.19), (2.17), and (2.12), which must be integrated, subject to the boundary data (2.6), on the five respective subintervals of $(-L_\beta, L_\beta)$.

We begin the analysis with equation (2.9) for $\bar{\theta}_R(x,y)$ and make the simplifying assumption that for $0 \le y \le d(x), l_\beta \le x \le L_\beta$

$$\left|\frac{\partial^2 \bar{\theta}_R}{\partial x^2}\right|, \left|\frac{\partial \bar{\theta}_R}{\partial x}\right| \ll \left|\frac{\partial^2 \bar{\theta}_R}{\partial y^2}\right|, \tag{2.21}$$

in which case, if we set $\zeta = -\mu/\kappa$, (2.9) reduces to

$$\frac{\partial^2 \bar{\theta}_R}{\partial y^2} = \zeta \bar{\mathcal{A}}^R(x,y), \tag{2.22}$$

for $0 \le y \le d(x), l_\beta < x < L_\beta$.

It is important to understand that in using the assumption (2.21) to reduce (2.9) to (2.22) we have not, e.g., set $\dfrac{\partial \bar{\theta}_R}{\partial x} = 0$ in (2.22). What we are saying here is that in many cases, because of the small deviation of the channel from a parallel-walled channel, a good *first approximation* to the temperature field $\bar{\theta}_R(x,y)$, in the region $0 \le y \le d(x)$, $l_\beta < x < L_\beta$, is expected to be obtained by ignoring the contribution of the convective term $\rho c_p \bar{u}_R \dfrac{\partial \bar{\theta}_R}{\partial y}$ in (2.9) in comparison with the contribution of the conductive term $\kappa \dfrac{\partial^2 \bar{\theta}_R}{\partial y^2}$. In particular, as our results will show, this assumption still allows for a significant variation in $\bar{\theta}_R$ in the machine direction and a similar assumption with respect to $\bar{\theta}_{\mathcal{L}}$ allows for an even more pronounced variation in $\bar{\theta}_{\mathcal{L}}$ in the machine direction. Because the hypothesis (2.21) only produces what is considered to be a *first approximation* the validity of that approximation must be checked; several different methods for doing that, and for determining those situations in which the

mass flow rate in the channel may be so large that the convective term is significant (even for small temperature variations in the machine direction), are discussed in §7 along with techniques for computing higher order and more accurate approximations that involve the convective term.

The general solution of (2.22) has the form

$$\bar{\theta}_R(x,y) = \zeta \int^y \int^\xi \bar{A}^R(x,\gamma)d\gamma d\xi + \bar{F}_R(x)y + \bar{G}_R(x) \tag{2.23}$$

for $0 \le y \le d(x), l_\beta < x < L_\beta$, with $\bar{F}_R$ and $\bar{G}_R$ arbitrary functions of x. Carrying out the integrations in (2.23) we find that

$$\int^y \int^\xi \bar{A}^R(x,\gamma)d\gamma d\xi = d^{-2}(x)\sum_{k=0}^{4} \bar{p}_k^R(y)d^{-k}(x) \tag{2.24}$$

for $0 \le y \le d(x), l_\beta < x < L_\beta$, where the $\bar{p}_k^R, k = 0, 1, \ldots 4$, are given by (S2) of Appendix III. Thus

$$\bar{\theta}_R(x,y) = \zeta d^{-2}(x) \cdot \sum_{k=0}^{4} \bar{p}_k^R(y)d^{-k}(x) + F_R(x)y + G_R(x) \tag{2.25}$$

for $0 \le y \le d(x), l_\beta < x < L_\beta$, and $\bar{\theta}_R$ must satisfy the boundary conditions

$$\begin{cases} \bar{\theta}_R(x,0) = T_1 \\ \bar{\theta}_R(x,d(x)) = T_0 \end{cases} \quad l_\beta \le x \le L_\beta \tag{2.26}$$

Applying (2.26) to (2.25) we determine that

$$\bar{\theta}_R(x,y) = \zeta d^{-2}(x)\sum_{k=0}^{4} \bar{p}_k^R(y)d^{-k}(x) + \sum_{k=1}^{3} c_k^R d^{-k}(x)y + T_1 \tag{2.27}$$

for $0 \le y \le d(x), l_\beta \le x \le L_\beta$, with the coefficients $c_k^R, k = 1, 2, 3$, given by (S3) of Appendix III.

Remarks: It is a straightforward calculation to check that $\bar{\theta}_R(x,y)$ as given by (2.27), (S2), and (S3) satisfies

$$\max_{\substack{0\le y\le d(x) \\ l_\beta \le x \le L_\beta}} \left| \frac{\partial \bar{\theta}_R}{\partial x}(x,y) \right| \to 0, \text{ as } \beta \to 0 \tag{2.28}$$

and

$$\max_{\substack{0\le y\le d(x) \\ l_\beta \le x \le L_\beta}} \left| \frac{\partial^2 \bar{\theta}_R}{\partial x^2}(x,y) \right| \to 0, \text{ as } \beta \to 0 \tag{2.29}$$

while $\left| \frac{\partial^2 \bar{\theta}_R}{\partial y^2}(x,y) \right|$ is bounded away from zero, as $\beta \to 0$, for $0 \le y \le d(x), l_\beta \le x \le L_\beta$.

Under the auspices of the same reasoning as described in the argument following (2.22), we now assume, as a first approximation, that, for $0 \leq y \leq d(x), -L_\beta < x < -l_\beta$,

$$\left|\frac{\partial \bar{\theta}_{\mathcal{L}}}{\partial x}\right|, \left|\frac{\partial^2 \bar{\theta}_{\mathcal{L}}}{\partial x^2}\right| \ll \left|\frac{\partial^2 \bar{\theta}_{\mathcal{L}}}{\partial y^2}\right| \tag{2.30}$$

so that we have, in lieu of (2.12)

$$\frac{\partial^2 \bar{\theta}_{\mathcal{L}}}{\partial y^2} = \zeta \bar{\mathcal{A}}^{\mathcal{L}}(x, y) \tag{2.31}$$

for $0 \leq y \leq d(x), -L_\beta < x < -l_\beta$; thus,

$$\bar{\theta}_{\mathcal{L}}(x, y) = \zeta \int^y \int^\xi \bar{\mathcal{A}}^{\mathcal{L}}(x, \gamma) d\gamma d\xi + \bar{F}_{\mathcal{L}}(x) y + \bar{G}_{\mathcal{L}}(x) \tag{2.32}$$

with $\bar{F}_{\mathcal{L}}(x), \bar{G}_{\mathcal{L}}(x)$ determined by the boundary conditions

$$\begin{cases} \bar{\theta}_{\mathcal{L}}(x, 0) = T_1 \\ \bar{\theta}_{\mathcal{L}}(x, d(x)) = T_0 \end{cases} \quad -L_\beta \leq x \leq -l_\beta \tag{2.33}$$

Using (2.13), (2.14) in (2.32), and then applying the boundary conditions (2.33), we find that the temperature distribution $\bar{\theta}_{\mathcal{L}}$ is given by

$$\bar{\theta}_{\mathcal{L}}(x, y) = \zeta d^{-2}(x) \sum_{k=0}^{4} \bar{p}_k^{\mathcal{L}}(y) d^{-k}(x) + \sum_{k=1}^{3} c_k^{\mathcal{L}} d^{-k}(x) y + T_1 \tag{2.34}$$

for $0 \leq y \leq d(x), -L_\beta < x < -l_\beta$, where the coefficients $\bar{p}_k^{\mathcal{L}}, k = 0, \ldots, 4$ and $c_k^{\mathcal{L}}, k = 1, 2, 3$, are given, respectively by (S5) and (S6) of Appendix III. We note that $\bar{\theta}_{\mathcal{L}}(x, y)$, as given by (2.34), (S5), and (S6), also satisfies the criteria in the previous set of remarks, above, as $\beta \to 0$, on the domain: $0 \leq y \leq d(x), -L_\beta \leq x \leq -l_\beta$.

For $-l_\beta < x < l_\beta$, the temperature distribution $\bar{\theta}_c(x, y)$, is governed by (2.19), (2.20). Under the simplifying assumptions:

$$\left|\frac{\partial \theta_c}{\partial x}\right|, \left|\frac{\partial^2 \theta_c}{\partial x^2}\right| \ll \left|\frac{\partial^2 \theta_c}{\partial y^2}\right|$$

For $0 \leq y \leq d(x), -l_c < x < l_c$, (2.19) reduces to

$$\frac{\partial^2 \theta_c}{\partial y^2} = \zeta \mathcal{A}^c(x, y) \tag{2.35}$$

with $\mathcal{A}^c(x, y)$ given by (2.20), for $0 \leq y \leq d(x), -l_c < x < l_c$. Two consecutive integrations of (2.35) yield

$$\theta_c(x, y) = \zeta \int^y \int^\xi \mathcal{A}^c(x, \gamma) d\gamma d\xi + F_c(x) y + G_c(x) \tag{2.36}$$

Using (2.20) in (2.36) and applying the boundary conditions

$$\begin{cases} \theta_c(x,0) = T_1 \\ \theta_c(x,d(x)) = T_0 \end{cases} \quad -l_c \le x \le l_c \tag{2.37}$$

we find that

$$\theta_c(x,y) = \zeta \sum_{k=-2}^{2} p_k^c(y) d^k(x) + (T_0 - T_1) d^{-1}(x) y - \zeta \theta_c(x) y + T_1 \tag{2.38}$$

for $0 \le y \le d(x), -l_c < x < l_c$, where the $p_k^c(y), k = -2, \ldots, 2$, are given by (S9) of Appendix III, while $\theta_c(x), -l_c < x < l_c$, is given by (S8). We note that by virtue of (S2), (S5), and (S9),

$$\begin{cases} \bar{p}_k^R(0) = 0, & k = 0, \ldots, 4 \\ \bar{p}_k^{\mathcal{L}}(0) = 0, & k = 0, \ldots, 4 \\ \bar{p}_k^c(0) = 0, & k = -2, \ldots, 2 \end{cases} \tag{2.39}$$

Next, by imposing the assumption that

$$\left|\frac{\partial \tilde{\theta}_R}{\partial x}\right|, \left|\frac{\partial^2 \tilde{\theta}_R}{\partial x^2}\right| \ll \left|\frac{\partial^2 \tilde{\theta}_R}{\partial y^2}\right|$$

for $0 \le y \le d(x), l_c < x < l_\beta$, we find that (2.15) reduces to

$$\frac{\partial^2 \tilde{\theta}_R}{\partial y^2} = \zeta \tilde{A}^R(x,y) \tag{2.40}$$

with $\tilde{A}^R(x,y), 0 \le y \le d(x), l_c < x < l_\beta$, given by (2.16). Substituting for $\tilde{A}^R(x,y)$ in (2.40) from (2.16), integrating the resulting equation twice in succession, and applying the boundary conditions

$$\begin{cases} \tilde{\theta}_R(x,0) = T_1 \\ \tilde{\theta}_R(x,d(x)) = T_0 \end{cases} \quad l_c < x < l_\beta \tag{2.41}$$

we find that for $0 \le y \le d(x), l_c < x < l_\beta$,

$$\tilde{\theta}_R(x,y) = \frac{1}{2}\zeta s^2 y^2 d^{-2}(x) + [(T_0 - T_1) - \frac{1}{2}\zeta s^2] y d^{-1}(x) + T_1 \tag{2.42}$$

Finally, if we impose the assumptions

$$\left|\frac{\partial \tilde{\theta}_{\mathcal{L}}}{\partial x}\right|, \left|\frac{\partial^2 \tilde{\theta}_{\mathcal{L}}}{\partial x^2}\right| \ll \left|\frac{\partial^2 \tilde{\theta}_{\mathcal{L}}}{\partial y^2}\right|$$

on $\tilde{\theta}_{\mathcal{L}}(x,y), 0 \le y \le d(x), -l_\beta < x < -l_c$, we see that (2.17) reduces to

$$\frac{\partial^2 \tilde{\theta}_{\mathcal{L}}}{\partial y^2} = \zeta \tilde{A}^{\mathcal{L}}(x,y) \tag{2.43}$$

where $\tilde{A}^{\mathcal{L}}(x,y), 0 \leq y \leq d(x), -l_\beta < x < -l_c$, is given by (2.16). Proceeding as in the computation of $\tilde{\theta}_R(x,y)$, and imposing the boundary conditions

$$\begin{cases} \tilde{\theta}_{\mathcal{L}}(x,0) = T_1 \\ \tilde{\theta}_{\mathcal{L}}(x,d(x)) = T_0 \end{cases} \quad -l_\beta < x < -l_c \tag{2.44}$$

we find that

$$\tilde{\theta}_{\mathcal{L}}(x,y) = \frac{1}{2}\zeta s^2 y^2 d^{-2}(x) + [(T_0 - T_1) - \frac{1}{2}\zeta s^2] y d^{-1}(x) + T_1 \tag{2.45}$$

for $0 \leq y \leq d(x), -l_\beta < x < -l_c$.

3 Heat Transfer from the Roll to the Lubricant

In this section we compute the net heat transferred from the CC roll to the lubricant, i.e. $Q_{r\to 0}$, as

$$Q_{r\to 0} = \bar{q}^R_{r\to 0} + \tilde{q}^R_{r\to 0} + \bar{q}^c_{r\to 0} + \tilde{q}^{\mathcal{L}}_{r\to 0} + \bar{q}^{\mathcal{L}}_{r\to 0} \tag{3.1}$$

where $\bar{q}^R_{r\to 0}, \tilde{q}^R_{r\to 0}, q^c_{r\to 0}, \tilde{q}^{\mathcal{L}}_{r\to 0}$, and $\bar{q}^{\mathcal{L}}_{r\to 0}$ are the quantities of heat transferred from the roll to the lubricant in those regions of the bearing where the corresponding temperature distributions are given by $\bar{\theta}_R, \tilde{\theta}_R, \theta_c, \tilde{\theta}_{\mathcal{L}}$, and $\bar{\theta}_{\mathcal{L}}$.

We begin by noting that the heat transfer per unit cross-directional width under the solid part of the shoe in the right-hand subchannel is given by

$$\bar{q}^R_{r\to 0} = \int_{l_\beta}^{L_\beta} (-\kappa \frac{\partial \bar{\theta}_R}{\partial y}\,|_{y=0}) dx \tag{3.2}$$

where κ is the (temperature-independent) thermal conductivity of the lubricant. Using (2.27), (S2), and (S3), and making note of the fact that $p_k^{R\,\prime}(0) = 0, k = 0, \ldots, 4$, we find that

$$\frac{\partial \bar{\theta}_R}{\partial y}\,|_{y=0} = \sum_{k=1}^{3} c_k^R d^{-k}(x), l_\beta < x < L_\beta \tag{3.3}$$

If we substitute $d(x) = d_0 - x\tan\beta$ in (3.3), and then the resulting expression in (3.2), the integration indicated in (3.2) leads to

$$\begin{aligned} \bar{q}^R_{r\to 0} &= \frac{\kappa[(T_0 - T_1) - 3\zeta s^2]}{\tan\beta} \ln\left[\frac{d(L_\beta)}{d(l_\beta)}\right] - \frac{8\kappa\zeta\dot{m}_R s}{\rho\tan\beta}\left[\frac{1}{d(L_\beta)} - \frac{1}{d(l_\beta)}\right] \\ &+ \frac{3\kappa\zeta\dot{m}_R^2}{\rho^2\tan\beta}\left[\frac{1}{d^2(L_\beta)} - \frac{1}{d^2(l_\beta)}\right] \end{aligned} \tag{3.4}$$

Next, we have that

$$\tilde{q}^R_{r\to 0} = \int_{l_c}^{l_\beta} \left(-\kappa \frac{\partial \tilde{\theta}_R}{\partial y}\,|_{y=0}\right) dx \tag{3.5}$$

From (2.42) we compute that

$$\frac{\partial \tilde{\theta}_R}{\partial y}\,|_{y=0} = [(T_0 - T_1) - \frac{1}{2}\zeta s^2] d^{-1}(x), \tag{3.6}$$

for $l_c < x < l_\beta$, and using this result in (3.5) yields

$$\tilde{q}^R_{r\to 0} = \frac{\kappa[(T_0 - T_1) - \frac{1}{2}\zeta s^2]}{\tan\beta} \ln\left[\frac{d(l_\beta)}{d(l_c)}\right] \tag{3.7}$$

Remarks: Assume $T_1 > T_0$. As $d(l_c) > d(l_\beta)$, we infer from (3.7), and the fact that $\zeta < 0$, that for $|T_0 - T_1|$ sufficiently large and/or s sufficiently small, $\tilde{q}^R_{r\to 0} > 0$. However, for $|T_0 - T_1|$

fixed, say, we may also infer that, because $\zeta < 0$, we will have $\tilde{q}^R_{r\to 0} < 0$ for s sufficiently large, a phenomena that may be attributed directly to the dumping of heat into the lubricant at high speeds as a consequence of the mechanism of viscous dissipation.

For the center subchannel, i.e., $-l_c < x < l_c$, we have

$$q^c_{r\to 0} = \int_{-l_c}^{l_c} \left(-\kappa \frac{\partial \theta_c}{\partial y} |_{y=0} \right) dx \tag{3.8}$$

By virtue of (2.38), (S8), and (S9) we have

$$\frac{\partial \theta_c}{\partial y} |_{y=0} = [(T_0 - T_1) - \frac{1}{2}\zeta s^2] d^{-1}(x) - \frac{1}{6}\zeta \Gamma_c^2 d^3(x) + \frac{1}{3}\zeta \Gamma_c s d(x) \tag{3.9}$$

where $\Gamma_c = (\tilde{p}_{\mathcal{L}} - \tilde{p}_R)/4\mu l_c$ and we have used the fact that the coefficients $p^c_k(y)$ in (2.38) satisfy $p^{c\,\prime}_R(0) = 0, k = -2, \ldots, 2$. From (3.8), (3.9) we compute that

$$\begin{aligned} q^c_{r\to 0} &= \frac{\kappa[(T_0 - T_1) - \frac{1}{2}\zeta s^2]}{\tan\beta} \ln\left[\frac{d(l_c)}{d(-l_c)}\right] - \frac{\zeta \kappa \Gamma_c^2}{24 \tan\beta}[d^4(l_c) - d^4(-l_c)] \\ &+ \frac{\zeta \kappa \Gamma_c s}{6 \tan\beta}[d^2(l_c) - d^2(-l_c)] \end{aligned} \tag{3.10}$$

Next, in the region of the channel under the recesses in the left-hand subchannel

$$\tilde{q}^{\mathcal{L}}_{r\to 0} = \int_{-l_\beta}^{-l_c} \left(-\kappa \frac{\partial \tilde{\theta}_{\mathcal{L}}}{\partial y} |_{y=0} \right) dx \tag{3.11}$$

However, by (2.45)

$$\frac{\partial \tilde{\theta}_{\mathcal{L}}}{\partial y} |_{y=0} = [(T_0 - T_1) - \frac{1}{2}\zeta s^2] d^{-1}(x), \tag{3.12}$$

for $-l_\beta < x < -l_c$, in which case, by (3.11)

$$\tilde{q}^{\mathcal{L}}_{r\to 0} = \frac{\kappa[(T_0 - T_1) - \frac{1}{2}\zeta s^2]}{\tan\beta} \ln\left[\frac{d(-l_c)}{d(-l_\beta)}\right] \tag{3.13}$$

Finally,

$$\bar{q}^{\mathcal{L}}_{r\to 0} = \int_{-L_\beta}^{-l_\beta} \left(-\kappa \frac{\partial \bar{\theta}_{\mathcal{L}}}{\partial y} |_{y=0} \right) dx \tag{3.14}$$

From (2.34), (S5), (S6) and the fact that $\bar{p}^{\mathcal{L}\,\prime}_k(0) = 0, k = 0, \ldots, 4$ we have

$$\frac{\partial \bar{\theta}^{\mathcal{L}}}{\partial y} |_{y=0} = \sum_{k=1}^{3} c^{\mathcal{L}}_k d^{-k}(x), \tag{3.15}$$

for $-L_\beta < x < -l_\beta$, where the $c_k^{\mathcal{L}}, k = 1, 2, 3$, are given by (S6). Using (3.15) in (3.14), and carrying out the indicated integrations, we find that

$$\begin{aligned}\bar{q}_{\tau\to 0}^{\mathcal{L}} &= \frac{\kappa[(T_0 - T_1) - 3\zeta s^2]}{\tan\beta} \ln\left[\frac{d(-l_\beta)}{d(-L_\beta)}\right] + \frac{8\kappa\zeta\dot{m}_{\mathcal{L}} s}{\rho\tan\beta}\left[\frac{1}{d(-l_\beta)} - \frac{1}{d(-L_\beta)}\right] \\ &+ \frac{3\kappa\zeta}{\tan\beta}\left(\frac{\dot{m}_{\mathcal{L}}}{\rho}\right)^2\left[\frac{1}{d^2(-l_\beta)} - \frac{1}{d^2(-L_\beta)}\right] \end{aligned} \tag{3.16}$$

To compute the net heat transferred from the roll to the lubricant, i.e. $Q_{\tau\to 0}$, as given by (3.1), we sum the expressions in (3.4), (3.7), (3.10), (3.13), and (3.16); after some lengthy algebraic manipulations we find the following result:

$$\begin{aligned} Q_{\tau\to 0} &= \frac{\kappa[(T_0 - T_1) - 3\zeta s^2]}{\tan\beta} \ln\left[\frac{d(L_\beta)}{d(-L_\beta)}\right] + \frac{5}{2}\frac{\kappa|\zeta|s^2}{\tan\beta} \ln\left[\frac{d(-l_\beta)}{d(l_\beta)}\right] \\ &+ \frac{8\kappa|\zeta|s}{\rho\tan\beta}\left(\dot{m}_R\left[\frac{1}{d(L_\beta)} - \frac{1}{d(l_\beta)}\right] - \dot{m}_{\mathcal{L}}\left[\frac{1}{d(-l_\beta)} - \frac{1}{d(-L_\beta)}\right]\right) \\ &+ \frac{3\kappa\zeta}{\rho^2\tan\beta}\left(\dot{m}_R^2\left[\frac{1}{d^2(L_\beta)} - \frac{1}{d^2(l_\beta)}\right] + \dot{m}_{\mathcal{L}}^2\left[\frac{1}{d^2(-l_\beta)} - \frac{1}{d^2(-L_\beta)}\right]\right) \\ &+ \frac{\kappa|\zeta|\Gamma_c^2}{24\tan\beta}[d^4(l_c) - d^4(-l_c)] + \frac{\kappa\zeta\Gamma_c s}{6\tan\beta}[d^2(l_c) - d^2(-l_c)] \end{aligned} \tag{3.17}$$

4 Heat Transfer from the Lubricant to the Shoe

In this section we compute the net heat which is transferred from the channel to the internal shoe, i.e., $Q_{0\to sh}$, where

$$Q_{0\to sh} = \bar{q}^R_{0\to sh} + \tilde{q}^R_{0\to sh} + q^c_{0\to sh} + \tilde{q}^{\mathcal{L}}_{0\to sh} + \bar{q}^{\mathcal{L}}_{0\to sh} \tag{4.1}$$

and $\bar{q}^R_{0\to sh}, \tilde{q}^R_{0\to sh}, q^c_{0\to sh}, \tilde{q}^{\mathcal{L}}_{0\to sh}$, and $\bar{q}^{\mathcal{L}}_{0\to sh}$ are the quantities of heat which are transferred from the oil (lubricant) to the shoe in those regions of the channel where the corresponding temperature distributions are given by $\bar{\theta}_R, \tilde{\theta}_R, \theta_c, \tilde{\theta}_{\mathcal{L}}, \bar{\theta}_{\mathcal{L}}$.

We begin by noting that

$$\bar{q}^R_{0\to sh} = \int_{l_\beta}^{L_\beta} \left(-\kappa \frac{\partial \bar{\theta}_R}{\partial y} \Big|_{y=d(x)} \right) dx \tag{4.2}$$

Using (2.27), (S2), and (S3) we compute that

$$\frac{\partial \bar{\theta}_R}{\partial y} \Big|_{y=d(x)} = \frac{6\zeta \dot{m}_R^2}{\rho^2} d^{-3}(x) - \frac{4\zeta \dot{m}_R s}{\rho} d^{-2}(x) + (\zeta s^2 + (T_0 - T_1)) d^{-1}(x) \tag{4.3}$$

for $l_\beta < x < L_\beta$, where $d(x) = d_0 - x \tan\beta$. A straightforward computation based on (4.2) and (4.3) now yields

$$\begin{aligned} \bar{q}^R_{0\to sh} &= \frac{3\zeta\kappa\dot{m}_R^2}{\rho^2 \tan\beta} \left[\frac{1}{d^2(l_\beta)} - \frac{1}{d^2(L_\beta)} \right] + \frac{4\zeta\kappa\dot{m}_R s}{\rho \tan\beta} \left[\frac{1}{d(L_\beta)} - \frac{1}{d(l_\beta)} \right] \\ &+ \frac{\kappa(\zeta s^2 + (T_0 - T_1))}{\tan\beta} \ln \left[\frac{d(L_\beta)}{d(l_\beta)} \right] \end{aligned} \tag{4.4}$$

Next, we have

$$\tilde{q}^R_{0\to sh} = \int_{l_c}^{l_\beta} \left(-\kappa \frac{\partial \tilde{\theta}_R}{\partial y} \Big|_{y=d(x)} \right) dx \tag{4.5}$$

But, by (2.42)

$$\frac{\partial \tilde{\theta}_R}{\partial y} \Big|_{y=d(x)} = [(T_0 - T_1) + \frac{1}{2}\zeta s^2] d^{-1}(x), \tag{4.6}$$

for $l_c < x < l_\beta$. Therefore, as a direct consequence of (4.5) and (4.6) we find that

$$\tilde{q}_{0\to sh} = \frac{\kappa[(T_0 - T_1) + \frac{1}{2}\zeta s^2]}{\tan\beta} \ln \left[\frac{d(l_\beta)}{d(l_c)} \right] \tag{4.7}$$

In the center subchannel, i.e. $-l_c < x < l_c$,

$$q^c_{0\to sh} = \int_{l_c}^{l_c} \left(-\kappa \frac{\partial \theta_c}{\partial y} |_y = d(x) \right) dx \tag{4.8}$$

From (2.38), (S8), and (S9) it is easily computed that

$$\frac{\partial \theta_c}{\partial y}\Big|_{y=d(x)} = [(T_0 - T_1) + \frac{1}{2}\zeta s^2]d^{-1}(x) + \frac{1}{3}\zeta\Gamma_c s d(x) + \frac{1}{6}\zeta\Gamma_c^2 d^3(x), \tag{4.9}$$

for $-l_c < x < l_c$, where $\Gamma_c = (\tilde{p}_{\mathcal{L}} - \tilde{p}_R)/4\mu l_c$. Substituting (4.9) in (4.8), and performing the indicated integrations, we have

$$\begin{aligned} q^c_{0\to sh} &= \frac{\kappa[(T_0 - T_1) + \frac{1}{2}\zeta s^2]}{\tan\beta} \ln\left[\frac{d(l_c)}{d(-l_c)}\right] + \frac{\zeta\kappa\Gamma_c s}{6\tan\beta}[d^2(l_c) - d^2(-l_c)] \\ &+ \frac{\zeta\kappa\Gamma_c^2}{24\tan\beta}[d^4(l_c) - d^4(-l_c)] \end{aligned} \tag{4.10}$$

Moving into the region of the channel under the recesses in the left-hand subchannel, we next have that

$$\tilde{q}^{\mathcal{L}}_{0\to sh} = \int_{-l\beta}^{-l_c} \left(-\kappa\frac{\partial\tilde{\theta}_{\mathcal{L}}}{\partial y}|_y = d(x)\right) dx \tag{4.11}$$

However, by virtue of (2.45)

$$\frac{\partial\tilde{\theta}_{\mathcal{L}}}{\partial y}\Big|_{y=d(x)} = [(T_0 - T_1) + \frac{1}{2}\zeta s^2]d^{-1}(x) \tag{4.12}$$

for $-l_\beta < x < -l_c$. Combining (4.11) with (4.12) we now compute that

$$\tilde{q}^{\mathcal{L}}_{0\to sh} = \frac{\kappa[(T_0 - T_1) + \frac{1}{2}\zeta s^2]}{\tan\beta} \ln\left[\frac{d(-l_c)}{d(-l_\beta)}\right] \tag{4.13}$$

Finally,

$$\bar{q}^{\mathcal{L}}_{0\to sh} = \int_{-L_\beta}^{-l\beta} \left(-\kappa\frac{\partial\bar{\theta}_{\mathcal{L}}}{\partial y}\Big|_{y=d(x)}\right) dx \tag{4.14}$$

so using (2.34), (S5), and (S6) we have, for $-L_\beta < x < -l_\beta$,

$$\frac{\partial\bar{\theta}_{\mathcal{L}}}{\partial y}\Big|_{y=d(x)} = [\zeta s^2 + (T_0 - T_1)]d^{-1}(x) + 4\zeta s\left(\frac{\dot{m}_{\mathcal{L}}}{\rho}\right)d^{-2}(x) + 6\zeta\left(\frac{\dot{m}_{\mathcal{L}}}{\rho}\right)^2 d^{-3}(x) \tag{4.15}$$

and, then,

$$\begin{aligned} \bar{q}^{\mathcal{L}}_{0\to sh} &= \frac{\kappa[\zeta s^2 + (T_0 - T_1)]}{\tan\beta} \ln\left[\frac{d(-l_\beta)}{d(-L_\beta)}\right] - \frac{4\zeta\kappa s}{\tan\beta}\left(\frac{\dot{m}_{\mathcal{L}}}{\rho}\right)\left[\frac{1}{d(-l_\beta)} - \frac{1}{d(-L_\beta)}\right] \\ &- \frac{3\zeta\kappa}{\tan\beta}\left(\frac{\dot{m}_{\mathcal{L}}}{\rho}\right)^2\left[\frac{1}{d^2(-l_\beta)} - \frac{1}{d^2(-L_\beta)}\right] \end{aligned} \tag{4.16}$$

By summing up (4.4), (4.7), (4.10), (4.13), and (4.16), and carrying out some elementary algebraic manipulations, we find that

$$\begin{aligned} Q_{0\to sh} &= \frac{\kappa[(T_0-T_1)+\zeta s^2]}{\tan\beta}\ln\left[\frac{d(L_\beta)}{d(-L_\beta)}\right]+\frac{1}{2}\frac{\kappa\zeta s^2}{\tan\beta}\ln\left[\frac{d(-l_\beta)}{d(l_\beta)}\right] \\ &+ \frac{4\zeta\kappa s}{\rho\tan\beta}\left(\dot m_R\left[\frac{1}{d(L_\beta)}-\frac{1}{d(l_\beta)}\right]-\dot m_{\mathcal{L}}\left[\frac{1}{d(-l_\beta)}-\frac{1}{d(-L_\beta)}\right]\right) \\ &+ \frac{3|\zeta|r}{\rho^2\tan\beta}\left(\dot m_R^2\left[\frac{1}{d^2(L_\beta)}-\frac{1}{d^2(l_\beta)}\right]+\dot m_{\mathcal{L}}^2\left[\frac{1}{d^2(-l_\beta)}-\frac{1}{d^2(-L_\beta)}\right]\right) \\ &+ \frac{\zeta\kappa\Gamma_c s}{6\tan\beta}[d^2(l_c)-d^2(-l_c)]+\frac{\zeta\kappa\Gamma_c^2}{24\tan\beta}[d^4(l_c)-d^4(-l_c)] \end{aligned} \tag{4.17}$$

Remarks: One may take, as a measure of the "viscous heating" of the lubricant in the channel, the quantity

$$Q_f^v \equiv Q_{0\to sh}-Q_{r\to 0} \tag{4.18}$$

From (3.17) and (4.17) we have, therefore, the Q_f^v the expression:

$$\begin{aligned} Q_f^v &= \frac{3\kappa|\zeta|s^2}{\tan\beta}\ln\left[\frac{d(-l_\beta)}{d(l_\beta)}\right]+\frac{\kappa|\zeta|\Gamma_c^2}{12\tan\beta}[d^4(l_c)-d^4(-l_c)] \\ &+ \frac{12\kappa|\zeta|s}{\rho\tan\beta}\left(\dot m_R\left[\frac{1}{d(L_\beta)}-\frac{1}{d(l_\beta)}\right]-\dot m_{\mathcal{L}}\left[\frac{1}{d(-l_\beta)}-\frac{1}{d(-L_\beta)}\right]\right) \\ &- \frac{6\kappa|\zeta|}{\rho^2\tan\beta}\left(\dot m_R^2\left[\frac{1}{d^2(L_\beta)}-\frac{1}{d^2(l_\beta)}\right]+\dot m_{\mathcal{L}}^2\left[\frac{1}{d^2(-l_\beta)}-\frac{1}{d^2(-L_\beta)}\right]\right) \end{aligned} \tag{4.19}$$

Because $\zeta=0$ if $\mu=0$, we note that (4.19) implies that $Q_f^v|_{\mu=0}=0$; also, because $\dot m_R=\dot m_{\mathcal{L}}$ when $s=0$, in which case $\tilde p_R=\tilde p_{\mathcal{L}}$, it follows that $\Gamma_c=0$ when $s=0$ and, therefore, $Q_f^v|_{s=0}=0$. Thus, as would be expected, the 'viscous heating' of the lubricant vanishes both for the limiting case of zero viscosity as well as for the case of zero tangential speed of the roll. A detailed examination of Q_f^v for the degenerate case of a parallel-walled channel with fixed (stationary) walls is presented at the end of §5.

5 The Limiting Case as $\beta \to 0$.

In this section we will extract the limits

$$\begin{cases} \lim\limits_{\beta\to 0} & Q_{r\to 0} \\ \lim\limits_{\beta\to 0} & Q_{0\to sh} \\ \lim\limits_{\beta\to 0} & Q_f^v \end{cases} \tag{5.1}$$

of the respective expressions (3.17), (4.17), and (4.18), for the heat transferred from the roll to the oil (lubricant) the heat transferred from the oil to the shoe, and the 'viscous heating' of the lubricant; going to the limit in these expressions as $\beta \to 0$ corresponds to passing to the (physical) limiting case of a parallel wall channel.

In order to extract the limit: $\lim\limits_{\beta\to 0} Q_{r\to 0}$ we must extract the limit as $\beta \to 0$ in each component term in (3.17). We now display the calculations for just one of these terms (i.e., the first one in (3.17)) and, thereafter, will only record the results. The β dependent part of the first term in (3.17) is, clearly,

$$\frac{1}{\tan\beta} \ln\left[\frac{d(L_\beta)}{d(-L_\beta)}\right]$$

Using L'Hospital's rule we compute that

$$\begin{aligned} &\lim_{\beta\to 0}\left(\frac{1}{\tan\beta}\ln\left[\frac{d(L_\beta)}{d(-L_\beta)}\right]\right) \\ &= \lim_{\beta\to 0}\frac{1}{\tan\beta}\ln\left[\frac{d_0 - L_T\sin\beta}{d_0 + L_T\sin\beta}\right] \\ &= \lim_{\beta\to 0}\frac{1}{\sec^2\beta}\cdot\left(\frac{d_0 + L_T\sin\beta}{d_0 - L_T\sin\beta}\right)\frac{d}{d\beta}\left(\frac{d_0 - L_T\sin\beta}{d_0 + L_T\sin\beta}\right) \\ &= \lim_{\beta\to 0}\frac{1}{\sec^2\beta}\left(\frac{d_0 + L_T\sin\beta}{d_0 - L_T\sin\beta}\right)\left(\frac{-d_0 L_T\cos\beta}{[d_0 + L_T\sin\beta]^2}\right) \\ &= \lim_{\beta\to 0}\left(\frac{-d_0 L_T\cos\beta}{\sec^2\beta}\right)\cdot\left(\frac{1}{d_0^2 - L_T^2\sin^2\beta}\right) \end{aligned}$$

or

$$\lim_{\beta\to 0}\left(\frac{1}{\tan\beta}\ln\left[\frac{d(L_\beta)}{d(-L_\beta)}\right]\right) = -\frac{L_T}{d_0}$$

so that

$$\lim_{\beta\to 0}\frac{\kappa[(T_0 - T_1) - 3\zeta s^2]}{\tan\beta}\cdot\ln\left[\frac{d(L_\beta)}{d(-L_\beta)}\right] = \kappa[(T_1 - T_0) + 3\zeta s^2]\frac{L_T}{d_0} \tag{5.2}$$

Moving on to the other terms in (3.17) we have the following:

$$\lim_{\beta\to 0}\frac{1}{\tan\beta}\ln\left[\frac{d(-l_\beta)}{d(l_\beta)}\right] = \frac{L_{rec}}{d_0}$$

so that

$$\lim_{\beta\to 0}\frac{5}{2}\cdot\frac{\kappa|\zeta|s^2}{\tan\beta}\ln\left[\frac{d(-l_\beta)}{d(l_\beta)}\right]=\frac{5}{2}\frac{\kappa|\zeta|L_{rec}\cdot s^2}{d_0} \tag{5.3}$$

Next,

$$\lim_{\beta\to 0}\frac{1}{\tan\beta}\left[\frac{1}{d(L_\beta)}-\frac{1}{d(l_\beta)}\right]=\frac{L_T-L_{rec}}{d_0^2}$$

and, also,

$$\lim_{\beta\to 0}\frac{1}{\tan\beta}\left[\frac{1}{d(-l_\beta)}-\frac{1}{d(-L_\beta)}\right]=\frac{L_T-L_{rec}}{d_0^2}$$

so that

$$\lim_{\beta\to 0}\frac{8\kappa|\zeta|s}{\rho\tan\beta}\left(\dot{m}_R\left[\frac{1}{d(L_\beta)}-\frac{1}{d(l_\beta)}\right]-\dot{m}_{\mathcal{L}}\left[\frac{1}{d(-l_\beta)}-\frac{1}{d(-L_\beta)}\right]\right)$$
$$=\frac{8\kappa|\zeta|s}{\rho}\cdot\frac{(L_T-L_{rec})}{d_0^2}(\dot{m}_R-\dot{m}_{\mathcal{L}})|_{\beta=0} \tag{5.4}$$

Moving on to the next expression in (3.17) we have

$$\lim_{\beta\to 0}\frac{1}{\tan\beta}\left(\frac{1}{d^2(L_\beta)}-\frac{1}{d^2(l_\beta)}\right)=\frac{2(L_T-L_{rec})}{d_0^3}$$

and, also,

$$\lim_{\beta\to 0}\frac{1}{\tan\beta}\left(\frac{1}{d^2(-l_\beta)}-\frac{1}{d^2(-L_\beta)}\right)=\frac{2(L_T-L_{rec})}{d_0^3}$$

which imply that

$$\lim_{\beta\to 0}\frac{3\kappa\zeta}{\rho^2\tan\beta}\left(\dot{m}_R^2\left[\frac{1}{d^2(L_\beta)}-\frac{1}{d^2(l_\beta)}\right]+\dot{m}_{\mathcal{L}}^2\left[\frac{1}{d^2(-l_\beta)}-\frac{1}{d^2(-L_\beta)}\right]\right)$$
$$=\frac{-6\kappa|\zeta|}{\rho^2}\cdot\frac{(L_T-L_{rec})}{d_0^3}(\dot{m}_R^2-\dot{m}_{\mathcal{L}}^2)|_{\beta=0} \tag{5.5}$$

For the next expression we need

$$\lim_{\beta\to 0}\frac{1}{\tan\beta}[d^2(l_c)-d^2(-l_c)]=-4d_0L_c$$

so that

$$\lim_{\beta\to 0}\frac{\kappa\zeta\Gamma_c s}{6\tan\beta}[d^2(l_c)-d^2(-l_c)]=\frac{2}{3}\cdot\kappa|\zeta|d_0\cdot L_c\cdot s\cdot\Gamma_c(0)$$

where $\Gamma_c(0)=\dfrac{\tilde{p}_{\mathcal{L}}-\tilde{p}_R}{4\mu l_c}|_{\beta=0}$. As $l_c=L_c\cos\beta, l_c=L_c$, for $\beta=0$, and

$$\lim_{\beta\to 0}\frac{\kappa\zeta\Gamma_c s}{6\tan\beta}[d^2(l_c)-d^2(-l_c)]=\frac{1}{6}\frac{\kappa|\zeta|}{\mu}(\tilde{p}_{\mathcal{L}}(0)-\tilde{p}_R(0))d_0\cdot s \tag{5.6}$$

with $\tilde{p}_{\mathcal{L}}(0) = \tilde{p}_{\mathcal{L}}|_{\beta=0}$ and $\tilde{p}_R(0) = \tilde{p}_R|_{\beta=0}$.

Finally,

$$\lim_{\beta\to 0} \frac{1}{\tan\beta}[d^4(l_c) - d^4(-l_c)] = -8d_0^3 L_c$$

so

$$\lim_{\beta\to 0} \frac{\kappa|\zeta|\Gamma_c^2}{24\tan\beta}(d^4(l_c) - d^4(-l_c)) = -\frac{1}{3}\kappa|\zeta|d_0^3 \cdot L_c \cdot \Gamma_c^2(0)$$

from which it follows that

$$\lim_{\beta\to 0} \frac{\kappa|\zeta|\Gamma_c^2}{24\tan\beta}(d^4(l_c) - d^4(-l_c)) = -\frac{1}{48}\frac{\kappa|\zeta|}{\mu^2}(\tilde{p}_{\mathcal{L}}(0) - \tilde{p}_R(0))^2 \cdot \frac{d_0^3}{L_c} \tag{5.7}$$

Employing the limiting expressions in (5.2)-(5.7) we now compute that

$$\begin{aligned}
\lim_{\beta\to 0} Q_{r\to 0} &= \frac{\kappa(T_1 - T_0)}{d_0}L_T - \frac{\kappa|\zeta|s^2}{2d_0}(6L_T - 5L_{rec}) + \frac{8\kappa|\zeta|}{\rho d_0^2}s(L_T - L_{rec})(\dot{m}_R(0) - \dot{m}_{\mathcal{L}}(0)) \\
&- \frac{6\kappa|s|}{\rho^2}\frac{(L_T - L_{rec})}{d_0^3}(\dot{m}_R^2(0) + \dot{m}_{\mathcal{L}}^2(0)) + \frac{1}{6}\frac{\kappa|s|}{\mu}(\tilde{p}_{\mathcal{L}}(0) - \tilde{p}_R(0))s \\
&- \frac{1}{48}\frac{\kappa|\zeta|}{\mu^2}(\tilde{p}_{\mathcal{L}}(0) - \tilde{p}_R(0))^2\frac{d_0^3}{L_c}
\end{aligned} \tag{5.8}$$

with $\dot{m}_R(0) = \dot{m}_R|_{\beta=0}$ and $\dot{m}_{\mathcal{L}}(0) = \dot{m}_{\mathcal{L}}|_{\beta=0}$. Because the various terms in (4.17) exhibit the same dependence on β as did the corresponding terms in (3.17), we may compute, based on our results, above, that

$$\begin{aligned}
\lim_{\beta\to 0} Q_{0\to sh} &= \frac{\kappa(T_1 - T_0)}{d_0}L_T + \frac{\kappa|\zeta|s^2}{2d_0}(2L_T - L_{rec}) - \frac{4\kappa|\zeta|s}{\rho d_0^2}(L_T - L_{rec})(\dot{m}_R(0) - \dot{m}_{\mathcal{L}}(0)) \\
&+ \frac{6\kappa|\zeta|}{\rho^2}\frac{(L_T - L_{rec})}{d_0^3}(\dot{m}_R^2(0) + \dot{m}_{\mathcal{L}}^2(0)) + \frac{1}{6}\frac{\kappa|\zeta|}{\mu}(\tilde{p}_{\mathcal{L}}(0) - \tilde{p}_R(0))d_0 \\
&+ \frac{1}{48}\frac{\kappa|\zeta|}{\mu^2}(\tilde{p}_{\mathcal{L}}(0) - \tilde{p}_R(0))^2\frac{d_0^3}{L_c}
\end{aligned} \tag{5.9}$$

and, in view of (4.18), (5.8), and (5.9)

$$\begin{aligned}
\lim_{\beta\to 0} Q_f^v &= \frac{\kappa|\zeta|s^2}{d_0}(4L_T - 3L_{rec}) - 12\frac{\kappa|\zeta|s}{\rho d_0^2}(L_T - L_{rec})(\dot{m}_R(0) - \dot{m}_{\mathcal{L}}(0)) \\
&+ \frac{12\kappa|\zeta|}{\rho^2 d_0^3}(L_T - L_{rec})(\dot{m}_R^2(0) + \dot{m}_{\mathcal{L}}^2(0)) + \frac{\kappa|\zeta|}{24\mu^2}(\tilde{p}_{\mathcal{L}}(0) - \tilde{p}_R(0))^2\frac{d_0^3}{L_c}
\end{aligned} \tag{5.10}$$

Remarks: If we both extract the limit as $\beta \to 0$ in the expression for Q_f^v and, also, set $s = 0$, then $\tilde{p}_{\mathcal{L}}(0) = \tilde{p}_R(0)$ when $s = 0, \dot{m}_R(0) = \dot{m}_{\mathcal{L}}(0) \equiv \dot{m} > 0$, and (5.10) reduces to

$$\lim_{\beta \to 0} Q_f^v|_{s=0} = \frac{24\kappa|\zeta|}{\rho^2 d_0^3}(L_T - L_{rec})\dot{m}^2 \tag{5.11}$$

While it is difficult, even in this limiting case of a parallel wall channel, to make definitive statements about the behavior of $Q_{r\to 0}$, $Q_{0\to sh}$, and Q_f^v, (because, in general, the channel thickness d_0 will be a function of the roll speed s, given that all other physical parameters, such as the load exerted on the shoe, are fixed) it appears that the following will be valid:
(i) For s sufficiently small, $Q_{r\to 0} > 0$, but for s sufficiently large $Q_{r\to 0} < 0$
(ii) If $T_1 - T_0$ is sufficiently large, then for all $s, Q_{0\to sh} > 0$, with $Q_{0\to sh}$ growing as the roll speed s increases.
(iii) For all s, $Q_f^v > 0$, with Q_f^v growing as the roll speed s increases.

In fact, for a parallel wall domain, both the temperature and velocity fields are independent of x, i.e., $\theta = \theta(y), u = u(y)$, and θ satisfies

$$\kappa\theta''(y) = -\left(\frac{\mu}{c}\right) u'^2(y) < 0 \tag{5.12}$$

so that the graph of $\theta = \theta(y)$ is concave (down) and satisfies $\theta(0) = T_1 > T_0 = \theta(d_0)$. The two possible scenarios which apply here are indicated in figure 11.

For $s < s_c$ (s_c a critical speed) the oil temperature near the wall representing the roll is less than T_1 so heat flow goes from the roll to the lubricant; but for $s > s_c$ oil temperature near this wall is greater than T_1 and heat flows from the lubricant to the roll.

On the other hand, for all s, it would appear that the oil temperature near the wall representing the shoe is always greater than T_0 so that heat flows from the lubricant to the bottom surface of the shoe; in order for this result to, indeed, hold for all s it may be necessary that the difference $T_1 - T_0$ be sufficiently large.

Some further analytical insight into this problem can be achieved by looking at an even simpler problem in which oil flows in a parallel wall channel whose depth is held constant, say, at one unit; the channel has length L, the pressure difference $c_0 = p_0 - p_{atm} > 0$ is constant, the upper wall is held fixed, the bottom wall moves to the right with speed s, and the constant temperatures at the bottom and top wall are, respectively T_1 and $T_0 (T_0 < T_1)$. This situation is depicted in figure 12.

It is easily shown that the velocity distribution is given by

$$u(y) = \frac{c_0}{2\mu}y^2 - \left(\frac{c_0}{2\mu} + s\right) y + s \tag{5.13}$$

and

$$\theta(y) = \frac{\zeta c_0^2}{12\mu^2}y^4 - \frac{\zeta}{6}\left(\frac{2c_0 s}{\mu} + \frac{c_0^2}{\mu^2}\right)y^3 + \frac{\zeta}{2}\left(\frac{c_0^2}{4\mu^2} + \frac{c_0 s}{\mu} + s^2\right)y^2 + K_s y + T_1 \tag{5.14}$$

where

$$K_s = (T_0 - T_1) - \frac{\zeta c_0^2}{12\mu^2} + \frac{\zeta}{6}\left(\frac{2c_0 s}{\mu} + \frac{c_0^2}{\mu^2}\right) - \frac{\zeta}{2}\left(\frac{c_0^2}{4\mu^2} + \frac{c_0 s}{\mu} + s^2\right) \tag{5.15}$$

and $\zeta = \dfrac{-\mu}{\kappa}$.

From (5.14) we easily find the two relations

$$\begin{aligned} Q_{r\to 0} &= -\kappa L \frac{d\theta}{dy}|_{y=0} \\ &= -\kappa L K_s \end{aligned} \tag{5.16}$$

and

$$\begin{aligned} Q_{0\to sh} &= -\kappa L \frac{d\theta}{dy}|_{y=1} = -\kappa L K_s + (\mu)\left[\frac{c_0^2}{12\mu^2} + s^2 L\right] \\ &= Q_{r\to 0} + (\mu)\left[\frac{c_0^2 L}{12\mu^2} + s^2 L\right] \end{aligned} \tag{5.17}$$

The viscous heating of the oil is then given by

$$Q_{0\to sh} - Q_{r\to 0} = (\mu)\left[\frac{c_0^2 L}{12\mu^2} + s^2 L\right] \equiv Q_f^v \tag{5.18}$$

so that $Q_f^v \geq 0$ with $Q_f^v = 0$ iff both $c_0 = 0$ and $s = 0$. Also, Q_f^v as a function of s increases like s^2 as $s \to \infty$. From (5.15) and (5.16) we see that the term quadratic in s in the expression for $Q_{r\to 0}$ is just

$$q_s \equiv (-\kappa L)(-\frac{\zeta}{2})s^2 = \kappa\zeta\frac{L}{2}s^2 = -\frac{\mu L}{2}s^2 < 0 \tag{5.19}$$

so for s sufficiently large it is clear that $Q_{r\to 0} < 0$. By (5.18), then, the term quadratic in s in the expression for $Q_{0\to sh}$ is

$$q_s^* = \frac{-\mu L}{2}s^2 + \mu L\, s^2 = \frac{\mu L}{2}s^2 > 0 \tag{5.20}$$

so, for all s, $Q_{0\to sh} > 0$.

6 Some Numerical Results for CC Rolls

A. Computational Methods

Mathematical expressions for the velocity profiles (V1-V5), the temperature profiles (S1-S11), heat flow rate from the roll to the oil (S12-S17), and heat flow rate from the oil to the shoe (S18-S23), for each of the five regions between the bottom surface of the shoe and the inner surface of the roll were coded in a Fortran computer program using the Microsoft Fortran (version 5.1) on a 486 IBM-PC compatible microcomputer. The numerical results obtained from our previous study [4] for the lubricant mass flow rates, lubricant pressures, and geometric dimensions for the left and right sub-channels (e.g., thickness and length) associated with each operating condition were entered into the program. In the computer model a lubricant viscosity, density, and thermal conductivity of 56 centipoise, 873 Kg/m3; and 0.147 W/m°C were assumed, respectively. Calculations were performed for selected values of the shoe temperature (T_0) in the range of 100-160°C, and an inner roll surface temperature (T_1) in the range of 100-300°C.

B. Results and Discussion for a CC roll with $R = R_s$

In this section the results for a shoe/roll configuration in which the roll and the shoe are machined to the same radius of 508.13 mm ($R_s = R = 20.005$ in) are presented. Velocity and thermal characteristics were obtained for those operating conditions in which the shoe was subjected to an applied load of 350-1051 KN/m (2000-6000 PLI), and a roll speed of 305-1067 m/min (2000-3500 ft/min). In general, for the conditions analyzed in this study, the calculated net heat flow rate from the roll to the oil was negative which indicates that because of the viscous nature of the lubricant, and the large tangential speed of the roll, under steady state conditions, the temperature of the lubricant at the regions near the roll surface was greater than that of the inner surface of the roll, thus, under these conditions, the direction of heat transfer was actually from the oil to the roll. Energy absorbed by the lubricant because of viscous drag and inertial effects are expected to be very important in determination of thermal performance of the press roll. Therefore, in this section we will characterize this viscous heat dissipation as a function of various boundary and operating contortions.

Shown in figures 13a and 13b are the velocity and temperature profiles at the entrance to each channel ($x = 0$), at the end of the left-hand channel ($x = -L_\beta$), and at the end of the right-hand channel ($x = L_\beta$) for the roll speed of 610 m/min (2000 ft/min), and an applied load of 350 KN/m (2000 PLI). Note that in all figures referred in this section the subscript β has been suppressed, e.g., the points at the end of the left-hand and right- hand subchannels are identified by $-L$ and L, respectively. The velocity profiles are plotted as seen by an observer who considers as positive the direction from left to right; thus, except for the regions closer to the moving boundary (roll), in other locations the velocity profile in the left-hand channel is negative, and in general the profile at the beginning of the channels ($x = 0$) lies between those of the left-hand and right-hand channels. As was shown in the

previous study [4], because of the clockwise rotation of the shoe, the thickness of the channel at $x = -L_\beta$ becomes greater than that at $x = L_\beta$. For the operating conditions shown in figure 13a, the maximum lubricant velocity occurs in the right-hand channel slightly below the mid-point of the channel. We show in figure 13b the corresponding lubricant temperature profiles when the top and bottom boundaries are maintained at 100°C. In the left-hand channel, because the lubricant is flowing in the opposite direction to motion of the roll, viscous heat dissipation is greater than that in the right-hand channel. This results in a greater temperature increase for the lubricant flowing in the left-hand channel as compared with the corresponding points in the right-hand channel. Under these operating conditions, the lubricant temperature increases up to 30°C above the wall temperatures at the end of the left-hand (i.e., as much as 30% above the wall temperature), and up to 8°C at the end of the right-hand channel.

Shown in figures 14a and 14b are the lubricant velocity and temperature profiles for the same conditions as those described in the previous figures except that the applied load in these cases was increased from 350 KN/m to 700 KN/m. As shown in figure 14a, because of the influence of the external pressure and roll speed, in some regions the lubricant velocity becomes greater than the roll speed of 610 m/min (10.2 m/sec). The lubricant temperature increase for this case was approximately 70% above the wall temperature (figure 14b). Figures 15a-15c correspond to those profiles for an applied load of 1051 KN/m. As the magnitude of applied load increases, the shoe moves downwards and will also exhibit a smaller clockwise deflection. This will result in a smaller difference between the lubricant thicknesses at the end of the two sub-channels. As shown in these figures, an increase in applied load results in more symmetrical velocity distributions for the left-hand and right-hand channels with respect to the distribution at $x = 0$. As the applied load increases, the influence of the pressure terms in the calculated velocity for the profile at $x = 0$, becomes less significant (see equation V5), and this profile will approach a straight line (figure 15a). This same behavior is observed in the temperature profile (figure 15b). An increase in applied load from 350 KN/m to 1051 KN/m results in a significant increase in the mass flow rates, and a significant reduction in the lubricant thickness along the left hand channel [4]. Thus, the fluid velocity in this channel increases significantly with applied load.

For instance, the absolute value of the maximum lubricant velocity for an applied load of 1051 KN/m is 26 m/sec (figure 15a) which is approximately 2.5 times greater than the roll velocity. Figures 14b and 15b indicate that the maximum oil temperature at the end of the right-hand channel occurs in the region closer to the shoe, while for the left-hand channel it occurs in regions closer to the roll. Note that the two boundaries are maintained at the same temperature of 100°C, however, the lubricant temperature differential in the thickness direction is as high as 125°C (figure 15b). This has occurred because of heat dissipation within the fluid which is strongly influenced by the oil viscosity and relative motions of the lubricant and the moving boundary. Such a temperature variation along the film thickness is expected to have a major effect in the oil viscosity.

It should be emphasized that in the analytical solution performed in this study it was

assumed that in each region of the channel (i.e., under the solid part of the shoe in the right-hand channel) the variation of the temperature along the machine direction is much smaller than that along the thickness direction (see equation (2.21)). Plots of the temperature profiles at the entrance to this region of the channel ($x = l_\beta = 116.3$ mm), and at the end of the channel ($x = L_\beta = 187.4$ mm) are shown in figure 16c. Considering the fact that under the solid part of the shoe, the thickness of the channel (0.42 mm or less) is much smaller than the machine direction width of the channel (71.1 mm), the approximation used in equation (2.21) appears to be supported by this figure. However, justification for simplifying equation (2.9) to equation (2.22) in which the convective term was assumed to be negligible, depends on lubricant velocity, and the thermal and physical properties of the oil, and should be further investigated by a numerical approach.

Analysis of thermal behavior of hydrostatic and hydrodynamic bearing with conventional recess and pad design and subjected to adiabatic or isothermal boundary conditions has been studied extensively [10,11]. A classical solution for a flow of an incompressible Newtonian fluid between two coaxial cylinders in which the outer cylinder rotates and results in viscous heat generation within the fluid is given in [9]. Some studies have analyzed the effect of a more complex bearing geometry and variable rheological behavior of the lubricant [10,11]. However, the thermal solution for a crown compensated roll design such as the one described in this study, in which the lubricant is subjected to an external pressure, and flows through a series of capillary tubes located in the central region of the shoe as it enters into the channel formed by the bottom surface of the shoe and inner surface of the roll, and then flows through the left-hand and right-hand sides of the channel, is not available. For the sake of simplification, in this initial study, the influence of the variation of lubricant viscosity with temperature was not considered. This viscosity variation not only occurs along the machine direction width of the channel, but also across the film thickness, and should be considered in future studies. The purpose of this initial investigation was to develop a closed-form analytical solution to gain more insight into the fluid and thermal characteristics of the press roll. Using numerical techniques such as finite difference or finite element analysis, future studies should consider all terms in the energy equation, and take viscosity to be a function of temperature. In this regard we refer the reader to the discussion in section 7. One advantage of numerical techniques over analytical methods is that, in general, they are more flexible with regard to handling complex geometric and boundary conditions. However, to assure validity, accuracy, and convergence, such results should be compared with experimental data, or analytical solutions.

Lubricant temperature profiles for a shoe temperature of 100°C and roll temperatures of 200°C and 300°C are shown in figures 16a and 16b, respectively. Again, because in the left-hand channel the lubricant flows against the direction of rotation of the roll, the oil temperature increase in this sub-channel is greater than that in the right-hand channel. An equivalent interpretation is that the square of the gradient of the velocity profile at each point along the thickness of the left-hand channel is greater than that at the corresponding point in the right-hand channel (see equation 2.4). As expected, under these conditions,

the maximum lubricant temperature occurs near the roll which is maintained at a higher temperature than the shoe. Temperature profiles at three locations along the channel for a roll inner surface temperature of 100°C and a shoe temperature of 160°C are shown in figure 17. Note that the temperature profile at $x = 0$, which is approximately linear, indicates that for this operating condition, in this region, the influence of viscous dissipation on the temperature gradient is negligible, and the dominant mode of heat transfer within the fluid is by conduction. In other words, under these conditions, the heat transfer through the lubricant at $x = 0$ is similar to that of heat transfer through a solid body. Shown in figure 18 are the temperature profiles at the end of the left-hand channel ($x = -L_\beta$) for an inner roll temperature of 200°C and various shoe temperatures between 100-160°C. Under these conditions, the location of the maximum lubricant temperature is independent of the shoe temperature and occurs approximately 0.13 mm above the inner surface of the roll.

The influence of the roll speed on the lubricant velocity and temperature profiles at the end of the left-hand channel are shown in figures 19a and 19b, respectively.

Figure 19b indicates that with both boundaries at 100°C, the maximum oil temperature occurs closer to the moving boundary (roll). A comparison of these figures indicates that an increase in roll speed has a more pronounced effect on the temperature profiles than on the velocity profiles. Temperature profiles for an inner roll temperature of 300°C are shown in figure 19c. Figures 20a and 20b depict the oil velocity and temperature profiles at the entrance of the channels ($x = 0$) when the shoe and roll temperatures are maintained at 100°C for various roll speeds. As the speed of the roll increases from 305 m/min to 1067 m/min, the viscous heat dissipation within the lubricant increases which results in a significant change in the temperature profile. Temperature profiles for an inner roll temperature of 300°C are shown in figure 20c. The corresponding plots for the end of the right-hand channel are shown in figures 21a-21c. For the right-hand channel when the temperature of both boundaries are at 100°C (figure 21b), the maximum oil temperature occurs in those regions closer to the fixed boundary (shoe). Comparison of figures 20b and 21b indicates that at the entrance to the channel ($x = 0$), a roll speed of 305 m/min results in the smallest lubricant temperature differential along the thickness direction, while at the end of the right-hand channel ($x = L_\beta$), this roll speed results in the greatest temperature differential.

We show in figures 22a and 22b the oil temperature profiles at the end of each channel for the shoe temperature of 100°C and various inner roll temperatures. Note that when the inner surface of the roll is maintained at a higher temperature, the slope of the temperature profile near this surface is increased. Thus, gives a smaller heat flow from oil to the roll. It is anticipated that if one were to hold the shoe temperature fixed, under a fixed operating conditions with respect to roll speed and applied load continue to increase the roll temperature, eventually the slope of the temperature profile near the wall would become negative thus indicating that the heat transfer goes from roll to oil. For the condition where $T_1 = T_0$, the lower limit for the slope of the temperature profile corresponds to that of a straight line in which the transfer of heat from the roll to the shoe is controlled by the mode of conduction, independent of any viscous dissipation (e.g., see figures 20b and 20c). To

investigate the influence of applied load on the velocity and temperature profiles at various locations along the channel, these profiles are plotted for two loading conditions in figures 23a and 23b, respectively. An increase of the applied load from 350 to 700 KN/m will result in a smaller counterclockwise deflection for the shoe; this will result in a reduction of the lubricant thickness at $x = -L_\beta$ and an increase in the channel thickness at $x = L_\beta$. The temperature and velocity profiles at the entrance to the channels were not affected by the change in applied load. However, an increase in applied load from 350 to 700 KN/m, which results in a greater lubricant flow rate, and thus a greater flow velocity at the end of each channel, has caused a significant increase in the temperature profiles at these regions (figure 23b).

With both boundaries maintained at 100°C, the maximum oil temperature at $x = -L_\beta$ occurs in those regions closer to the roll while at $x = L_\beta$ it occurs in regions closer to the shoe.

Shown in figure 24a is a plot of the absolute value of the net heat flow rates per unit cross machine direction width of the channel (obtained from equation S17 as a function of roll inner surface temperature T_1, for each shoe temperature T_0, for the operating condition of 1051 KN/min (6000 PLI) load, and 610 m/min (2000 ft/min) roll speed. These results are plotted in figure 24b as a function of shoe temperature (T_0) for each roll inner surface temperature. The heat flow rate is inversely proportional to T_1 (figure 24a), and directly proportional to T_0 (figure 24b). A greater heat transfer from oil to roll occurs for a smaller roll temperature (e.g., $T = 100°C$), and a larger shoe temperature (e.g., $T_0 = 160°C$). As indicated, for a constant shoe temperature, if we continue to increase the roll inner surface temperature, the heat transfer from oil to roll will drop in magnitude (figure 24a) and eventually becomes negative indicating that the direction of heat transfer in this case will be from roll to oil. The heat flux for each region of the channel can be obtained by dividing the heat transfer in each region by the corresponding machine direction width of that region. Shown in figure 24c is the total net heat flux (which is equivalent to the total heat flow rate divided by the roll inner surface area along the cross machine direction). For a fixed shoe temperature of 160°C, the contributions of each region to the net thermal energy and heat flux transferred from the oil to the shoe are plotted as a function of the roll inner surface temperature in figures 25a and 25b, respectively. These figures indicate that the regions under the solid part of the shoe, which are associated with a greater fluid velocity, play a major roll in the transfer of heat from the oil to the roll.

The net heat transfer under the solid part of the shoe for the left-hand channel is much greater than that of the right-hand channel because of the greater lubricant thickness in this region, as well as the larger dissipated heat in the lubricant occupying the left-hand channel, (e.g., see temperature profile shown in figure 15b).

Shown in figures 26a and 26b are the net heat flow rate from oil to the shoe (see equation S-23) as a function of T_1 and T_0, respectively. A greater heat transfer from oil to shoe occurs for a greater roll inner surface temperature (e.g., $T_1 = 300°C$), and a smaller shoe temperature (e.g., $T_0 = 100°C$). The corresponding heat flux as a function of roll inner

surface temperature is plotted in figure 26c. For a constant shoe temperature of 160°C, the contributions of each region to the net heat transfer per unit of cross machine direction width of the roll, and to the net heat flux are plotted in figures 27a and 27b, respectively. Under these conditions, the calculated thermal energy and heat flux for the left-hand and right-hand recesses are identical. Shown in figures 28- 31c are the plots of the heat flow rate and heat flux for an operating condition of 1051 KN/m (6000 PLI) load, and 914 m/min (3500 ft/min) roll speed. Comparison of figures 24a and 28, and also figures 25a and 29a, indicates that an increase of the roll speed from 610 m/min to 914 m/min results in a greater heat transfer from the oil to the roll. However, the heat transfer under the recess was independent of the roll speed. Shown in figures 29b and 29c are the heat flux from the oil to the roll as a function of distance from the beginning of each sub-channel. The discontinuity in the profiles at the interface between two adjacent regions corresponds to the discontinuity in the velocity profile at that interface. For a fixed shoe temperature (T_0) of 100°C, and a roll inner surface temperature of 200°C, or higher, the viscous heat dissipation under the left-hand and right-hand recesses was negligible. For these conditions, the direction of heat transfer was from the roll to the oil (figure 29b). Similarly, for a fixed roll temperature of 100°C, and a shoe temperature of 160°C, in this region, the direction of heat transfer was from the shoe to the roll (figure 31c). The variation in heat flux under the solid part of the shoe is due to the variations in the dimension of the channels as well as the variation in the temperature profile along the cross machine direction (e.g., see figure 16c).

At the present time no experimental data for velocity or temperature across the film thickness or along the machine direction width of the channel is available to compare with the values predicted by the analytical model. Since the lubrication thickness is very small, and the variation of temperature along the thickness is relatively large, specific experimental methods should be developed to measure the velocity and temperature along this direction.

7 Some Directions for Future Research

In this section we will present some ideas that are directly related to carrying the initial effort presented in §1-6 forward; these include a finite-difference scheme for solving (2.9) with only the highest order derivatives in the machine direction deleted, a discussion of iterative and averaging schemes to gauge, more accurately, the relative importance of the convective term $\rho c_p u \dfrac{\partial \theta}{\partial x}$ in the heat transfer analysis, the inclusion of a temperature dependent viscosity $\mu = \mu(\theta)$, and a modification of the prescribed boundary conditions on the bottom surface of the shoe and the inside surface of the roll so as to cover a broader and more physically realistic set of possibilities on these boundaries. We begin by focusing on the subdomain in the channel under the solid part of the shoe, in the right-hand subchannel, and on recasting the original boundary-value problem there in a form more amenable to numerical computation of the temperature field.

In the subdomain of the lubrication channel in our model defined by $0 \leq y \leq d(x),\ l_\beta < x < L_\beta$, the equation for the temperature distribution has the form

$$\kappa \bigtriangledown^2 \theta_R(x,y) + b_R(x,y)\frac{\partial \theta_R}{\partial x} = f_R(x,y,\mu) \tag{7.1}$$

with

$$b_R(x,y) = -\rho c_p u_R(x,y);\ f(x,y;\mu) = -\mu_R \left(\frac{\partial u}{\partial y}\right)^2 \tag{7.2}$$

In addition, the full set of boundary conditions has the form

$$\theta(x,0) = T_1,\ \theta(x,d(x)) = T_0, l_\beta < x < L_\beta \tag{7.3a}$$

and

$$\begin{cases} \theta(L_\beta, y) = \alpha(y), & 0 \leq y \leq d(L_\beta) \\ \theta(l_\beta, y) = \beta(y), & 0 \leq y \leq d(l_\beta) \end{cases} \tag{7.3b}$$

Let

$$\theta^* = \frac{y}{d(x)}(T_0 - T_1) + T_1 \tag{7.4}$$

then

$$\theta^*(x,0) = T_1,\ \theta^*(x,d(x)) = T_0, l_\beta \leq x \leq L_\beta \tag{7.5a}$$

and

$$\begin{cases} \theta^*(L_\beta, y) = \dfrac{y}{d(L_\beta)}(T_0 - T_1) + T_1, & 0 \leq y \leq d(L_\beta) \\ \theta^*(l_\beta, y) = \dfrac{y}{d(l_\beta)}(T_0 - T_1) + T_1, & 0 \leq y \leq d(l_\beta) \end{cases} \tag{7.5b}$$

so if we set

$$\Theta(x,y) = \theta(x,y) - \theta^*(x,y) \tag{7.6}$$

then

$$\Theta(x,0) = \Theta(x,d(x)) = 0, l_\beta \le x \le L_\beta \tag{7.7a}$$

and

$$\begin{cases} \Theta(L_\beta,y) = \alpha(y) - \left[\dfrac{y}{d(L_\beta)}(T_0 - T_1) + T_1\right], & 0 \le y \le d(L_\beta) \\ \Theta(l_\beta,y) = \beta(y) - \left[\dfrac{y}{d(-L_\beta)}(T_0 - T_1) + T_1\right], & 0 \le y \le d(l_\beta) \end{cases} \tag{7.7b}$$

In particular, if $\alpha(y), \beta(y)$ are chosen, respectively, to be linear interpolations of the temperatures T_0, T_1 at $x = L_\beta$ and $x = l_\beta$, then $\Theta(L_\beta, y) = 0, 0 \le y \le d(L_\beta)$, and $\Theta(l_\beta, y) = 0, 0 \le y \le d(l_\beta)$. Using (7.6) in (7.1) we may compute, directly, that $\Theta(x,y)$ satisfies

$$\kappa \bigtriangledown^2 \Theta_R + b_R(x,y)\frac{\partial \Theta_R}{\partial x} = g_R(x,y;\mu) \tag{7.8}$$

with

$$g_R(x,y;\mu) = f_R(x,y;\mu) - \kappa(T_0 - T_1)y \cdot (d^{-1}(x))'' - (T_0 - T_1)b_R(x,y) \cdot y \cdot (d^{-1}(x))'$$

But, as $d(x) = d_0 - x\tan\beta, (d^{-1}(x))' = \tan\beta/d^2(x)$, while $(d^{-1}(x))'' = 2\tan^2\beta/d^3(x)$, and, therefore,

$$g_R(x,y;\mu) = f_R(x,y;\mu) + \frac{2\kappa(T_1 - T_0)\tan^2\beta \cdot y}{d^3(x)} + \frac{(T_1 - T_0)\tan\beta \cdot y \cdot b_R(x,y)}{d^2(x)} \tag{7.9}$$

We now transform the domain $D = \{(x,y) | 0 \le y \le d(x), l_\beta \le x \le L_\beta\}$ which approximates that part of the subchannel formed by the bottom surface of the shoe and the inside surface of the roll between l_β and L_β. Consider the change of independent variables given by

$$\begin{cases} \bar{x} = f_1(x,y) = x \\ \bar{y} = f_2(x,y) = y/d(x) \end{cases} \tag{7.10}$$

Under the mapping $(x,y) \to (\bar{x},\bar{y}), D$ is mapped onto the domain $\bar{D} = \{(\bar{x},\bar{y}) | l_\beta \le \bar{x} \le L_\beta, 0 \le \bar{y} \le 1\}$ (figure 32a). The Jacobian of this mapping is

$$J = \left|\frac{\partial(\bar{x},\bar{y})}{\partial(x,y)}\right| = \begin{vmatrix} 1 & 0 \\ \dfrac{-yd'(x)}{d^2(x)} & \dfrac{1}{d(x)} \end{vmatrix} = \frac{1}{d(x)} > 0 \tag{7.11}$$

so the mapping $(x, y) \rightarrow (\bar{x}, \bar{y})$ is non-singular and, thus, invertible. The inverse mapping is, in fact, given by

$$\begin{cases} x = \bar{f}_1(\bar{x}, \bar{y}) = \bar{x} \\ y = \bar{f}_2(\bar{x}, \bar{y}) = d(\bar{x})\bar{y} \end{cases} \tag{7.12}$$

We now define $\bar{\Theta}, \bar{g}$, and $\bar{b}$ by

$$\begin{cases} \Theta_R(x, y) & \equiv \Theta_R(\bar{f}_1(\bar{x}, \bar{y}), \bar{f}_2(\bar{x}, \bar{y})) = \Theta_R(\bar{x}, d(\bar{x})\bar{y}) \\ & = \bar{\Theta}_R(\bar{x}, \bar{y}) \\ g_R(x, y; \mu) & \equiv g_R(\bar{x}, d(\bar{x})\bar{y}; \mu) = \bar{g}_R(\bar{x}, \bar{y}; \mu) \\ b_R(x, y) & \equiv b_R(\bar{x}, d(\bar{x})\bar{y}) = \bar{b}_R(\bar{x}, \bar{y}) \end{cases} \tag{7.13}$$

so that $\bar{\Theta}_R, \bar{g}_R$, and $\bar{b}_R$ are defined for $l_\beta \leq \bar{x} \leq L_\beta, 0 \leq \bar{y} \leq 1$. From (7.13), tedious but straightforward calculations yield

$$\begin{cases} \dfrac{\partial \Theta_R}{\partial x} = \dfrac{\partial \bar{\Theta}_R}{\partial \bar{x}} + \tan\beta \left(\dfrac{\bar{y}}{d(\bar{x})}\right) \dfrac{\partial \bar{\Theta}_R}{\partial \bar{y}} \\ \dfrac{\partial \Theta_R}{\partial y} = \dfrac{\partial \bar{\Theta}_R}{\partial \bar{y}} \cdot \dfrac{1}{d(\bar{x})} \end{cases} \tag{7.14}$$

and

$$\begin{cases} \dfrac{\partial^2 \Theta_R}{\partial x^2} & = \dfrac{\partial^2 \bar{\Theta}_R}{\partial \bar{x}^2} + 2\tan\beta \left(\dfrac{\bar{y}}{d(\bar{x})}\right) \dfrac{\partial^2 \bar{\Theta}_R}{\partial \bar{x} \partial \bar{y}} \\ & \quad + 2\tan^2\beta \left(\dfrac{\bar{y}}{d^2(\bar{x})}\right) \dfrac{\partial \bar{\Theta}_R}{\partial \bar{y}} + \tan^2\beta \left(\dfrac{\bar{y}}{d(\bar{x})}\right) \dfrac{\partial^2 \bar{\Theta}_R}{\partial \bar{y}^2} \\ \dfrac{\partial^2 \Theta_R}{\partial y^2} & = \dfrac{1}{d^2(\bar{x})} \dfrac{\partial^2 \bar{\Theta}_R}{\partial \bar{y}^2} \end{cases} \tag{7.15}$$

From (7.15) we then have, for $l_\beta \leq \bar{x} \leq L_\beta, 0 \leq \bar{y} \leq 1$:

$$\begin{aligned} \nabla^2 \Theta_R &= \frac{\partial^2 \Theta_R}{\partial \bar{x}^2} + 2\tan\beta \left(\frac{\bar{y}}{d(\bar{x})}\right) \frac{\partial^2 \bar{\Theta}_R}{\partial \bar{x} \partial \bar{y}} + 2\tan^2\beta \left(\frac{\bar{y}}{d(\bar{x})}\right) \frac{\partial \bar{\Theta}_R}{\partial \bar{y}} \\ &\quad + \frac{1}{d^2(\bar{x})} \left(1 + \tan^2\beta \bar{y}^2\right) \frac{\partial^2 \bar{\Theta}_R}{\partial \bar{y}^2} \end{aligned} \tag{7.16}$$

As both $\tan\beta \approx 0$ and $\dfrac{\tan\beta}{d_0} \ll 1$ (i.e., [4]), if the derivatives

$$\frac{\partial^2 \bar{\Theta}_R}{\partial \bar{x} \partial \bar{y}}, \frac{\partial \bar{\Theta}_R}{\partial \bar{y}}, \text{ and } \frac{\partial^2 \bar{\Theta}_R}{\partial \bar{y}^2}$$

are bounded on the rectangle $\bar{D}$, then by (7.14), (7.16)

$$\begin{cases} \dfrac{\partial \Theta_R}{\partial x} & \approx \dfrac{\partial \bar{\Theta}_R}{\partial \bar{x}} \\ \\ \nabla^2 \Theta_R & \approx \dfrac{\partial \bar{\Theta}_R}{\partial \bar{x}^2} + \dfrac{1}{d_0^2} \dfrac{\partial^2 \bar{\Theta}_R}{\partial \bar{y}^2} \end{cases} \tag{7.17}$$

and (7.8) assumes the following form on $\bar{D}$:

$$\kappa \left(\frac{\partial^2 \bar{\Theta}_R}{\partial \bar{x}^2} + \frac{1}{d_0^2} \frac{\partial^2 \bar{\Theta}_R}{\partial \bar{y}^2} \right) + \bar{b}(\bar{x}, \bar{y}) \frac{\partial \bar{\Theta}_R}{\partial \bar{x}} = \bar{g}_R(\bar{x}, \bar{y}; \mu), \tag{7.18}$$

for $l_\beta \leq \bar{x} \leq L_\beta, 0 \leq \bar{y} \leq 1$, where $\bar{b}_R(\bar{x}, \bar{y})$ and $\bar{g}_R(\bar{x}, \bar{y}; \mu)$ are given by (7.13). Associated with (7.18) is the boundary data

$$\begin{cases} \bar{\Theta}_R(\bar{x}, 0) = \Theta_R(x, 0) = 0 \\ \bar{\Theta}_R(\bar{x}, 1) = \Theta_R(x, d(x)) = 0 \end{cases}, l_\beta < x < L_\beta \tag{7.19}$$

and

$$\begin{cases} \bar{\Theta}_R(L_\beta, \bar{y}) &= \Theta_R(L_\beta, d(L_\beta)\bar{y}) \\ &= \alpha(d(L_\beta)\bar{y}) - [\bar{y}(T_0 - T_1) + T_1],\ 0 \leq \bar{y} \leq 1 \\ \bar{\Theta}_R(l_\beta, \bar{y}) &= \Theta_R(l_\beta, d(l_\beta)\bar{y}) \\ &= \beta(d(l_\beta)\bar{y}) - [\bar{y}(T_0 - T_1) + T_1],\ 0 \leq \bar{y} \leq 1 \end{cases} \tag{7.20}$$

If $\alpha(y), \beta(y)$ have been chosen, respectively, as linear interpolations of T_0 and T_1, at $x = L_\beta, x = l_\beta$, then

$$\bar{\Theta}_R(L_\beta, \bar{y}) = 0, \bar{\Theta}_R(l_\beta, \bar{y}) = 0; 0 \leq \bar{y} \leq 1 \tag{7.21}$$

Once $\bar{\Theta}_R(\bar{x}, \bar{y})$ has been computed on $\bar{D}$ we may recover $\Theta_R(x, y)$ on D as

$$\Theta_R(x, y) = \bar{\Theta}_R(x, y/d(x)), 0 \leq y \leq d(x), l_\beta < x < L_\beta \tag{7.22}$$

and then, by (7.6),

$$\theta_R(x, y) = \Theta_R(x, y) + \frac{y}{d(x)}(T_0 - T_1) + T_1 \tag{7.23}$$

for $0 \leq y \leq d(x), l_\beta < x < L_\beta$

Because we have, in (7.18), $\dfrac{1}{d_0^2} >> 1$, a good approximation to the solution of the boundary-value problem (7.18)-(7.20) can be obtained by deleting the highest order spatial derivative in (7.18), in the machine direction, i.e., $\dfrac{\partial^2 \bar{\Theta}_R}{\partial x^2}$; in this case the first boundary condition in (7.20) is not needed and a finite-difference scheme may be applied to the resulting problem, i.e. to

$$\frac{\kappa}{d_0^2}\frac{\partial^2\bar{\Theta}_R}{\partial x^2} + \bar{b}_R(\bar{x},\bar{y})\frac{\partial\bar{\Theta}_R}{\partial\bar{x}} = \bar{g}_R(\bar{x},\bar{y},\mu) \quad (7.24)$$

$$\bar{\Theta}_R(\bar{x},0) = \bar{\Theta}_R(\bar{x},1) = 0,\ l_\beta < x < L_\beta \quad (7.25)$$

$$\bar{\Theta}_R(\ell_\beta,\bar{y}) = \beta(d(l_\beta)\bar{y}) - [\bar{y}(T_0 - T_1) + T_1], 0 \le \bar{y} \le 1 \quad (7.26)$$

as follows:

First a domain such as the one shown in figure 32b will be generated in which the top, the bottom, and the left boundaries are assumed to have known values of nodal temperature. The objective is to determine the nodal temperatures for $\bar{\Theta}_{I,J}$ where $I = 2, 3, ...m$ and $J = 2, 3, ..., j+1$.

Using a central difference approximation, for all the derivatives involving $\bar{y}$, and a backward difference approximation for all derivatives involving $\bar{x}$, a system of linear equations for all nodal points in a specific column (e.g. $I = 2$) will be generated. For instance in the system of equation for the nodes located at the second column ($I = 2$), nodal temperatures of $\bar{\Theta}_{2,J}$ ($J = 2, 3, ..., j+1$) are unknown, and are expressed in terms of some known quantities such as the nodal velocities, the boundary temperatures, and the thermal and geometric properties. The nodal velocities are obtained from the mathematical expressions for the velocity fields (e.g., equations $V1$ and $V2$). This system of equations for $I = 2$ will be solved numerically and the nodal temperatures for $\bar{\Theta}_{2,J}$, $J = 2, 3, ..., j+1$ will be determined. Then using a similar approach, another system of equations for the nodal temperatures at $I = 3$ will be generated which are now in terms of known quantities such as the nodal temperatures at $I = 2$. Again the system of equations will be solved numerically and this process of marching down the channel will be continued until the temperatures at the channel exit (e.g., $\bar{\Theta}_{I,J}$ for $I = m$, $J = 2, 3, ..., j+1$) are determined. As examples for development of this scheme we note the following finite difference expressions for the nodes located at $I = 2$:

For $I = 2$, $J = 2$, the finite difference approximation of the governing equation (where we suppress the R subscript) (7.24) is:

$$\frac{k}{d_0^2}\frac{\bar{\Theta}_{2,3} - 2\bar{\Theta}_{2,2} + \bar{\Theta}_{2,1}}{(\Delta\bar{y})^2} + \bar{b}_{2,2}\frac{\bar{\Theta}_{2,2} - \bar{\Theta}_{1,2}}{(\Delta\bar{x})} = \bar{g}_{2,2}$$

For $I = 2$, $J = 3$:

$$\frac{k}{d_0^2}\frac{\bar{\Theta}_{2,4} - 2\bar{\Theta}_{2,3} + \bar{\Theta}_{2,2}}{(\Delta\bar{y})^2} + \bar{b}_{2,3}\frac{\bar{\Theta}_{2,3} - \bar{\Theta}_{1,3}}{(\Delta\bar{x})} = \bar{g}_{2,3}$$

$\vdots$

For $I = 2, j$:

$$\frac{k}{d_0^2}\frac{\bar{\Theta}_{2,j+1} - \bar{\Theta}_{2,j} + \bar{\Theta}_{2,j-1}}{(\Delta\bar{y})^2} + \bar{b}_{2,j}\frac{\bar{\Theta}_{2,j} - \bar{\Theta}_{1,j}}{(\Delta\bar{x})} = \bar{g}_{2,j}$$

and for $I = 2, j+1$

$$\frac{k}{d_0^2}\,\frac{\bar{\Theta}_{2,n}-\bar{\Theta}_{2,j+1}+\bar{\Theta}_{2,j}}{(\Delta\bar{y})^2}+\bar{b}_{2,j+1}\frac{\bar{\Theta}_{2,j+1}-\bar{\Theta}_{1,j+1}}{(\Delta\bar{x})}=\bar{g}_{2,j+1}$$

where in the above equations, $\bar{\Theta}_{2,1}=\bar{\Theta}_{2,n}=0$,
and $\bar{\Theta}_{1,2}=\bar{\Theta}_{1,3}=...=\bar{\Theta}_{1,j}=\bar{\Theta}_{1,j+1}=\bar{\Theta}_I$ and $\bar{b}_{I,J}$ and $\bar{g}_{I,J}$ are know quantities that are given in terms of the nodal velocities and other parameters.

The scheme described above serves to determine (by (7.22) and (7.23)) $\bar{\theta}_R(x,y)$ for $0\leq y\leq d(x), l_\beta<x<L_\beta$.

To evaluate the importance of the convective term $\rho c_p u\dfrac{\partial\theta}{\partial x}$, which has been passed over in generating the results presented in §1-6, we may proceed in one of several other ways:

(i) Consider the subdomain in the right-hand channel defined by $0\leq y\leq d(x),\ l_\beta<x<L_\beta$, and the "zeroth-order" iterative given by (2.27), i.e.,

$$\begin{aligned}\bar{\theta}_R^{(0)}(x,y) &= \zeta d^{-2}(x)\sum_{R=0}^{4}\bar{p}_k^R(y)d^{-k}(x) \\ &+ \sum_{R=1}^{3}c_k^R d^{-k}(x)+T_1\end{aligned}\qquad(7.27)$$

where $\zeta=-\mu/\kappa$ and the $\bar{p}_k^R, c_k^R$ are given by (S5) and (S6), respectively, of Appendix III. Ignoring, once again, the highest order derivative in the machine direction, but employing (7.27) in the convective term, we may define a first-order iterative $\bar{\theta}_R^{(1)}(x,y)$ as the solution of the boundary-value problem (compare with (2.22) for $\bar{\theta}_R^{(0)}(x,y)$):

$$\frac{\partial^2\bar{\theta}_R^{(1)}}{\partial y^2}=\zeta\bar{A}^R(x,y)+\rho\frac{c_p}{\kappa}\bar{u}_R(x,y)\frac{\partial\bar{\theta}_R^{(0)}}{\partial x}\qquad(7.28a)$$

$$\bar{\theta}_R^{(1)}(x,0)=T_1,\ \bar{\theta}_R^{(1)}(x,d(x))=T_0, l_\beta<x<L_\beta\qquad(7.28b)$$

It may be shown that the general solution of (7.28a) is

$$\begin{aligned}\bar{\theta}_R^{(1)}(x,y) &= \zeta d^{-2}(x)\sum_{0}^{4}\bar{p}_k^R(y)d^{-k}(x)+m(x)y+n(x) \\ &+ \mu\tan\beta\left\{\frac{1}{2}D(x)y^5+\frac{1}{12}E(x)y^4+\frac{1}{6}F(x)y^3\right. \\ &+ \frac{4}{15}s^2y^6A_0(x)-\left[\frac{4\dot{m}_R s}{5\rho}y_6+\frac{4s^2}{21}y^7\right]A_1(x) \\ &+ \left.\left[\frac{3\dot{m}_k^2}{\zeta\rho^2}y^6+\frac{2\dot{m}_R s}{3\rho}y^7+\frac{3}{16}s^2y^8\right]A_2(x)\right.\end{aligned}$$

$$
\begin{aligned}
&- \left[\frac{4\dot{m}_R^2}{7\rho^2}y^7 + \frac{3\dot{m}_R s}{14\rho}y^8\right] A_3(x) + \frac{3\dot{m}_R^2}{14\rho^2}y^8 A_4(x) \\
&+ \frac{2}{5}s^2 y^5 B_0(x) - \left[\frac{6}{5\rho}\dot{m}_R s y^5 + \frac{4}{15}s^2 y^6\right] B_1(x) \\
&+ \left[\frac{9\dot{m}_R^2}{10\rho^2}y^5 + \frac{14\dot{m}_R s}{15\rho}y^6 + \frac{s^2}{14}y^7\right] B_2(x) \\
&- \left[\frac{4\dot{m}_R^2}{5\rho^2}y^6 + \frac{2\dot{m}_R s}{7\rho}y^7\right] B_3(x) + \frac{2\dot{m}_R^2}{7\rho^2}y^7 B_4(x) \\
&+ \frac{2}{3}s^2 y^4 C_0(x) - \left[\frac{2\dot{m}_R S}{\rho}y^4 + \frac{2}{5}s^2 y_5\right] C_1(x) \\
&+ \left[\frac{3}{2}\frac{\dot{m}_R^2}{\rho^2}y^4 + \frac{7\dot{m}_R s}{5\rho}y^5 + \frac{1}{10}s^2 y^6\right] C_2(x) \\
&- \left[\frac{6\dot{m}_R^2}{5\rho^2}y^5 + \frac{2\dot{m}_R s}{5\rho}y^6\right] C_3(x) + \frac{2\dot{m}_R^2}{5\rho^2}y^6 C_4(x)\Bigg\}
\end{aligned}
$$

where $m(x), n(x)$ are arbitrary functions of $x, l_\beta < x < L_\beta$, are to be determined by the boundary conditions (7.28b) and the coefficients $D(x), E(x), F(x), A_k(x), B_k(x)$, and $C_k(x)$ are given by

$$
\begin{aligned}
A_k(x) &= (k+2)d^{-k}(x)\left\{-\frac{6\zeta}{\rho}\dot{m}_R d^{-6}(x) + 3\zeta s d^{-5}(x)\right\} \\
B_k(x) &= (k+2)d^{-k}(x)\left\{\frac{6\zeta}{\rho}\dot{m}_R d^{-5}(x) - 4\zeta s d^{-4}(x)\right\} \\
D(x) &= \sum_1^3 k C_k^R d^{-k}(x)\left\{-\frac{6\dot{m}_R}{\rho}d^{-4}(x) + 3s d^{-3}(x)\right\} \\
E(x) &= \sum_1^3 k C_k^R d^{-k}(x)\left\{\frac{6\dot{m}_R}{\rho}d^{-3}(x) - 4s d^{-2}(x)\right\} \\
C_k(x) &= \zeta d^{-3}(x)(k+2)d^{-k}(x) \\
F(x) &= d^{-1}(x)\sum_1^3 k C_k^R d^{-k}(x)
\end{aligned}
$$

Once $m(x)$ and $n(x)$ are determined by the imposition of (7.28a), and the coefficients A_k, B_k, C_k, D, E_1 and F are substituted into the resulting expression, one may compute an upper bound for

$$
\max_{\substack{0\le y\le d(x)\\ l_\beta < x < L_\beta}} \left|\bar{\theta}_R^{(1)}(x,y) - \bar{\theta}_R^{(0)}(x,y)\right| \tag{7.29}
$$

and use it to gauge the error involved in not using the convective term in the computation of $\bar{\theta}_R^{(0)}(x,y)$.

(ii) If we let $\mathcal{D}_R = \{(x,y)|0 \leq y \leq d(x), l_\beta < x < L_\beta\}$, and for a function $f(x,y)$ defined on $\mathcal{D}_R$ use the average given by

$$\bar{f} = \frac{1}{\mathcal{A}_{\mathcal{D}_R}} \int_{l_\beta}^{L_\beta} \int_0^{d(x)} f(x,y) dx dy, \tag{7.30}$$

where $\mathcal{A}_{\mathcal{D}_R}$ is the area of $\mathcal{D}_R$, then we may compare directly the "averaged" values

$$\overline{\kappa \frac{\partial^2 \bar{\theta}^{(0)}}{\partial y^2}(x,y)} \quad \text{vs.} \quad \overline{\rho c_p \bar{u}_R(x,y) \frac{\partial \bar{\theta}_R^{(0)}}{\partial x}} \tag{7.31}$$

so as to gauge the relative importance of the conductive term which was retained in the computation of $\bar{\theta}_R^{(0)}$ as compared with the convective term which was deleted.

As the lubricating oil employed in shoe/roll configuration in the impulse drying process has a viscosity which is strongly temperature dependent, an important area for future research involves redoing the work in [4], and this current report, to allow for a dependence of the form $\mu = \mu(\theta)$. Although, in this case, the lubrication and heat transfer aspects of the problem are coupled together, it is possible to solve the problem in a parallel-walled channel, analytically, map the result back onto the convergent walled channel generated in [4] and then set up and solve, numerically, the equilibrium equations which determine ψ and b (see, e.g., (1.1)); the analog of (1.1) in this case would involve, with respect to the parameter space $\mathcal{P}$ (see, (1.2)) the thermal boundary conditions on the walls of the channel, κ, c_p, and the functional form of the viscosity μ.

Finally, in any future work it will be important to modify the boundary conditions (2.6) so as to allow heat conduction at the walls bounding the channel to depend on the temperature along these walls; in the simplest scenario these conditions would assume the form

$$\begin{cases} \dfrac{\partial \theta}{\partial y}(x,0) = k_0 \theta(x,0), \ -L_\beta < x < L_\beta \\ \dfrac{\partial \theta}{\partial y}(x,d(x)) = k_1 \theta(x,d(x)), -L_\beta < x < L_\beta \end{cases} \tag{7.32}$$

with k_0, k_1, constant, in reality, the boundary conditions (2.6) can only be maintained by imposing restrictions on the ambient environment external to the lubrication channel which have not been specified in this initial work on the heat transfer problem.

8 CONCLUSIONS

1. The results of this study indicate that under the conditions where the two boundaries are maintained at the same temperature, the viscous heat dissipation within the lubricant, due to viscous drag and inertial effects, plays a major roll in the net heat transfer. However, when the inner surface temperature is much greater than that of the shoe, the effect of viscous heat dissipation is reduced significantly.

2. For the conditions analyzed in this study, the regions under the solid part of the shoe, which are associated with a greater lubricant velocity, had a significant influence on the magnitude of the heat transfer from the oil to the roll; because of a greater lubricant thickness for the left-hand sub-channel, the dissipated heat, and net heat transfer under the solid part in the left-hand sub-channel was greater than that for the corresponding region in the right-hand sub-channel.

3. Numerical techniques such as finite difference or finite element analysis should be utilized to determine the thermal performance of the press roll subjected to a temperature dependent viscosity, and other types of boundary conditions. The temperature distributions predicted from such a model should be incorporated in a finite element model to determine the stress distribution within the roll coating for various design and operating conditions.

References

1. Oroff, D.I., Yearly Report for Department of Energy Contract FG0285CE40738, DOE/CE/40738-T6, U.S. Dept. of Energy, Washington, 1991.

2. Orloff, D.I., "Method and Apparatus for Drying Web", U.S.pat.5353521 (Oct. 11, 1994).

3. Orloff, D.I., Phelan, P.M., and Crouse, J.W., "Linerboard Drying on a Sheet-fed Pilot Impulse Drying Shoe Press", Tappi J., 78(1), 129-141 (1995).

4. Bloom, F., Hojjatie, B., and Orloff, D.I., "Modeling of Fluid Flow and Heat Transfer in a Crown Compensated Roll I: The Lubrication Problem", Report 8, Institute of Paper Science and Technology, 1994.

5. Schlichting, H., *Boundary Layer Theory*, McGraw-Hill, 1960.

6. Batchelor, G.K., *An Introduction to Fluid Dynamics*, Cambridge University Press, 1990.

7. Bassani, R., and Piccigallo, B., Hydrostatic lubrication, Elsevier, 1992.

8. Pinkus O., Thermal Aspects of Fluid Film Tribology, ASME Press, 1990.

9. Bird, R.B., Stewart W.E., Lightfoot, E.N.; Transport Phenomena; Wiley and Sons, pp. 780, 1960.

10. Thermal Effects in Externally Pressurized Conical Bearing with variable Viscosity, ASME Trans, J. of Tribology, 201-211, (110) 1988.

11. Braun, M., Mullen, R. and Hendricks, R.C., "An Analysis of Temperature Effect in a Finite Journal Bearing with Spatial Tilt and Viscous Dissipation", ASLE Trans., pp 405-412, Vol 27, no. 4, 1984.

Acknowledgements

The work reported here was supported by member companies of the IPST and by the U.S. Department of Energy, Office of Industrial Programs, through Grant No. DE-FG02-8SCE40738. Their support is gratefully acknowledged.

Appendix I: Nomenclature

Design Parameters

Φ - angular opening of the shoe

ϕ - $\frac{1}{2}\Phi$

w_{sh} - width of the shoe

n_c - number of capillaries on each side of the shoe

l_{sh} - length of the shaft of the shoe

$\hat{l} = \frac{1}{2} l_{sh}$

l^* - half-width of the confinement shaft

$\tilde{l}_{eff}$ - effective length of a capillary

$\tilde{R}_{eff}$ - effective radius of a capillary

w_{rec} - width of the inside of a recess

α_r - distance of the middle rib on the shaft of the shoe from the top of the shaft (measured to the middle of that rib)

β_r - distance that the middle rib protrudes beyond the neighboring ribs

R_s - radius of the shoe

R - radius of the roll

H_s - height of the shoe

$$\delta = \tan^{-1}\left(\frac{R_s - H_s}{\hat{l}}\right)$$

L_c - distance (measured along the bottom surface of the shoe) from the midpoint on the bottom surface to the beginning of the recess

L_{rec} - distance (measured along the bottom surface of the shoe) from the midpoint on the bottom surface to the end of the recess

$L_T = R_s \cdot \varphi$

Geometrical Parameters

ψ - angle between the center line through the shoe and the vertical direction

$(a, R+b)$ - location of the center of the circle that the arc forming the bottom surface of the shoe lies on

d_0 - depth of the lubrication channel along the line through $(a, R+b)$ and the point at the middle of the arc forming the bottom surface of the shoe

PV - location of the pivot point for the shoe along the wall of the confinement shaft

$m_{\mathcal{L}} = \cot(\varphi + \psi)$

$m_c = \cot\psi$

$m_R = \cot(\psi - \varphi)$

θ_1 - angle between the positive x-axis and the secant line (segment) joining the endpoints of the lubrication channel along its bottom wall (arc)

θ_2 - angle between the positive x-axis and the secant line (segment) joining the endpoints of the lubrication channel along its upper wall (arc)

$\beta = \theta_1 - \theta_2$ - angular deviation between the (secant) line segments forming the upper and lower walls of the approximating lubrication channel (wedge)

$(d_R(x) = d_0 - x\tan\beta)$ - thickness of the approximating lubrication channel (wedge) x units to the right of the middle of that channel

$(d_{\mathcal{L}}(x) = d_0 + x\tan\beta)$ - thickness of the approximating lubrication channel (wedge) x units to the left of the middle of that channel

$d(x) = d_0 - x\tan\beta, -L_\beta \le x \le L_\beta$, - thickness of the approximating lubrication channel (wedge) at any x in the interval $[-L_\beta, L_\beta]$

$l_c = L_c\cos\beta$

$l_\beta = L_{rec}\cos\beta$

$L_\beta = L_T\cos\beta$

$d_R(l_\beta)$ - trailing edge thickness in the approximating lubrication channel (wedge)

$d_{\mathcal{L}}(l_\beta)$ - leading edge thickness in the approximating lubrication channel (wedge)

$$\lambda_R = \frac{d_R(l_\beta)d_R(L_\beta)}{d_R(l_\beta) + d_R(L_\beta)}$$

$$\delta_R = \frac{d_R^2(l_\beta)d_R^2(L_\beta)}{d_R^2(l_\beta) - d_R^2(L_\beta)}$$

$$\lambda_{\mathcal{L}} = \frac{d_{\mathcal{L}}(l_\beta)d_{\mathcal{L}}(L_\beta)}{d_{\mathcal{L}}(l_\beta) + d_{\mathcal{L}}(L_\beta)}$$

$$\delta_{\mathcal{L}} = \frac{d_{\mathcal{L}}^2(l_\beta)d_{\mathcal{L}}^2(L_\beta)}{d_{\mathcal{L}}^2(l_\beta) - d_{\mathcal{L}}^2(L_\beta)}$$

Physical Parameters

μ - viscosity of the lubricant (at a given temperature)

ρ - density of the lubricant (at a given temperature)

κ - thermal conductivity of the lubricating oil (at a given temperature)

c - heat capacitance of the lubricating oil (at a given temperature)

Ψ - viscous energy dissipation

T_1 - constant temperature along the lower wall of the lubrication channel (inside surface of the roll)

T_0 - constant temperature along the upper wall of the lubrication channel (bottom surface of the shoe)

$$\left.\begin{aligned} b(x,y) &= -\rho c u(x,y) \\ f(x,y;\mu) &= -\mu\left(\frac{\partial u}{\partial y}\right)^2 \end{aligned}\right\} \text{ with}$$

$u = u(x,y)$ - velocity field at any point (x,y) in the channel

$$\mathcal{A}(x,y) = \left(\frac{\partial u(x,y)}{\partial y}\right)^2$$

$\zeta = -\mu/\kappa$

s - (tangential) roll speed

F - load applied to the top of the shaft of the shoe

$\tilde{p}_R$ - pressure in the right-hand recesses

$\tilde{p}_{\mathcal{L}}$ - pressure in the left-hand recesses

p_{sh} - pressure exerted at the top of the shaft of the shoe

$p_{exit}(\equiv p_{atm})$ - exit pressure of the lubricant at the left and right-hand ends of the lubrication channel

Velocity and Temperature Fields (from the point of view of a single observer who looks at the lubrication channel from left to right):

$\bar{u}_R(x,y)$ - velocity field in the (approximate) right-hand sub-channel, $l_\beta \leq x \leq L_\beta$

$\bar{u}_{\mathcal{L}}(x,y)$ - velocity field in the (approximate) left-hand sub-channel, $-L_\beta \leq x \leq -l_\beta$

$\tilde{u}_R(x,y)$ - velocity field in the right-hand sub-channel beneath the recesses ($l_c \leq x \leq l_\beta$)

$\tilde{u}_{\mathcal{L}}(x,y)$ - velocity field in the left-hand sub-channel beneath the recesses ($-l_\beta \leq x \leq -l_c$)

$u^c(x,y)$ - velocity field in the center channel, $-l_c \leq x \leq l_c$

$\bar{\theta}_R(x,y)$ - temperature field in the (approximate) right-hand sub-channel, $l_\beta \leq x \leq L_\beta$

$\bar{\theta}_{\mathcal{L}}(x,y)$ - temperature field in the (approximate) left-hand sub-channel, $-L_\beta \leq x \leq -l_\beta$

$\tilde{\theta}_R(x,y)$ - temperature field in the right-hand sub-channel beneath the recesses ($l_c \leq x \leq l_\beta$)

$\tilde{\theta}_{\mathcal{L}}(x,y)$ - temperature field in the left-hand sub-channel beneath the recesses ($-l_\beta \leq x \leq -l_c$)

$\theta_c(x,y)$ - temperature field in the center channel, $-l_c \leq x \leq l_c$

$\dot{m}_R$- mass flow rate/unit depth in the right-hand channel

$\dot{m}_{\mathcal{L}}$ - mass flow rate/unit depth in the left-hand channel

$\tilde{q}^R_{r\to 0}$ - heat flow per unit width (in the cross-direction) per unit time (from the roll to the oil) in the right-hand subchannel, $l_\beta \le x \le L_\beta$

$\tilde{q}^{\mathcal{L}}_{r\to 0}$ - heat flow per unit width (in the cross-direction) per unit time (from the roll to the oil) in the left-hand subchannel, $-L_\beta \le x \le -l_\beta$

$\tilde{q}^R_{r\to 0}$ - heat flow per unit width (in the cross-direction) per unit time (from the roll to the oil) in the right-hand subchannel beneath the recesses ($l_c \le x \le l_\beta$)

$\tilde{q}^{\mathcal{L}}_{r\to 0}$ - heat flow per unit width (in the cross-direction) per unit time (from the roll to the oil) in the left-hand subchannel beneath the recesses ($-l_\beta \le x \le -l_c$)

$q^c_{r\to 0}$ - heat flow per unit width (in the cross-direction) per unit time (from the roll to the oil) in the center channel, $-l_c \le x \le l_c$

$Q_{r\to 0}$ - net heat flow per unit width (in the cross-direction) per unit time from the roll to the oil in the lubrication channel

$\tilde{q}^R_{0\to sh}$ - heat flow per unit width (in the cross-direction) per unit time (from the oil to the shoe) in the right-hand subchannel, $l_\beta \le x \le L_\beta$
$\tilde{q}^{\mathcal{L}}_{0\to sh}$ - heat flow per unit width (in the cross-direction) per unit time (from the oil to the shoe) in the left-hand subchannel, $-L_\beta \le x \le -l_\beta$

$\tilde{q}^R_{0\to sh}$ - heat flow per unit width (in the cross-direction) per unit time (from the oil to the shoe) in the right-hand subchannel beneath the recesses ($l_c \le x \le l_\beta$)

$\tilde{q}^{\mathcal{L}}_{0\to sh}$ - heat flow per unit width (in the cross-direction) per unit time (from the oil to the shoe) in the left-hand subchannel beneath the recesses ($-l_\beta \le x \le -l_c$)

$q^c_{0\to sh}$ - heat flow per unit width (in the cross-direction) per unit time (from the oil to the shoe) in the center channel, $-l_c \le x \le l_c$

$Q_{0\to sh}$ - net heat flow per unit width (in the cross-direction) per unit time from the oil to the shoe in the lubrication channel

$Q^v_f = (Q_{0\to sh} - Q_{r\to 0})$ - viscous heating of the lubricating oil per unit width (in the cross-direction) per unit time

Appendix II: Velocity Fields and Mass Flow Rates

(V1) $$\bar{u}_R(x,y) = -\frac{6\dot{m}_R}{\rho}y^2 d^{-3}(x) + \left[\frac{6\dot{m}_R}{\rho}y + 3sy^2\right] d^{-2}(x) - 4syd^{-1}(x) + s,$$
$$0 \le y \le d(x), l_\beta < x < L_\beta$$

(V2) $$\bar{u}_\mathcal{L}(x,y) = \frac{6\dot{m}_\mathcal{L}}{\rho}y^2 d^{-3}(x) - \left[\frac{6\dot{m}_\mathcal{L}}{\rho}y - 3sy^2\right] d^{-2}(x) - 4syd^{-1}(x) + s,$$
$$0 \le y \le d(x),\ -L_\beta < x < -l_\beta$$

(V3) $$\tilde{u}_R(x,y) = s(1 - yd^{-1}(x)), 0 \le y \le d(x),\ l_c < x < l_\beta$$
(V4) $$\tilde{u}_\mathcal{L}(x,y) = s(1 - yd^{-1}(x)), 0 \le y \le d(x),\ -l_\beta < x < -l_c$$

(V5) $$u_c(x,y) = \left(\frac{\tilde{p}_\mathcal{L} - \tilde{p}_R}{4\mu l_c}\right) y(d(x) - y) + s(1 - yd^{-1}(x)), 0 \le y \le d(x), -l_c < x < l_c$$

(m1) $$\frac{\dot{m}_R}{\rho} = \frac{(p_{sh} - p_{atm}) + \dfrac{6\mu s}{\tan\beta}\left(\dfrac{\lambda_R}{\delta_R}\right)}{\left[\dfrac{6\mu}{\tan\beta \cdot \delta_R} + \left(\dfrac{w_{sh}}{n_c}\right)\dfrac{8\mu\tilde{l}_{eff}}{\pi\tilde{R}^4_{eff}}\right]}$$

(m2) $$\frac{\dot{m}_\mathcal{L}}{\rho} = \frac{(p_{sh} - p_{atm}) + \dfrac{6\mu s}{\tan\beta}\left(\dfrac{\lambda_\mathcal{L}}{\delta_\mathcal{L}}\right)}{\left[\dfrac{6\mu}{\tan\beta \cdot \delta_\mathcal{L}} - \left(\dfrac{w_{sh}}{n_c}\right)\dfrac{8\mu\tilde{l}_{eff}}{\pi\tilde{R}^4_{eff}}\right]}$$

Appendix III: Technical Summary

In this technical summary we will write $d(x) \equiv d_R(x) = d_0 - x\tan\beta, -L_\beta \le x \le L_\beta$.

(S1) $$\bar{\theta}_R(x,y) = \zeta d^{-2}(x)\sum_{k=0}^{4}\bar{p}_k^R(y)d^{-k}(x) + \sum_{k=1}^{3}c_k^R d^{-k}(x)y + T_1, l_\beta < x < L_\beta$$

(S2) $$\begin{cases} \bar{p}_4^R(y) &= \dfrac{12\dot{m}_R^2}{\rho^2}y^4 \\ \bar{p}_3^R(y) &= -\left[\dfrac{24\dot{m}_R^2}{\rho^2}y^3 + \dfrac{12\dot{m}_R}{\rho}sy^4\right] \\ \bar{p}_2^R(y) &= \dfrac{18\dot{m}_R^2}{\rho^2}y^2 + \dfrac{28\dot{m}_R s}{\rho}y^3 + 3s^2y^4 \\ \bar{p}_1^R(y) &= -\left[\dfrac{24\dot{m}_R s}{\rho}y^2 + 8s^2y^3\right] \\ \bar{p}_0^R(y) &= 8s^2y^2 \end{cases}$$

(S3) $$\begin{cases} c_1^R &= (T_0 - T_1) - 3\zeta s^2 \\ c_2^R &= \dfrac{8\zeta\dot{m}_R s}{\rho} \\ c_3^R &= \dfrac{-6\zeta\dot{m}_R^2}{\rho^2} \end{cases}$$

(S4) $$\bar{\theta}_{\mathcal{L}}(x,y) = \zeta d^{-2}(x)\sum_{k=0}^{4}\bar{p}_k^{\mathcal{L}}(y)d^{-k}(x) + \sum_{k=1}^{3}c_k^{\mathcal{L}}d^{-k}(x)y + T_1, -L_\beta < x < -l_\beta$$

$$\text{(S5)}\quad \begin{cases} \bar{p}_4^{\mathcal{L}}(y) &= 12\left(\dfrac{\dot{m}_{\mathcal{L}}}{\rho}\right)^2 y^4 \\ \bar{p}_3^{\mathcal{L}}(y) &= -\left[24\left(\dfrac{\dot{m}_{\mathcal{L}}}{\rho}\right)^2 y^3 - 12\left(\dfrac{\dot{m}_{\mathcal{L}}}{\rho}\right) s y^4\right] \\ \bar{p}_2^{\mathcal{L}}(y) &= 18\left(\dfrac{\dot{m}_{\mathcal{L}}}{\rho}\right)^2 y^2 - 28\left(\dfrac{\dot{m}_{\mathcal{L}}}{\rho}\right) s y^3 + 3s^2 y^4 \\ \bar{p}_1^{\mathcal{L}}(y) &= 24\left(\dfrac{\dot{m}_{\mathcal{L}}}{\rho}\right) s y^2 - 8s^2 y^3 \\ \bar{p}_0^{\mathcal{L}}(y) &= 8s^2 y^2 \end{cases}$$

$$\text{(S6)}\quad \begin{cases} c_1^{\mathcal{L}} = (T_0 - T_1) - 3\zeta s^2 \\ c_2^{\mathcal{L}} = -8\zeta\left(\dfrac{\dot{m}_{\mathcal{L}}}{\rho}\right) s \\ c_3^{\mathcal{L}} = -6\zeta\left(\dfrac{\dot{m}_{\mathcal{L}}}{\rho}\right)^2 \end{cases}$$

$$\text{(S7)}\quad \theta_c(x,y) = \zeta \sum_{k=-2}^{2} p_k^c(y) d^k(x) + (T_0 - T_1) d^{-1}(x) y + T_1 - \zeta \theta_c(x) y, -l_c < x < l_c$$

$$\text{(S8)}\quad \begin{cases} \theta_c(x) = \frac{1}{6}\Gamma_c^2 d^3(x) - \frac{1}{3}\Gamma_c s d(x) + \frac{1}{2} s^2 d^{-1}(x) \\ \Gamma_c = \dfrac{\tilde{p}_{\mathcal{L}} - \tilde{p}_R}{4\mu l_c} \end{cases}$$

$$\text{(S9)}\quad \begin{cases} p_2^c(y) = \frac{1}{2}\Gamma_c^2 y^2 \\ p_1^c(y) = -\frac{2}{3}\Gamma_c^2 y^3 \\ p_0^c(y) = \frac{1}{3}\Gamma_c^2 y^4 - \Gamma_c s y^2 \\ p_{-1}^c(y) = \frac{2}{3}\Gamma_c s y^3 \\ p_{-2}^c(y) = \frac{1}{2} s^2 y^2 \end{cases}$$

(S10) $$\tilde{\theta}_R(x,y) = \frac{\zeta}{2}s^2y^2d^{-2}(x) + [(T_0 - T_1) - \frac{1}{2}\zeta s^2]yd^{-1}(x) + T_1, l_c < x < l_\beta$$

(S11) $$\tilde{\theta}_{\mathcal{L}}(x,y) = \frac{\zeta}{2}s^2y^2d^{-2}(x) + [(T_0 - T_1) - \frac{1}{2}\zeta s^2]yd^{-1}(x) + T_1, -l_\beta < x < -l_c$$

(S12) $$\tilde{q}^R_{r\to 0} = \frac{\kappa[(T_0 - T_1) - 3\zeta s^2]}{\tan\beta}\ln\left[\frac{d(L_\beta)}{d(l_\beta)}\right] - \frac{8\kappa\zeta\dot{m}_R s}{\rho\tan\beta}\left[\frac{1}{d(L_\beta)} - \frac{1}{d(l_\beta)}\right] + \frac{3\kappa\zeta\dot{m}_R^2}{\rho^2\tan\beta}\left[\frac{1}{d^2(L_\beta)} - \frac{1}{d^2(l_\beta)}\right]$$

(S13) $$\tilde{q}^R_{\kappa\to 0} = \frac{\kappa[(T_0 - T_1) - \frac{1}{2}\zeta s^2]}{\tan\beta}\ln\left[\frac{d(l_\beta)}{d(l_c)}\right]$$

(S14) $$q^c_{r\to 0} = \frac{\kappa[(T_0 - T_1) - \frac{1}{2}\zeta s^2]}{\tan\beta}\ln\left[\frac{d(l_c)}{d(-l_c)}\right] - \frac{\zeta\kappa\Gamma_c^2}{24\tan\beta}[d^4(l_c) - d^4(-l_c)] + \frac{\zeta\kappa}{6}\cdot\frac{\Gamma_c s}{\tan\beta}[d^2(l_c) - d^2(-l_c)]$$

(S15) $$\tilde{q}^{\mathcal{L}}_{r\to 0} = \frac{\kappa[(T_0 - T_1) - \frac{1}{2}\zeta s^2]}{\tan\beta}\ln\left[\frac{d(-l_c)}{d(-l_\beta)}\right]$$

(S16) $$\tilde{q}^{\mathcal{L}}_{r\to 0} = \frac{\kappa[(T_0 - T_1) - 3\zeta s^2]}{\tan\beta}\ln\left[\frac{d(-l_\beta)}{d(-L_\beta)}\right] + \frac{8\kappa\zeta\dot{m}_{\mathcal{L}} s}{\rho\tan\beta}\left[\frac{1}{d(-l_\beta)} - \frac{1}{d(-L_\beta)}\right] + \frac{3\kappa\zeta}{\tan\beta}\left(\frac{\dot{m}_{\mathcal{L}}}{\rho}\right)^2\left[\frac{1}{d^2(-l_\beta)} - \frac{1}{d^2(-L_\beta)}\right]$$

$$(S17)\quad Q_{r\to 0} = \frac{\kappa[(T_0-T_1)-3\zeta s^2]}{\tan\beta}\ln\left[\frac{d(L_\beta)}{d(-L_\beta)}\right] + \frac{5}{2}\cdot\frac{\kappa|\zeta|s^2}{\tan\beta}\ln\left[\frac{d(-l_\beta)}{d(l_\beta)}\right]$$
$$+\frac{8\kappa|\zeta|s}{\rho\tan\beta}\left(\dot m_R\left[\frac{1}{d(L_\beta)}-\frac{1}{d(l_\beta)}\right]-\dot m_{\mathcal{L}}\left[\frac{1}{d(-l_\beta)}-\frac{1}{d(-L_\beta)}\right]\right)$$
$$+\frac{3\kappa\zeta}{\rho^2\tan\beta}\left(\dot m_R^2\left[\frac{1}{d^2(L_\beta)}-\frac{1}{d^2(l_\beta)}\right]+\dot m_{\mathcal{L}}^2\left[\frac{1}{d^2(-l_\beta)}-\frac{1}{d^2(-L_\beta)}\right]\right)$$
$$+\frac{\kappa|\zeta|\Gamma_c^2}{24\tan\beta}[d^4(l_c)-d^4(-l_c)]+\frac{\kappa\zeta\Gamma_c s}{6\tan\beta}[d^2(l_c)-d^2(-l_c)]$$

$$(S18)\quad \bar q^R_{0\to sh} = \frac{3\zeta\kappa\dot m_R^2}{\rho^2\tan\beta}\left[\frac{1}{d^2(l_\beta)}-\frac{1}{d^2(L_\beta)}\right]+\frac{4\zeta\kappa\dot m_R s}{\rho\tan\beta}\left[\frac{1}{d(L_\beta)}-\frac{1}{d(l_\beta)}\right]$$
$$+\frac{\kappa(\zeta s^2+(T_0-T_1))}{\tan\beta}\ln\left[\frac{d(L_\beta)}{d(l_\beta)}\right]$$

$$(S19)\quad \tilde q^R_{0\to sh} = \frac{\kappa[(T_0-T_1)+\frac{1}{2}\zeta s^2]}{\tan\beta}\ln\left[\frac{d(l_\beta)}{d(l_c)}\right]$$

$$(S20)\quad q^c_{0\to sh} = \frac{\kappa[(T_0-T_1)+\frac{1}{2}\zeta s^2]}{\tan\beta}\ln\left[\frac{d(l_c)}{d(-l_c)}\right]+\frac{\zeta\kappa\Gamma_c s}{6\tan\beta}[d^2(l_c)-d^2(-l_c)]$$
$$+\frac{\zeta\kappa\Gamma_c^2}{24\tan\beta}[d^4(l_c)-d^4(-l_c)]$$

$$(S21)\quad \tilde q^{\mathcal{L}}_{0\to sh} = \frac{\kappa[(T_0-T_1)+\frac{1}{2}\zeta s^2]}{\tan\beta}\ln\left[\frac{d(-l_c)}{d(-l_\beta)}\right]$$

$$(S22)\quad \bar q^{\mathcal{L}}_{0\to sh} = \frac{\kappa[\zeta s^2+(T_0-T_1)]}{\tan\beta}\ln\left[\frac{d(-l_\beta)}{d(-L_\beta)}\right]-\frac{4\zeta\kappa s}{\tan\beta}\cdot\frac{\dot m_{\mathcal{L}}}{\rho}\left[\frac{1}{d(-l_\beta)}-\frac{1}{d(-L_\beta)}\right]$$
$$-\frac{3\zeta\kappa}{\tan\beta}\left(\frac{\dot m_{\mathcal{L}}}{\rho}\right)^2\left[\frac{1}{d^2(-l_\beta)}-\frac{1}{d^2(-L_\beta)}\right]$$

$$(S23)\quad Q_{0\to sh} = \frac{\kappa[(T_0-T_1)+\zeta s^2]}{\tan\beta}\ln\left[\frac{d(L_\beta)}{d(-L_\beta)}\right]+\frac{1}{2}\frac{\kappa\zeta s^2}{\tan\beta}\ln\left[\frac{d(-l_\beta)}{d(l_\beta)}\right]$$
$$+\frac{4\zeta\kappa s}{\rho\tan\beta}\left(\dot m_R\left[\frac{1}{d(L_\beta)}-\frac{1}{d(l_\beta)}\right]-\dot m_{\mathcal{L}}\left[\frac{1}{d(-l_\beta)}-\frac{1}{d(-L_\beta)}\right]\right)$$
$$+\frac{3|\zeta|\kappa}{\rho^2\tan\beta}\left(\dot m_R^2\left[\frac{1}{d^2(L_\beta)}-\frac{1}{d^2(l_\beta)}\right]+\dot m_{\mathcal{L}}^2\left[\frac{1}{d^2(-l_\beta)}-\frac{1}{d^2(-L_\beta)}\right]\right)$$

$$+\frac{\zeta\kappa\Gamma_c s}{6\tan\beta}[d^2(l_c)-d^2(-l_c)]+\frac{\zeta\kappa\Gamma_c^2}{24\tan\beta}[d^4(l_c)-d^4(-l_c)]$$

$$\text{(S24)}\quad Q_f^v=\frac{3\kappa|\zeta|s^2}{\tan\beta}\ln\left[\frac{d(-l_\beta)}{d(l_\beta)}\right]+\frac{12\kappa|\zeta|s}{\rho\tan\beta}\left(\dot m_R\left[\frac{1}{d(L_\beta)}-\frac{1}{d(l_\beta)}\right]-\dot m_{\mathcal L}\left[\frac{1}{d(-l_\beta)}-\frac{1}{d(-L_\beta)}\right]\right)$$
$$-\frac{6\kappa|\zeta|}{\rho^2\tan\beta}\left(\dot m_R^2\left[\frac{1}{d^2(L_\beta)}-\frac{1}{d^2(l_\beta)}\right]+\dot m_{\mathcal L}^2\left[\frac{1}{d^2(-l_\beta)}-\frac{1}{d^2(-L_\beta)}\right]\right)$$
$$+\frac{|\zeta|\kappa\Gamma_c^2}{12\tan\beta}[d^4(l_c)-d^4(-l_c)]$$

$$\text{(S25)}\quad \lim_{\beta\to0}Q_{r\to0}=\frac{\kappa[T_1-T_0]}{d_0}L_T-\frac{\kappa|\zeta|s^2}{2d_0}(6L_t-5L_{rec})+\frac{8\kappa|\zeta|s}{\rho d_0^2}(L_T-L_{rec})(\dot m_R-\dot m_{\mathcal L})$$
$$-\frac{6\kappa|\zeta|}{\rho^2d_0^3}(L_T-L_{rec})(\dot m_R^2+\dot m_{\mathcal L}^2)-\frac{\kappa|\zeta|}{48\mu^2}(\tilde p_{\mathcal L}-\tilde p_R)^2\cdot\frac{d_0^3}{L_c}-\frac{\kappa|\zeta|}{6\mu}(\tilde p_R-\tilde p_{\mathcal L})\cdot d_0\cdot s$$

Remarks In all the expressions in (S25), above, $\dot m_R, \dot m_{\mathcal L}, \tilde p_{\mathcal L}$ and $\tilde p_R$ are to be evaluated in the limit as $\beta\to0$.

$$\text{(S26)}\quad \lim_{\beta\to0}Q_{0\to sh}=\frac{\kappa[T_1-T_0]}{d_0}L_T+\frac{\kappa|\zeta|s^2}{2d_0}(2L_T-L_{rec})-\frac{4\kappa|\zeta|s}{\rho d_0^2}(L_T-L_{rec})(\dot m_R-\dot m_{\mathcal L})$$
$$+\frac{6|\zeta|\kappa}{\rho^2d_0^3}(L_T-L_{rec})(\dot m_R^2+\dot m_{\mathcal L}^2)-\frac{1}{6}\frac{|\zeta|\kappa s}{\mu}(\tilde p_R-\tilde p_{\mathcal L})d_0+\frac{1}{48}\frac{|\zeta|\kappa}{\mu^2}(\tilde p_{\mathcal L}-\tilde p_R)^2\cdot\frac{d_0^3}{L_c}$$

In (S26) $\tilde p_R, \dot m_R, \tilde p_{\mathcal L}$, and $\dot m_{\mathcal L}$ are taken in the limit as $\beta\to0$.

$$\text{(S27)}\quad \lim_{\beta\to0}Q_f^v=\frac{\kappa|\zeta|s^2}{d_0}[4L_T-3L_{rec}]-\frac{12\kappa|\zeta|s}{\rho d_0^2}(L_T-L_{rec})(\dot m_R-\dot m_{\mathcal L})$$
$$+\frac{12\kappa|\zeta|}{\rho^2d_0^3}(L_T-L_{rec})(\dot m_R^2+\dot m_{\mathcal L}^2)+\frac{\kappa|\zeta|}{48\mu^2L_c}(\tilde p_{\mathcal L}-\tilde p_R)^2d_0^3$$

In (S27), $\tilde p_R, \dot m_R, \tilde p_{\mathcal L}$ and $\dot m_{\mathcal L}$ are to be evaluated in the limit as $\beta\to0$.

$$\text{(S28)}\quad \lim_{\beta\to0}Q_f^v|_{s=0}=\frac{24\kappa|\zeta|\dot m^2}{\rho^2d_0^2}(L_T-L_{rec})$$
where $\tilde p_R=\tilde p_{\mathcal L}$ for $s=0$ and $\dot m_R=\dot m_{\mathcal L}=\dot m$.

$$\text{(S29)}\quad\begin{cases}\bar\Theta_R(\bar x,\bar y)=\Theta_R(\bar x,d(\bar x)\bar y);\ \bar x=x,\bar y=y/d(x)\\ \Theta_R(x,y)=\theta_R(x,y)-\left[\dfrac{y}{d(x)}(T_0-T_1)+T_1\right]\end{cases}$$

$$\text{(S30)}\quad \kappa\left(\frac{\partial^2\bar{\Theta}_R}{\alpha\bar{x}^2}+\frac{1}{d_0^2}\frac{\partial^2\bar{\Theta}_R}{\partial\bar{y}^2}\right)+\bar{b}_R(\bar{x},\bar{y})\frac{\partial\bar{\Theta}_R}{\partial\bar{x}}=\bar{g}_R(\bar{x},\bar{y};\mu)$$

$$\text{on } \bar{D}=\{(\bar{x},\bar{y})|l_\beta\le\bar{x}\le L_\beta;\ 0\le\bar{y}\le 1\}$$

$$\text{(S31)}\quad \begin{cases}\bar{g}_R(\bar{x},\bar{y};\mu)=g_R(\bar{x},d(\bar{x})\bar{y};\mu)\\ \bar{b}_R(\bar{x},\bar{y})=b_R(\bar{x},d(\bar{x})\bar{y})\end{cases}$$

with

$$\text{(S32)}\quad g_R(x,y;\mu)=f_R(x,y;\mu)+\frac{2\kappa(T_1-T_0)\tan^2\beta\cdot y}{d^3(x)}+\frac{(T_1-T_0)\tan\beta\cdot y\cdot b_R(x,y)}{d^2(x)}$$

$$\text{(S33)}\quad \bar{\Theta}_R(\bar{x},0)=0,\bar{\Theta}_R(\bar{x},1)=0,l_\beta\le x\le L_\beta$$

$$\text{(S34)}\quad \begin{cases}\bar{\Theta}_R(L_\beta,\bar{y})=\alpha(d(L_\beta)\bar{y})-\bar{y}(T_0-T_1)-T_1,0\le\bar{y}\le 1\\ \alpha(d(L_\beta)\bar{y})=\theta(L_\beta,d(L_\beta)\bar{y})\end{cases}$$

$$\text{(S35)}\quad \begin{cases}\bar{\Theta}_R(l_\beta,\bar{y})=\beta(d(l_\beta)\bar{y})-\bar{y}(T_0-T_1)-T_1\\ \beta(d(l_\beta)\bar{y})=\theta_R(l_\beta,d(-L_\beta)\bar{y})\end{cases}$$

Appendix IV: Figures

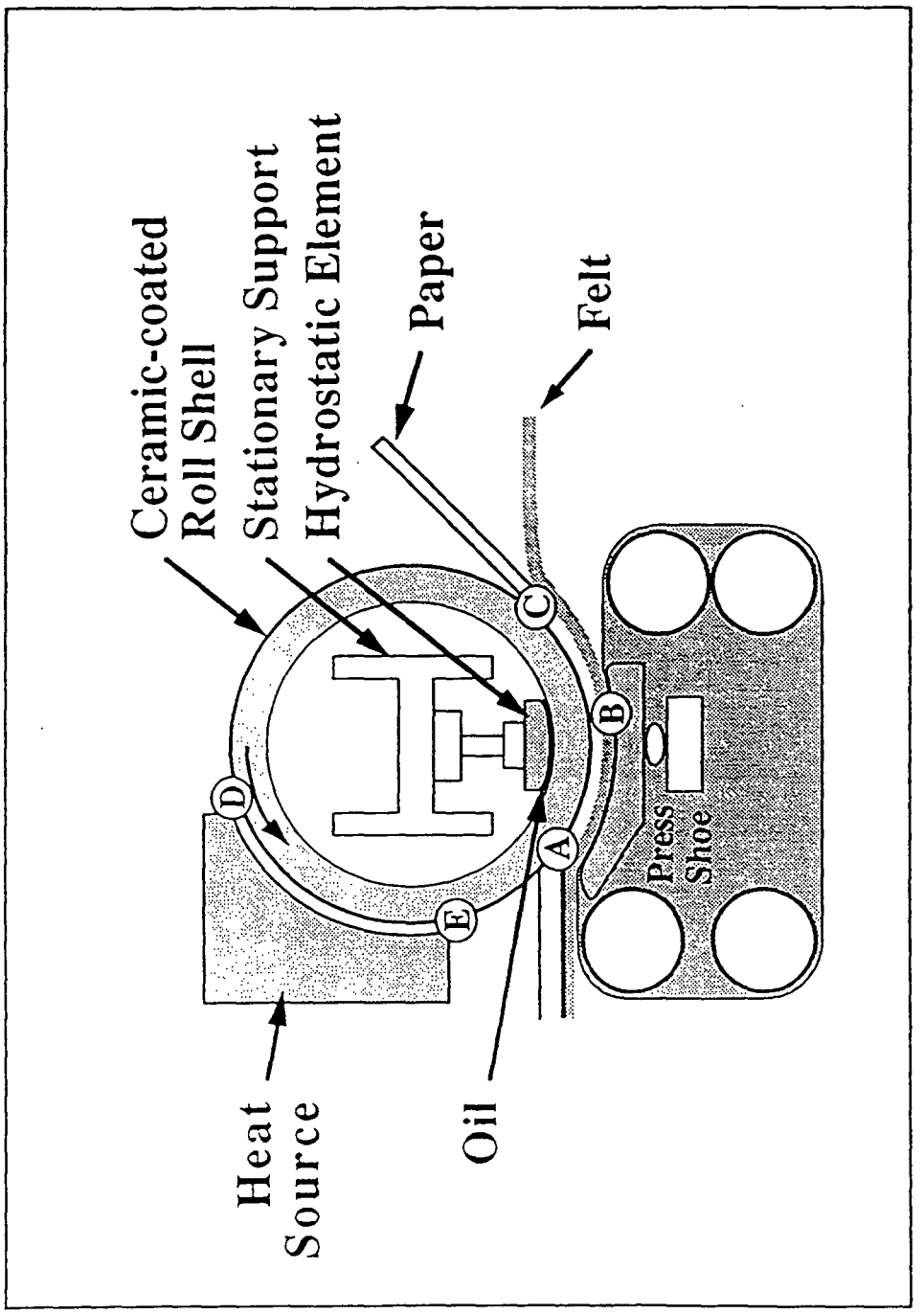

Figure 1 . The Crown Compensated Impulse Drying Press Roll (not shown to scale).

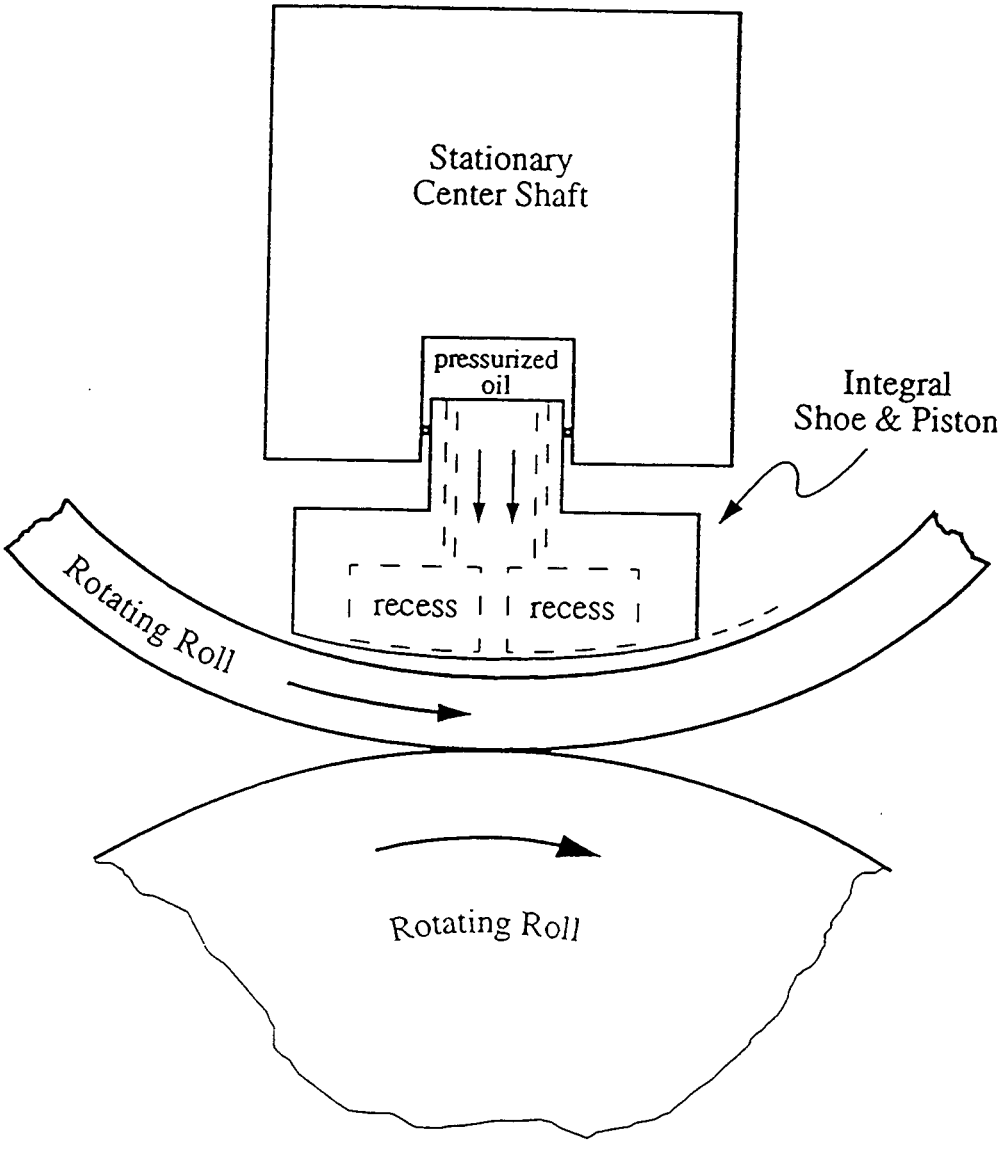

Figure 2. Cross sectional view of the shoe and the rotating shell.

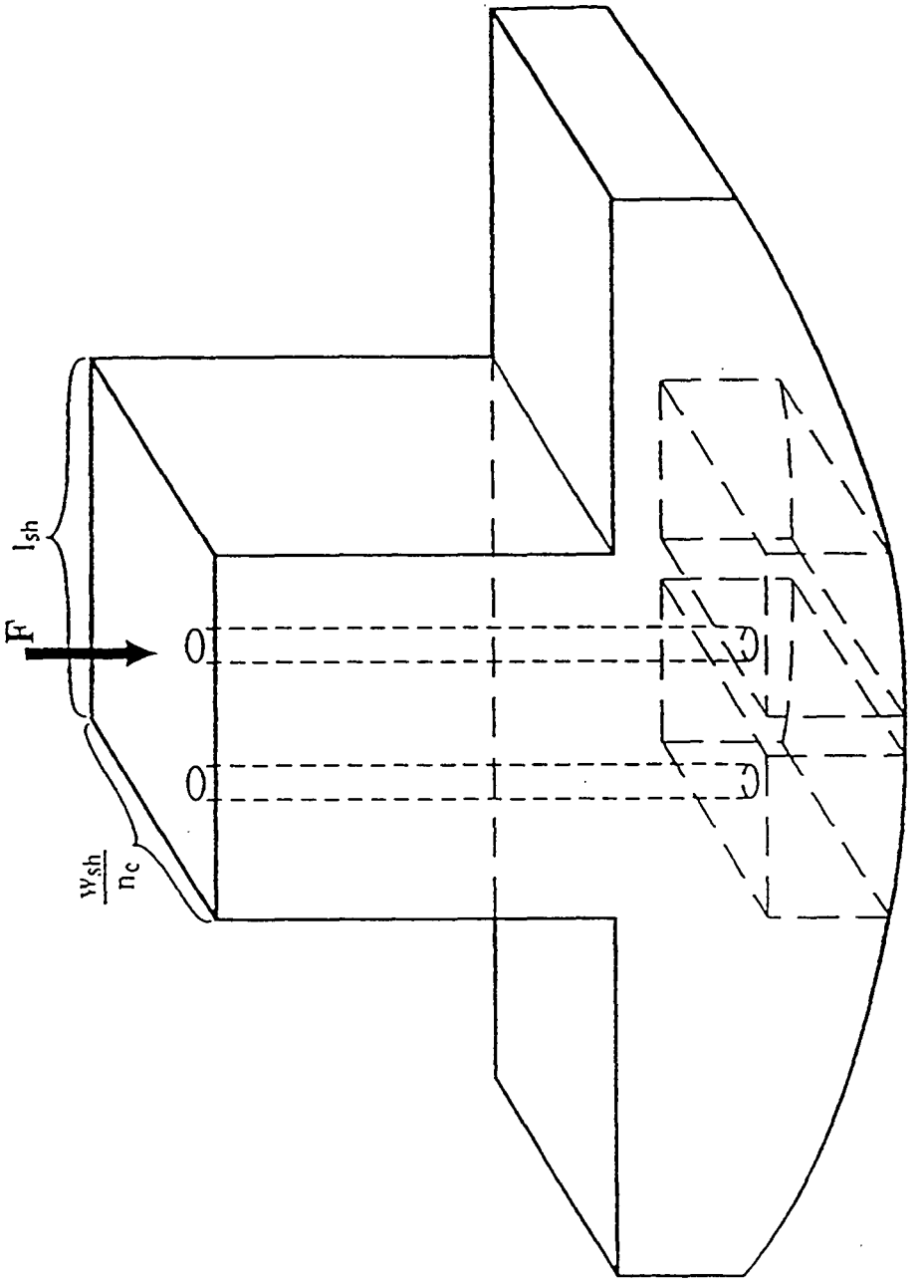

Figure 3. Shoe cross section depicting capillaries entering the recesses (not shown to scale).

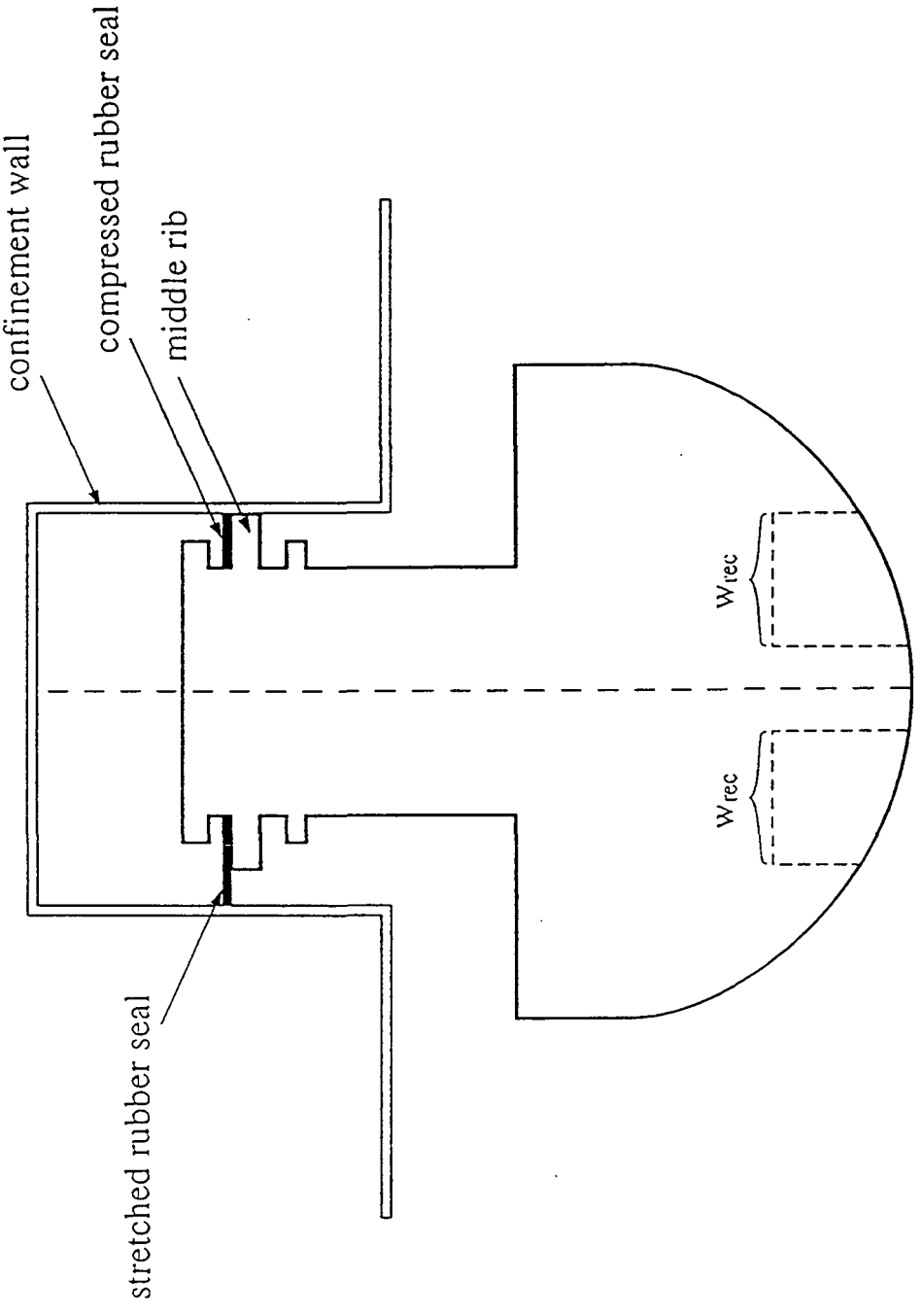

Figure 4. Contact between the shaft of the hydrostatic shoe and the wall of the confinement.

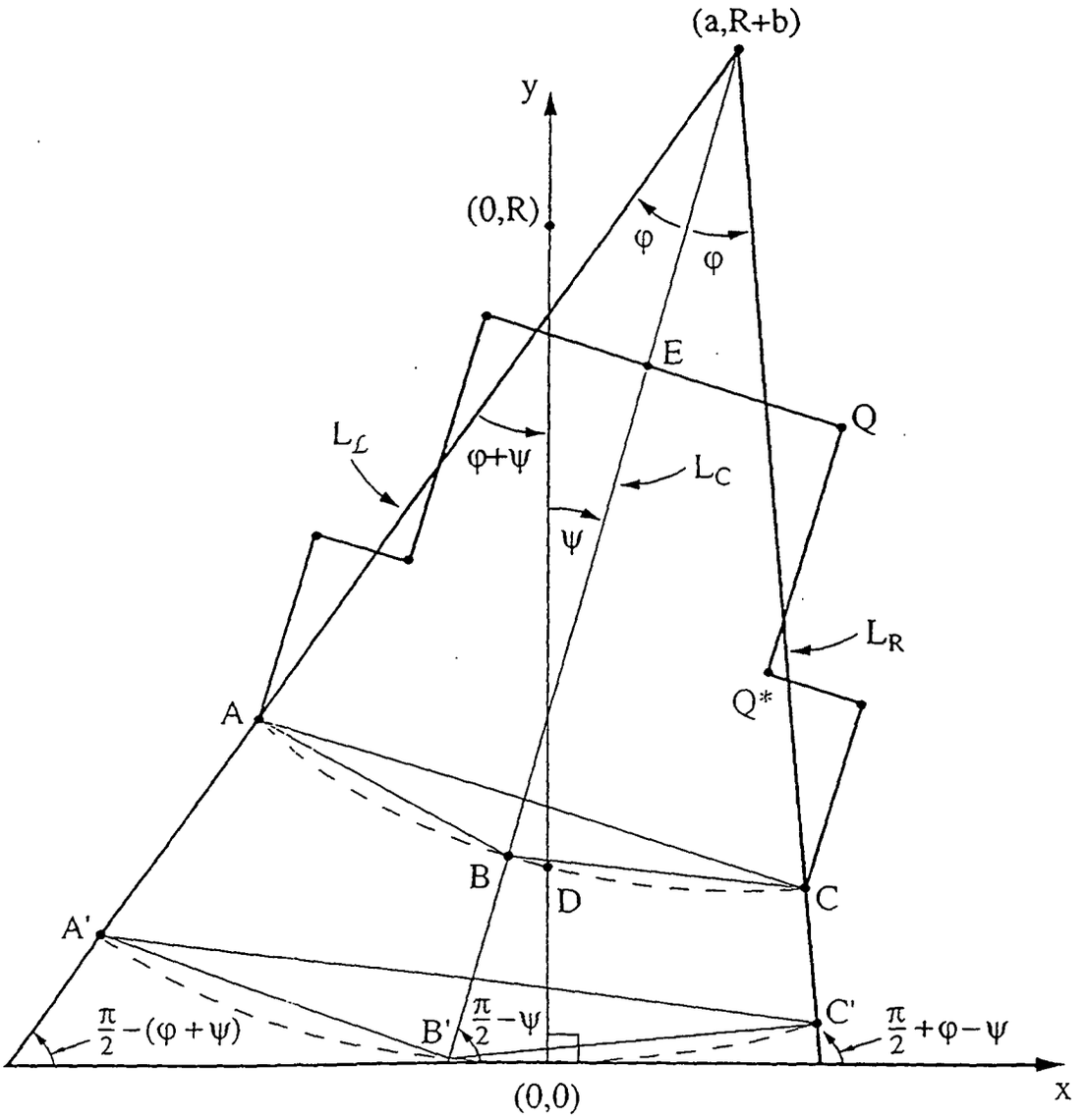

Figure 5. Motion of the hydrostatic shoe.

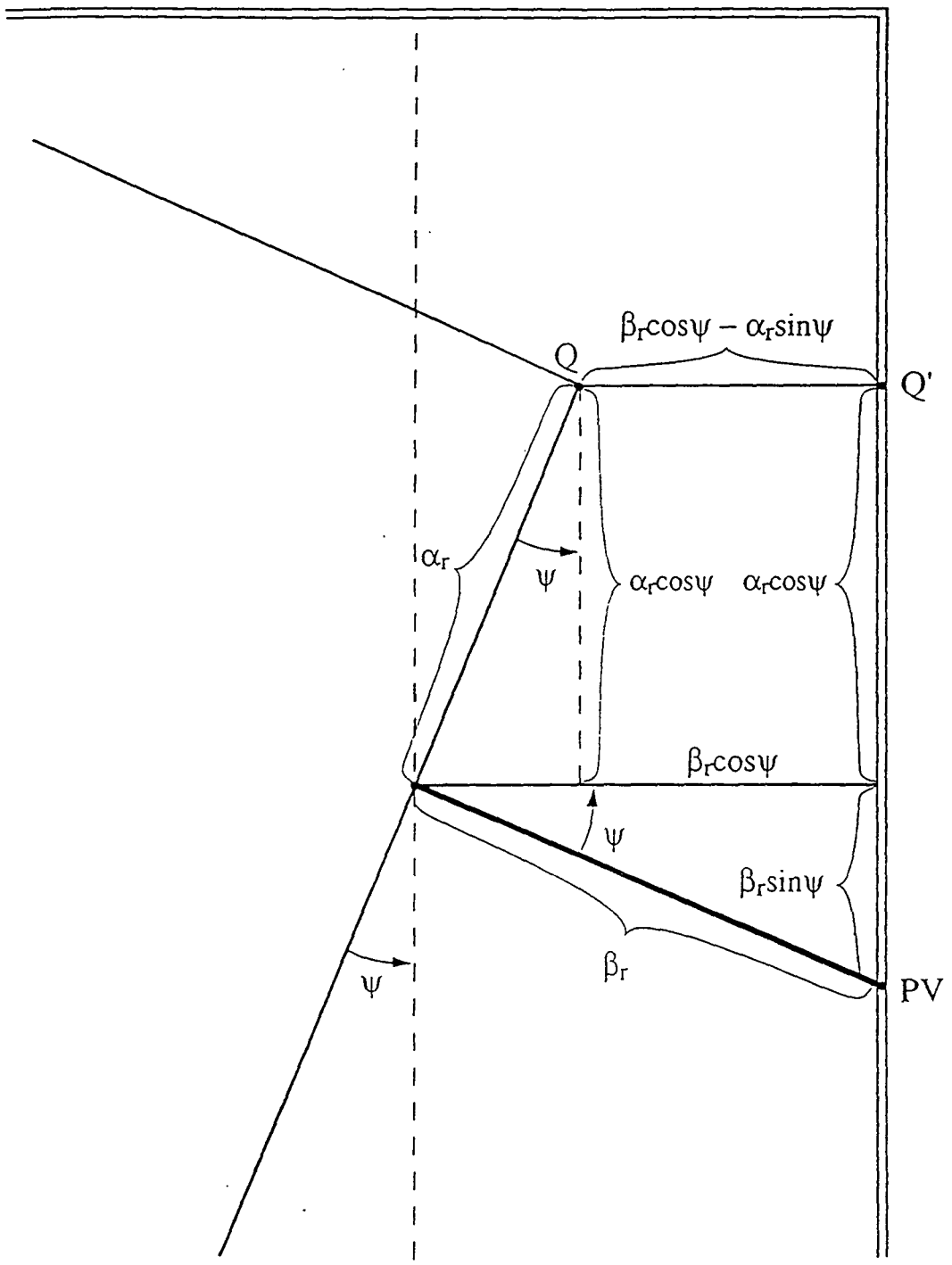

Figure 6. Geometry for the pivoting of the shaft of the hydrostatic shoe.

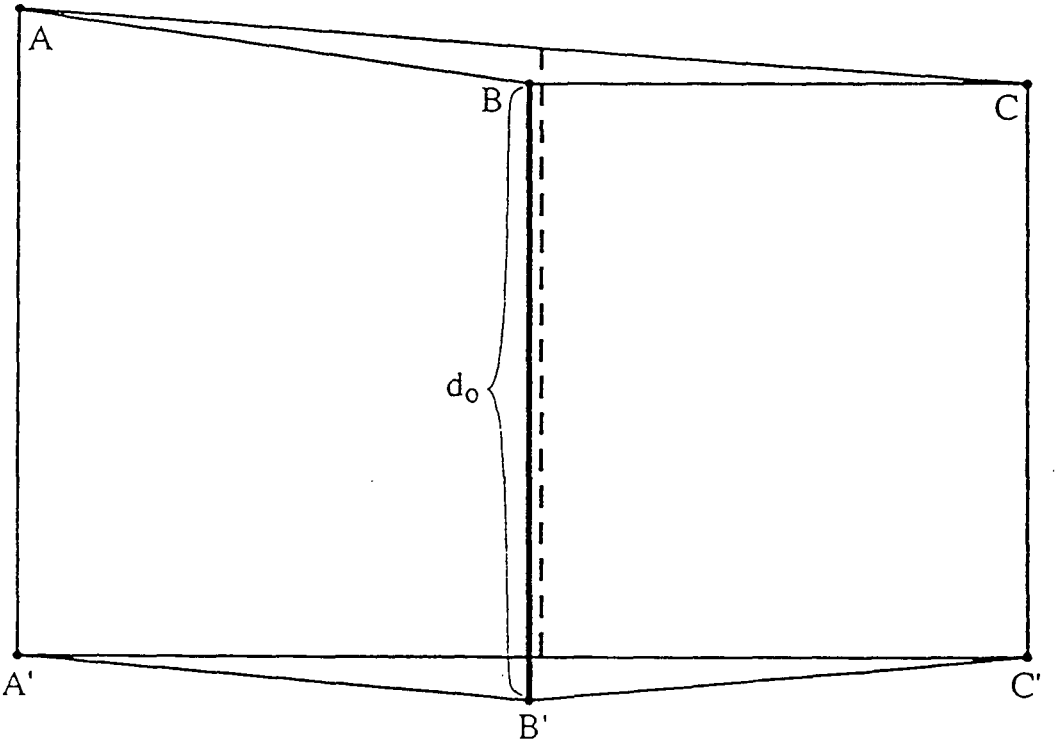

Figure 7. Approximate geometry of the lubrication channel.

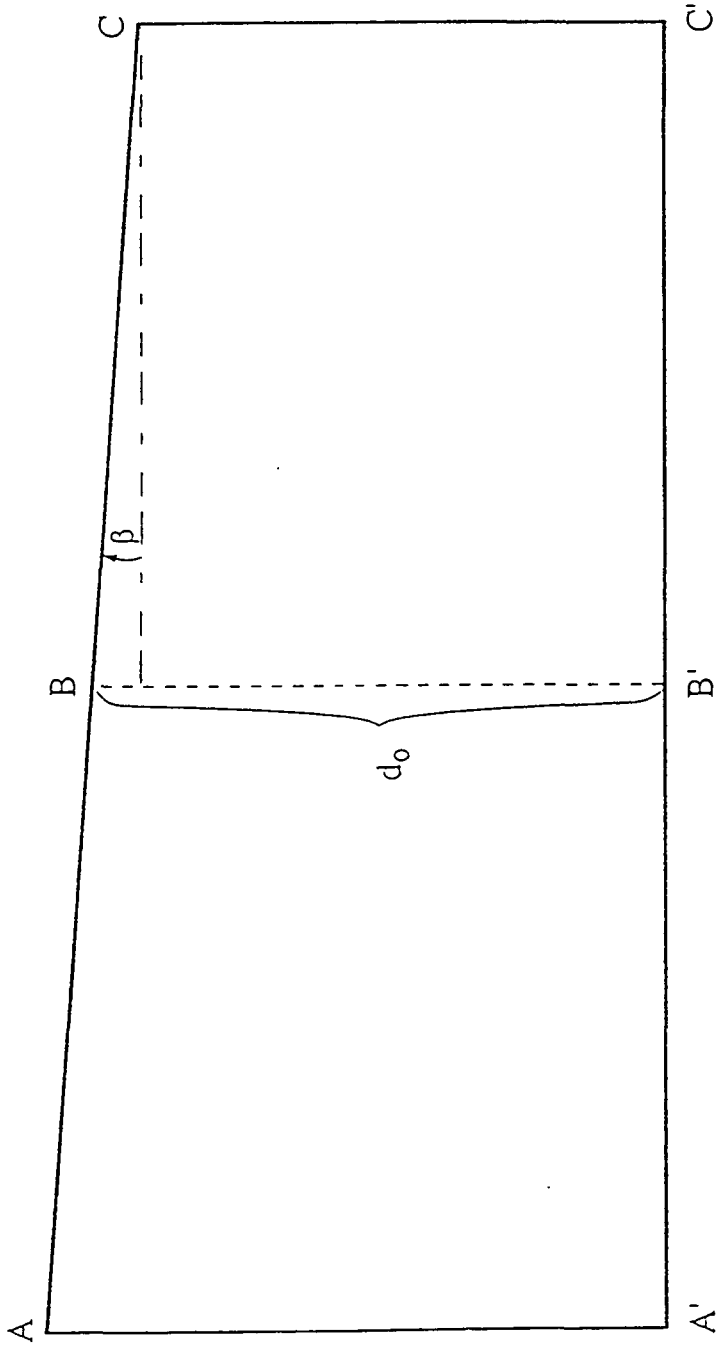

Figure 8. The approximate wedge-shaped channel.

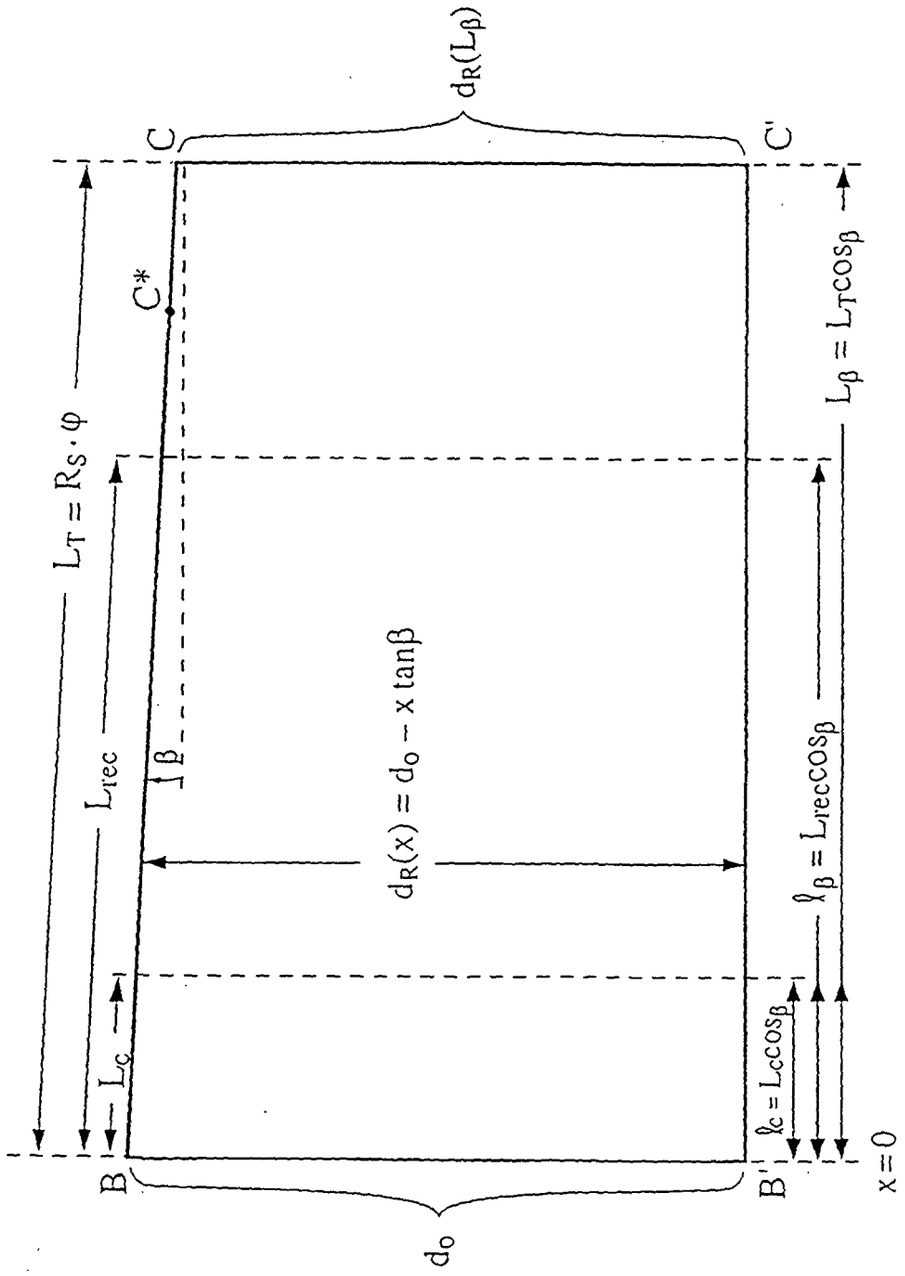

Figure 9. The right-hand subchannel.

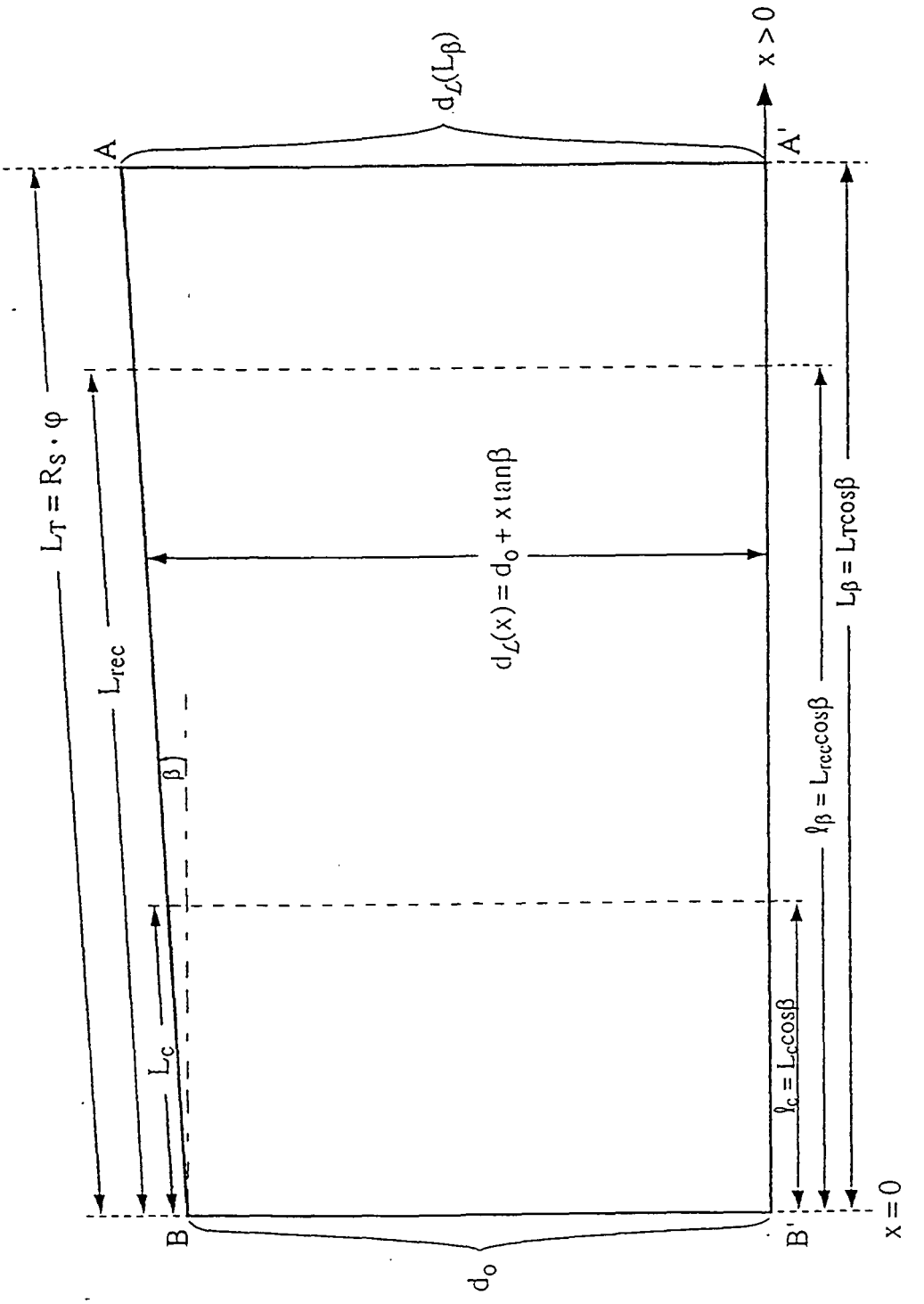

Figure 10. The left-hand subchannel.

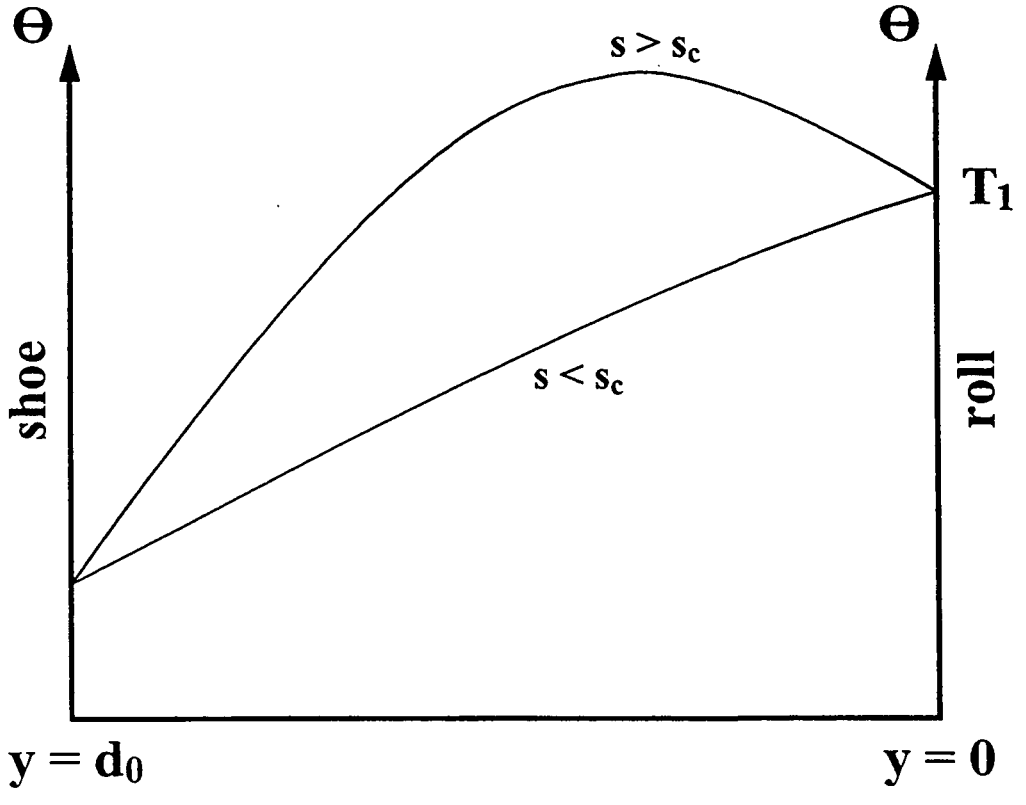

Figure 11. Expected dependence of the temperature profile on the speed of the roll.

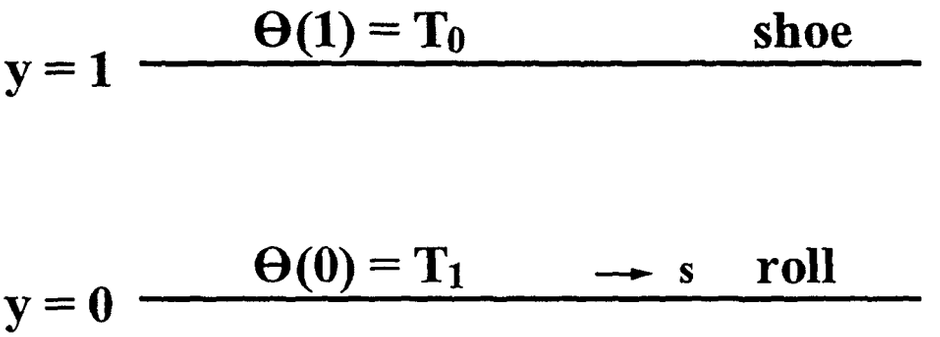

Figure 12. Temperature boundary conditions in a parallel wall channel.

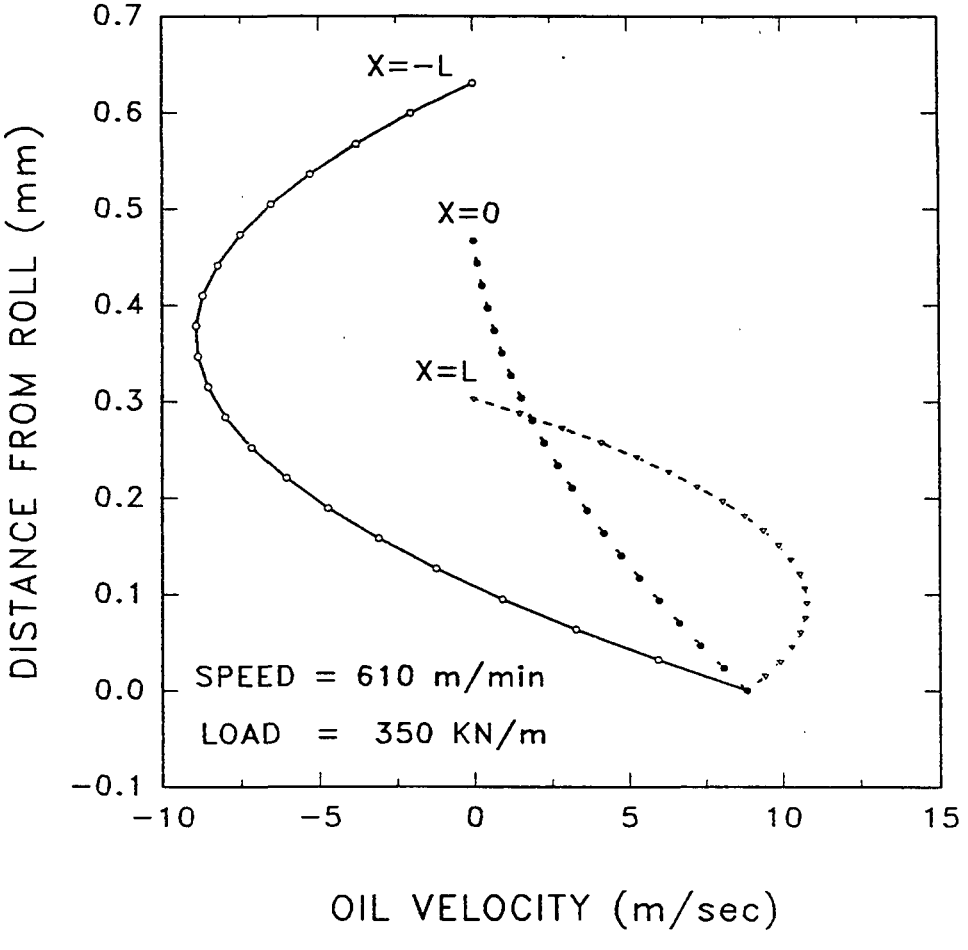

Figure 13a. Lubricant velocity profile at three locations along the left-hand and right-hand sub-channels for the roll speed of 610 m/min and applied load of 350 KN/m.

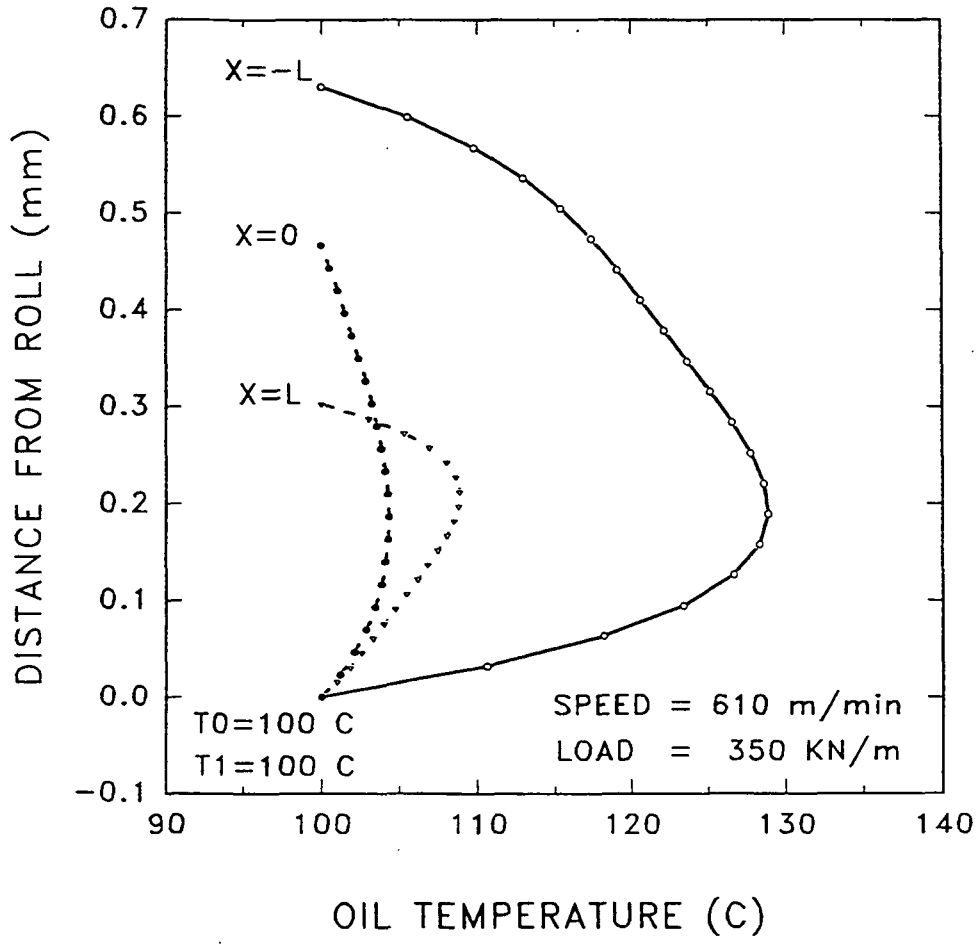

Figure 13b. Lubricant temperature profile at three locations along the left-hand and right-hand sub-channels for the roll speed of 610 m/min and applied load of 350 KN/m ($T_0 = T_1 = 100°C$).

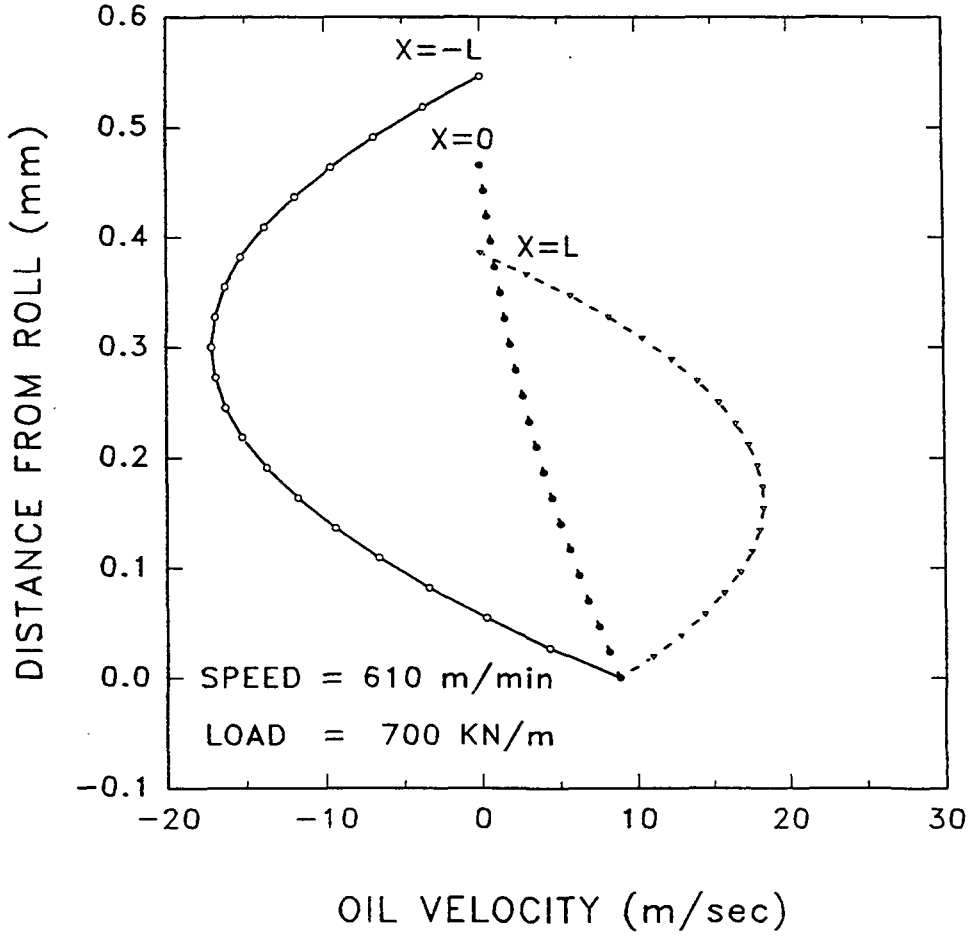

Figure 14a. Lubricant velocity profile at three locations along the left-hand and right-hand sub-channels for the roll speed of 610 m/min and applied load of 700 KN/m.

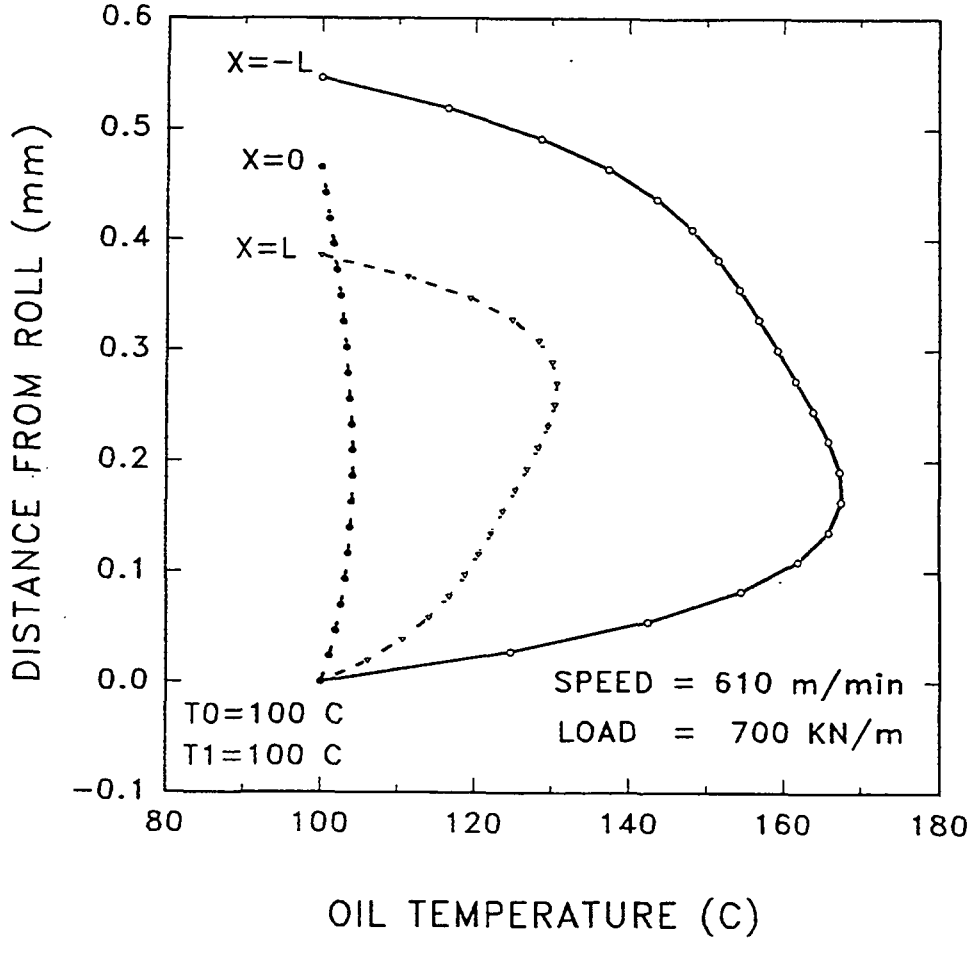

Figure 14b. Lubricant temperature profile at three locations along the left-hand and right-hand sub-channels for the roll speed of 610 m/min and applied load of 700 KN/m ($T_0 = T_1 = 100°C$).

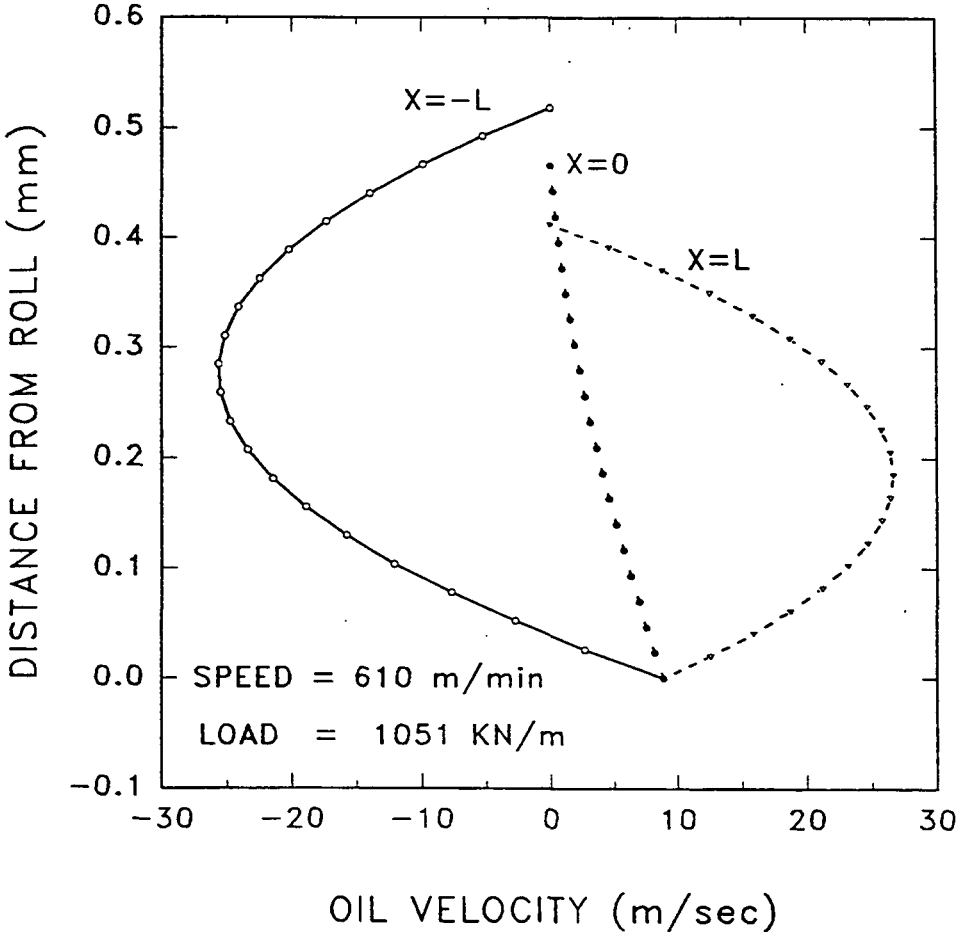

Figure 15a. Lubricant velocity profile at three locations along the left-hand and right-hand sub-channels for the roll speed of 610 m/min and applied load of 1051 KN/m.

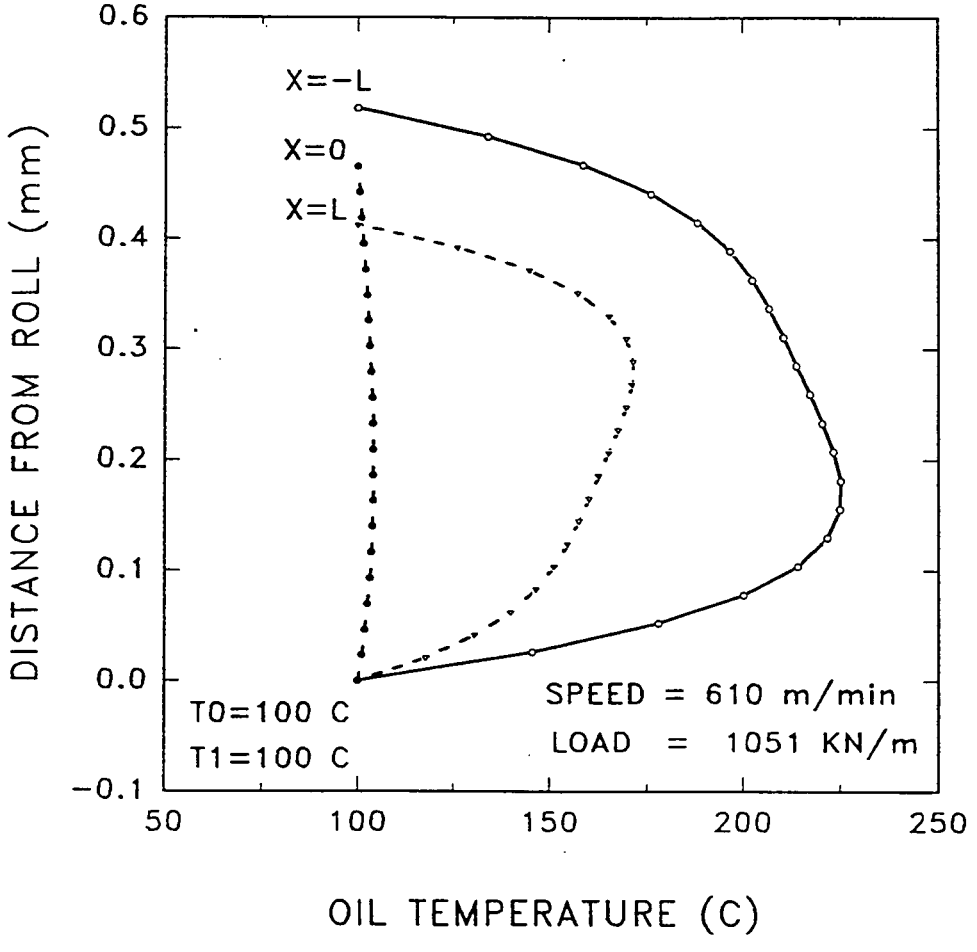

Figure 15b. Lubricant temperature profile at three locations along left-hand and the right-hand sub-channels for the roll speed of 610 m/min and applied load of 1051 KN/m ($T_0 = T_1 = 100°C$).

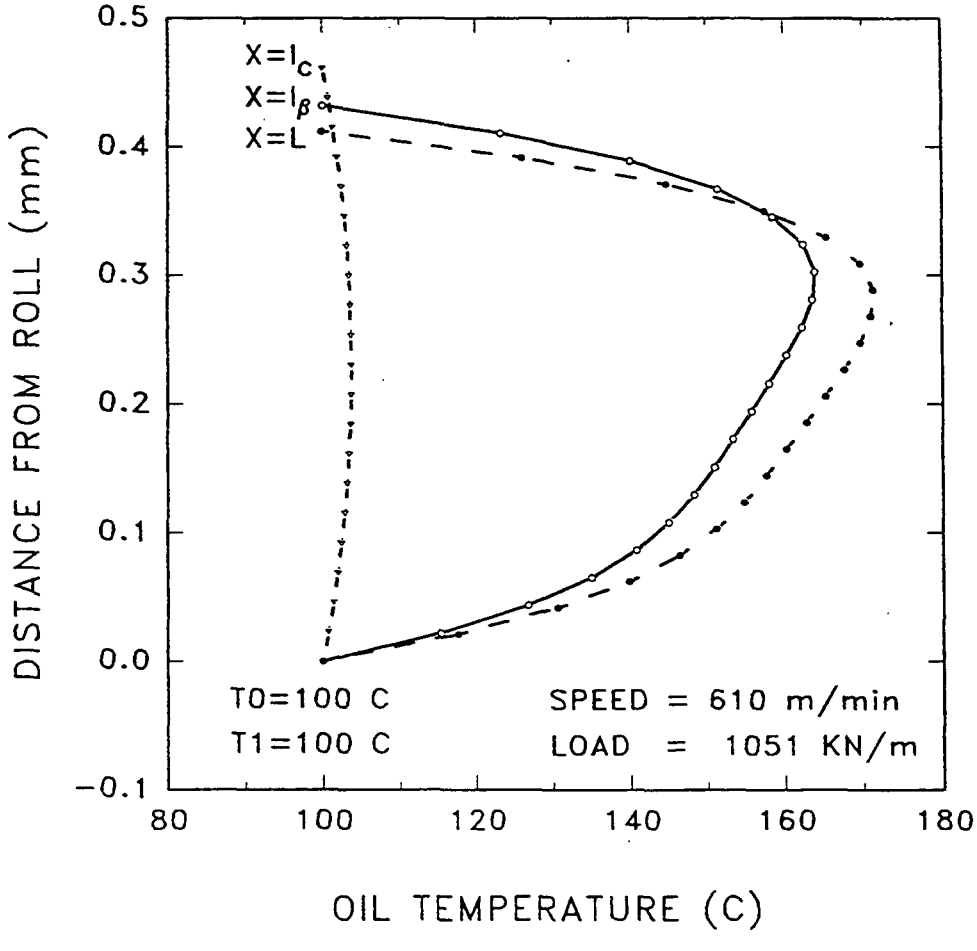

Figure 15c. Lubricant temperature profile at three locations along the right-hand sub-channel for the roll speed of 610 m/min and applied load of 1051 KN/m ($T_0 = T_1 = 100°C$).

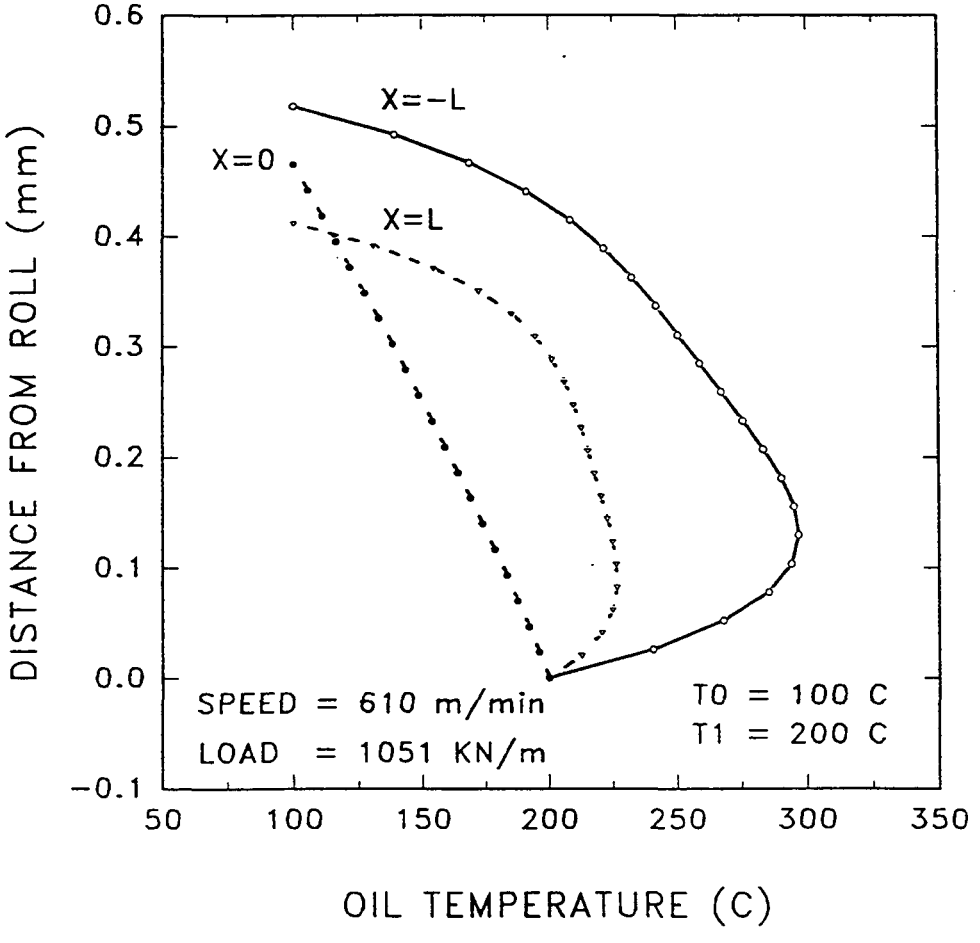

Figure 16a. Lubricant temperature profile at three locations along the left-hand and right-hand sub-channels for the roll speed of 610 m/min and applied load of 1051 KN/m (T_0 = 100°C, T_1 = 200°C).

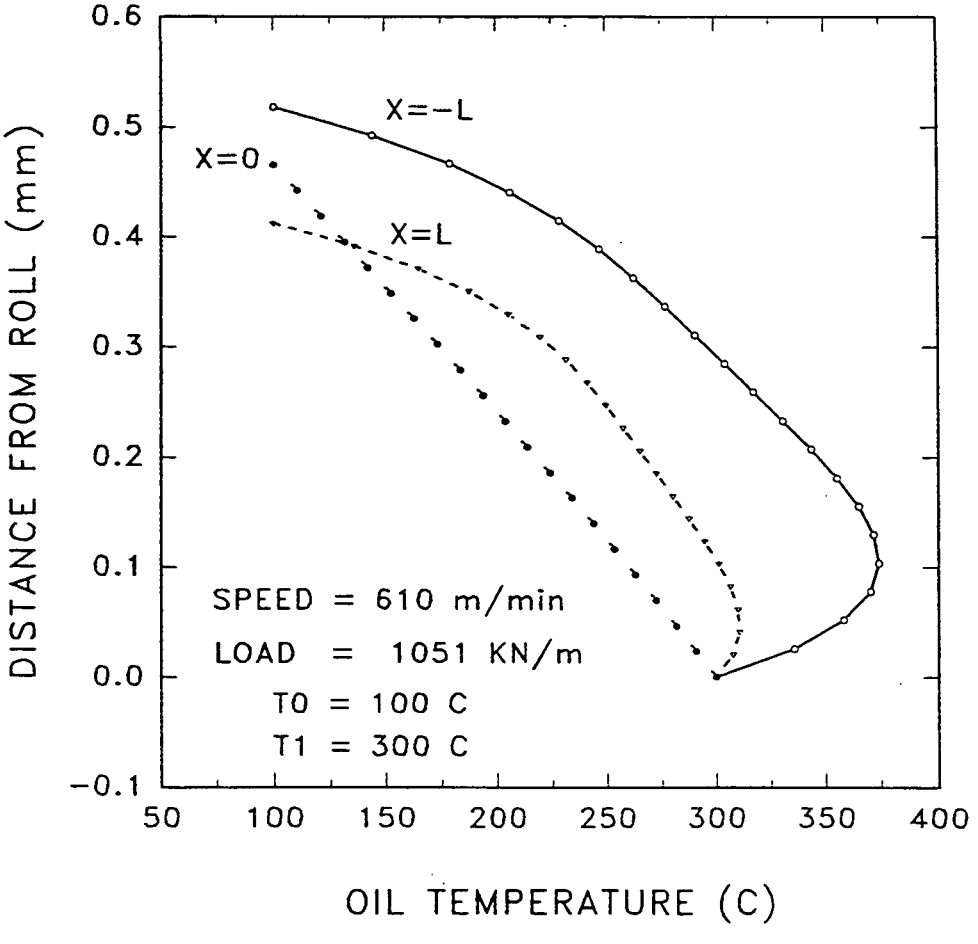

Figure 16b. Lubricant temperature profile at three locations along the left-hand and right-hand sub-channels for the roll speed of 610 m/min and applied load of 1051 KN/m (T_0 = 100°C, T_1 = 300°C).

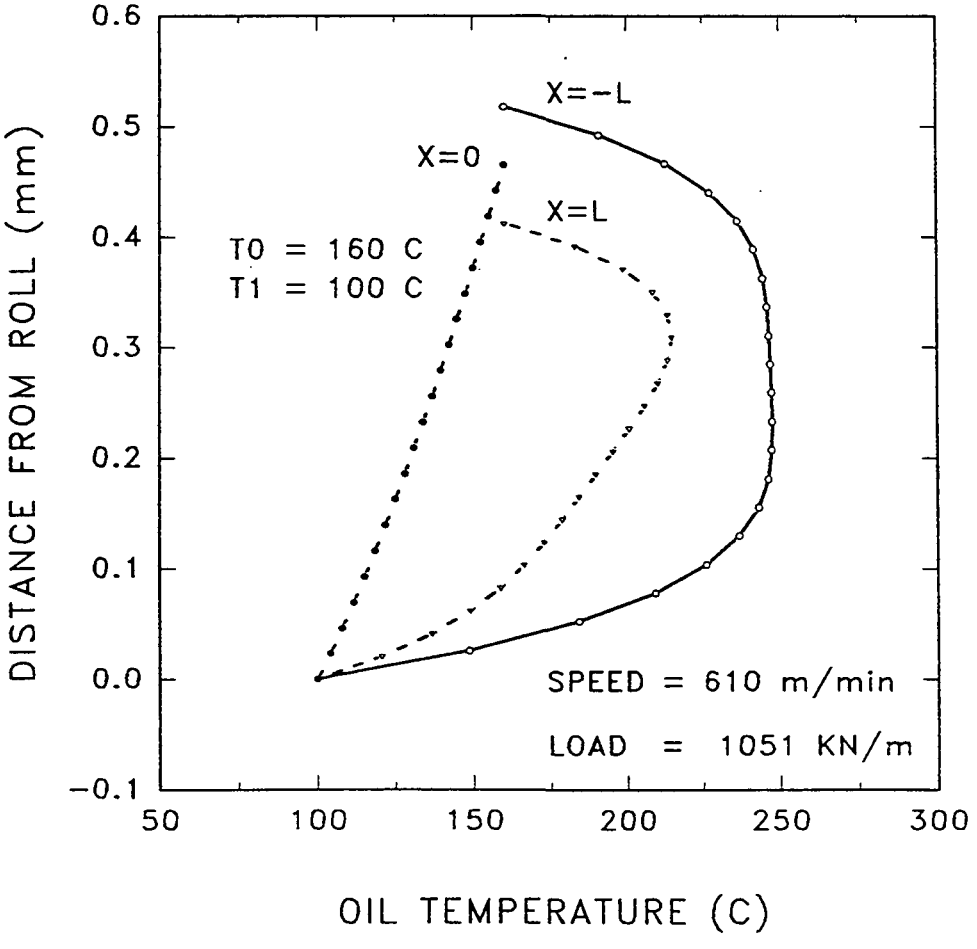

Figure 17. Lubricant temperature profile at three locations along left-hand and the right-hand sub-channels for the roll speed of 610 m/min and applied load of 1051 KN/m (T_0 = 160°C, T_1 = 100°C).

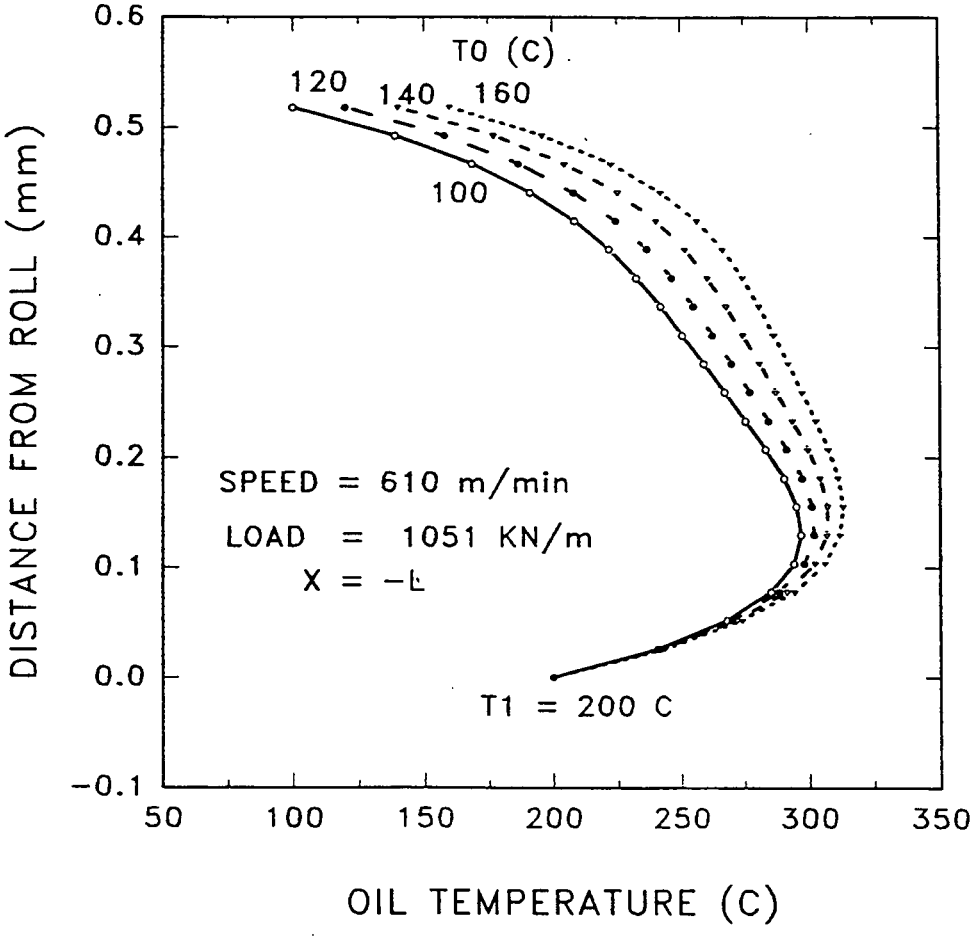

Figure 18. Lubricant temperature profile at the end of the left-hand sub-channels for the roll speed of 610 m/min and applied load of 1051 KN/m and for various shoe temperatures (T_1 = 200°C).

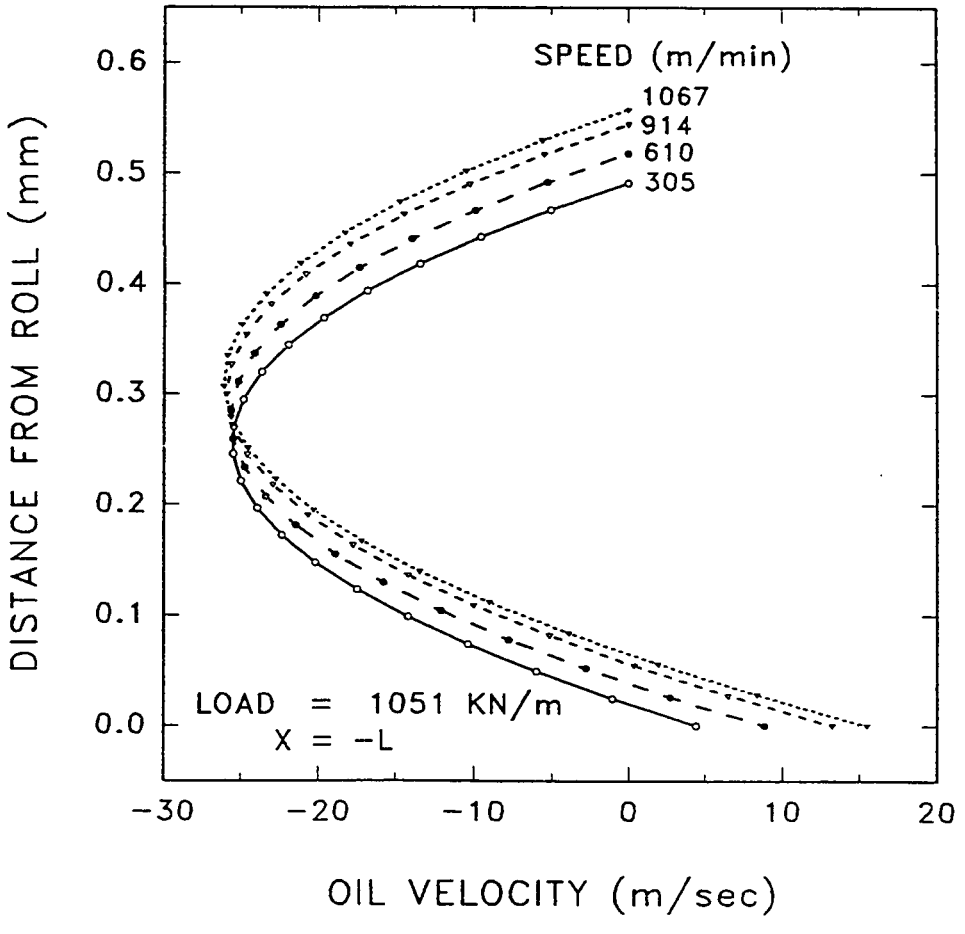

Figure 19a. Lubricant velocity profile at the end of the left-hand sub-channel for the an applied load of 1051 KN/m and various roll speeds.

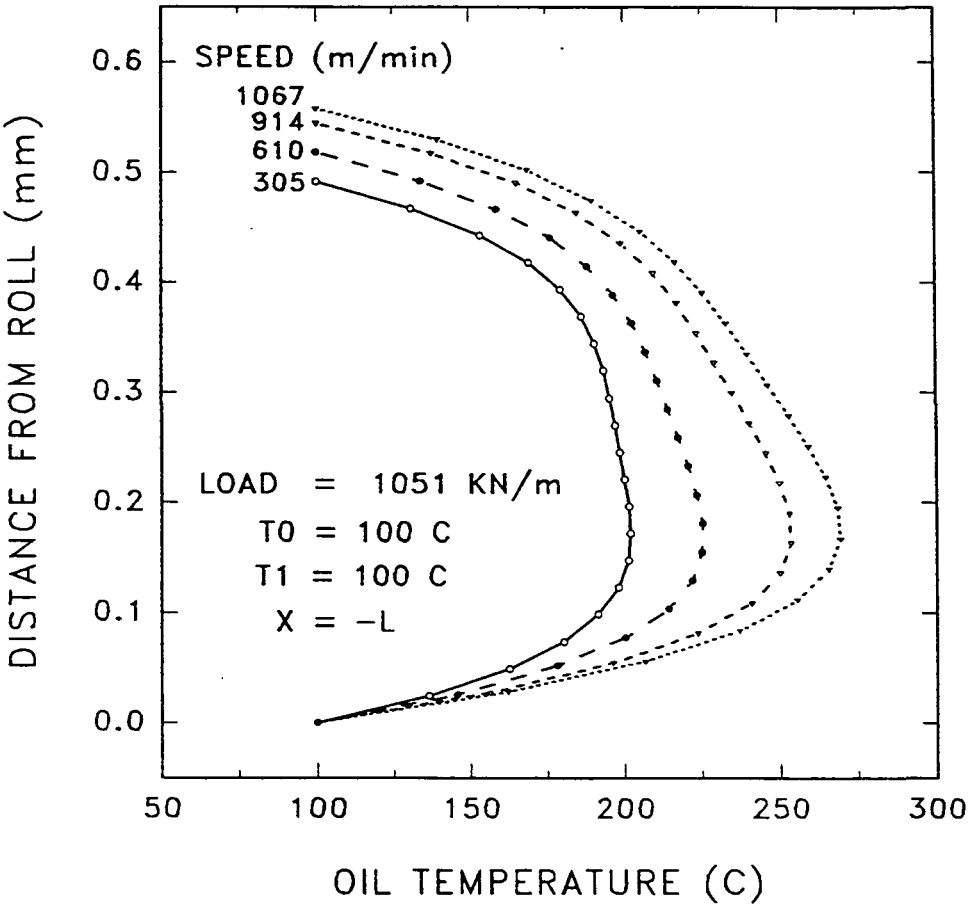

Figure 19b. Lubricant temperature profile at the end of the left-hand sub-channel for the an applied load of 1051 KN/m, and various roll speeds ($T_0 = T_1 = 100°C$).

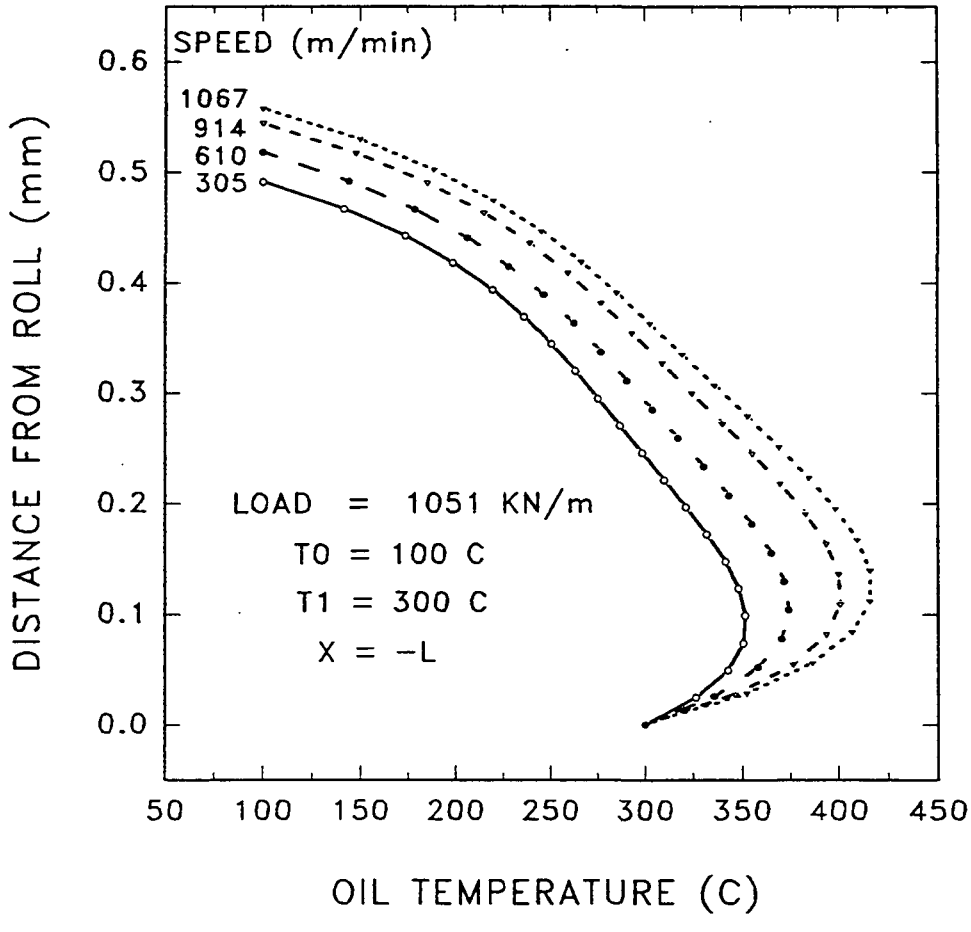

Figure 19c. Lubricant temperature profile at the end of the left-hand sub-channel for the an applied load of 1051 KN/m and various roll speeds (T_0 = 100°C, T_1 = 300°C).

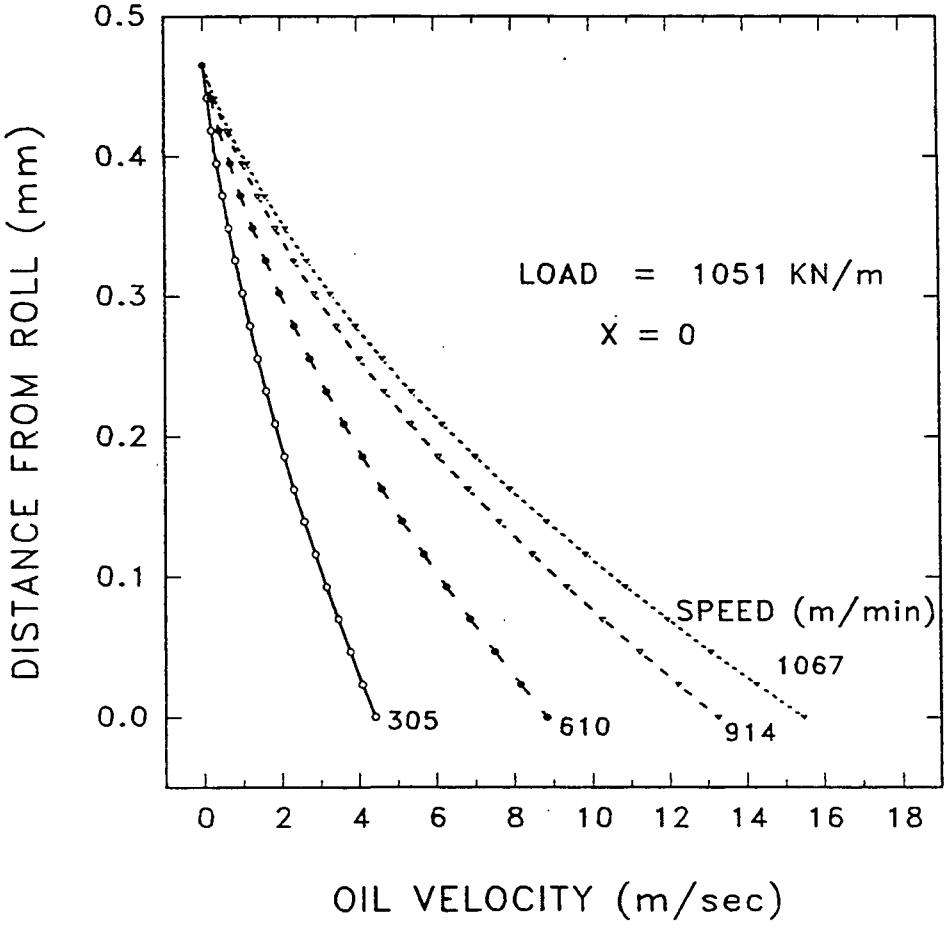

Figure 20a. Lubricant velocity profile at the entrance of each sub-channel for the an applied load of 1051 KN/m and various roll speeds.

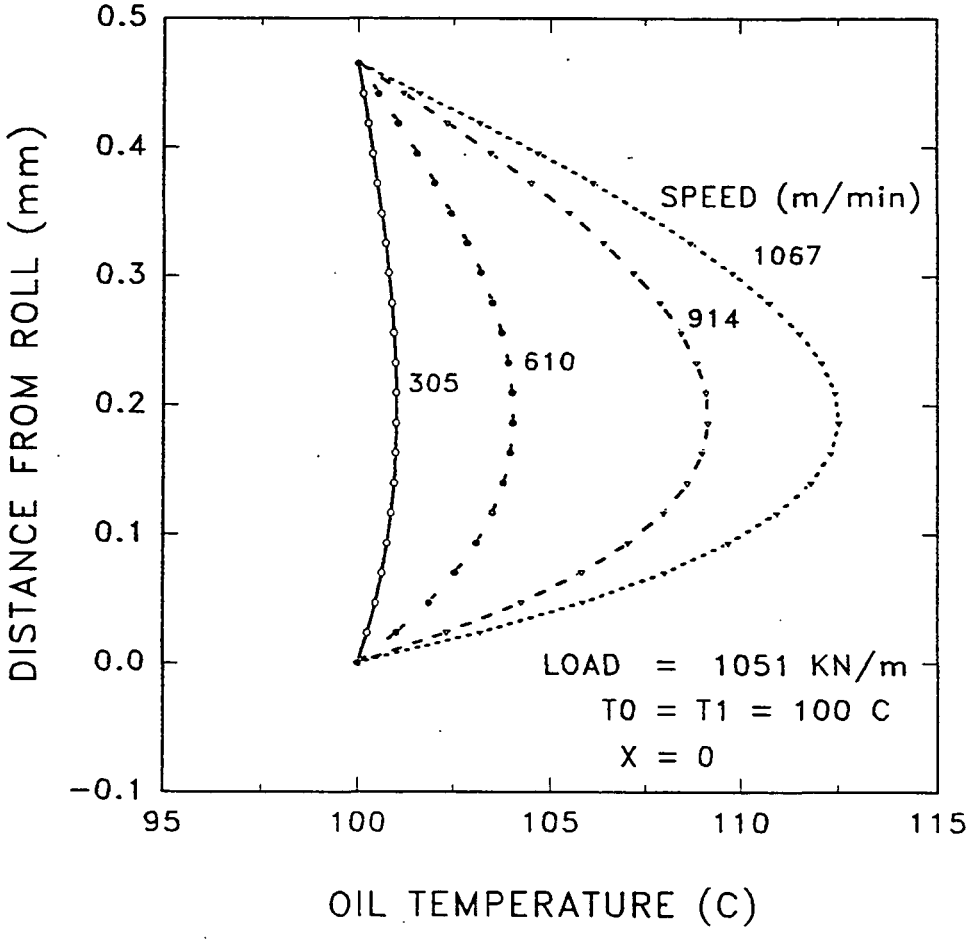

Figure 20b. Lubricant temperature profile at the entrance of each sub-channel for the an applied load of 1051 KN/m and various roll speeds ($T_0 = T_1 = 100°C$).

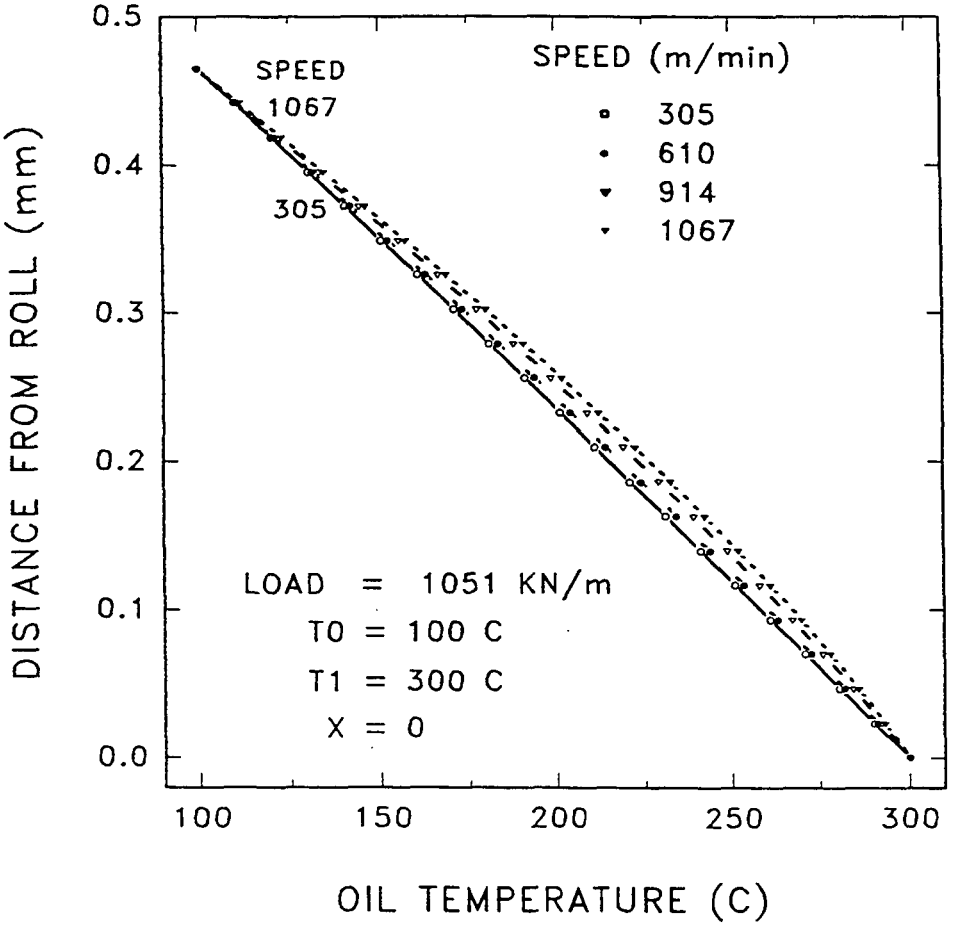

Figure 20c. Lubricant temperature profile at the entrance of each sub-channel for the an applied load of 1051 KN/m and various roll speeds (T_0 = 100 °C, T_1 = 300°C).

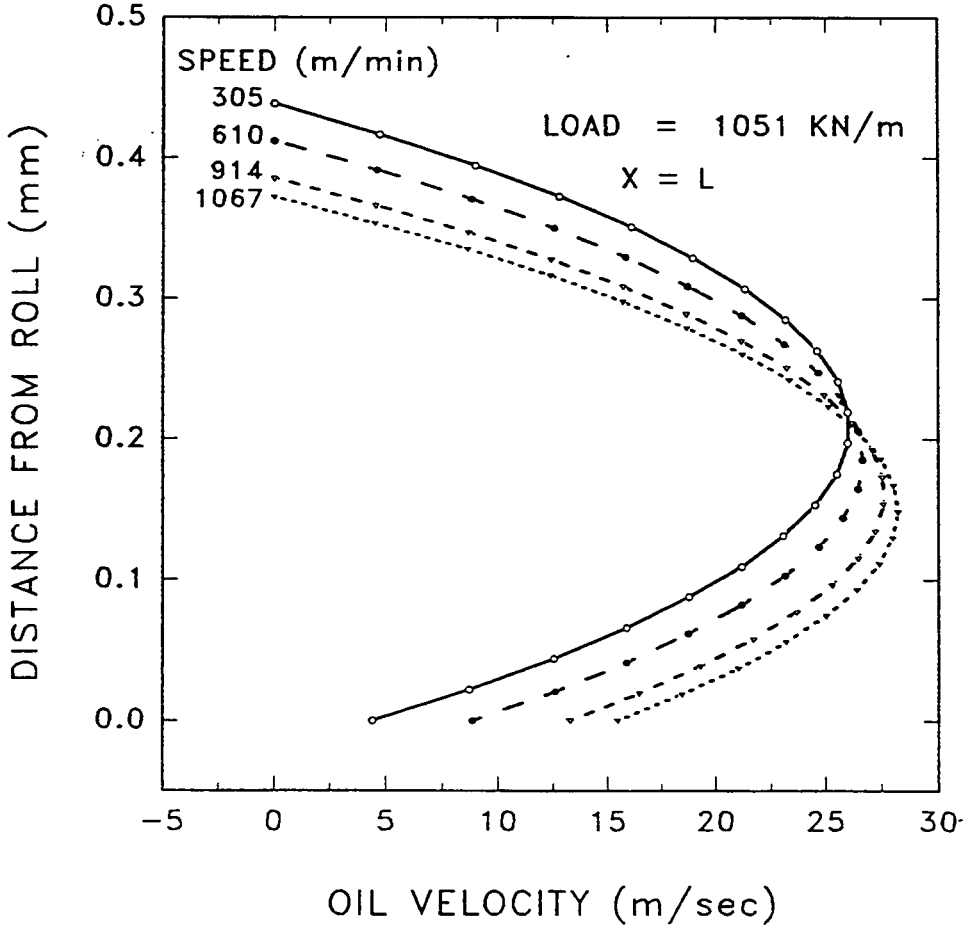

Figure 21a. Lubricant velocity profile at the end of the right-hand sub-channel for the an applied load of 1051 KN/m and various roll speeds.

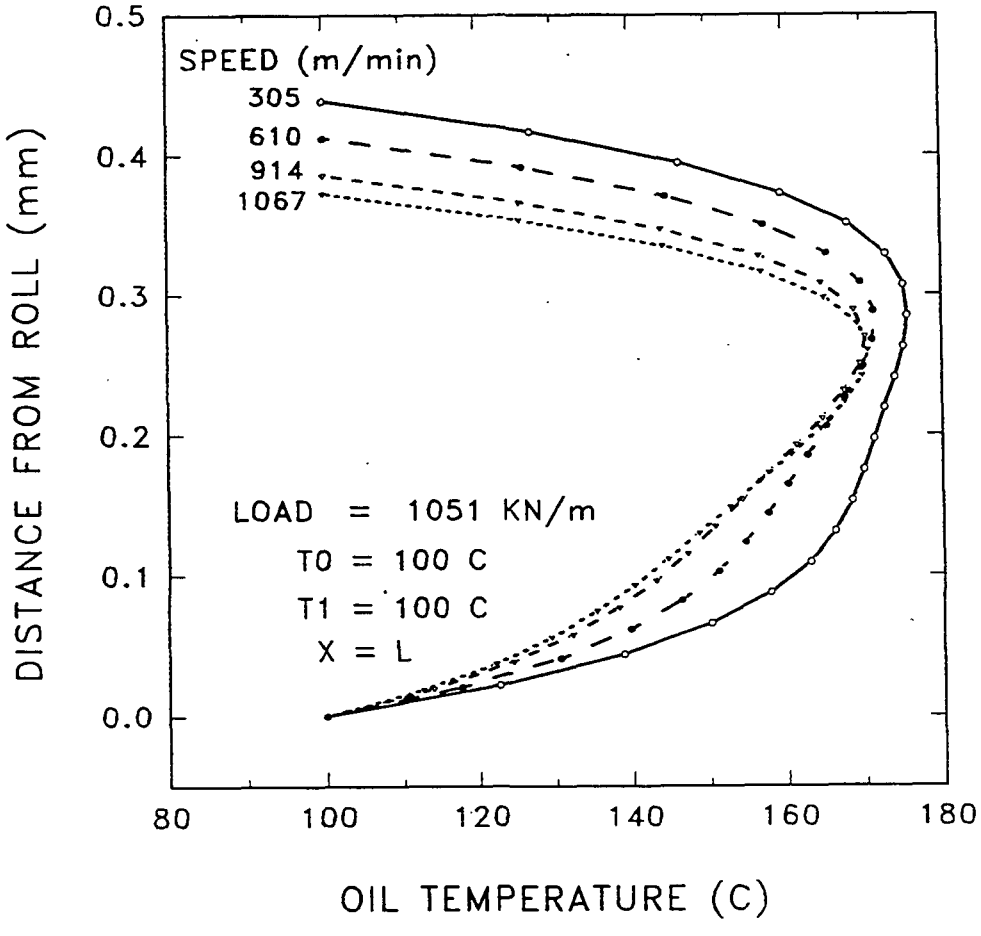

Figure 21b. Lubricant temperature profile at the end of the right-hand sub-channel for the an applied load of 1051 KN/m and various roll speeds ($T_0 = T_1 = 100°C$).

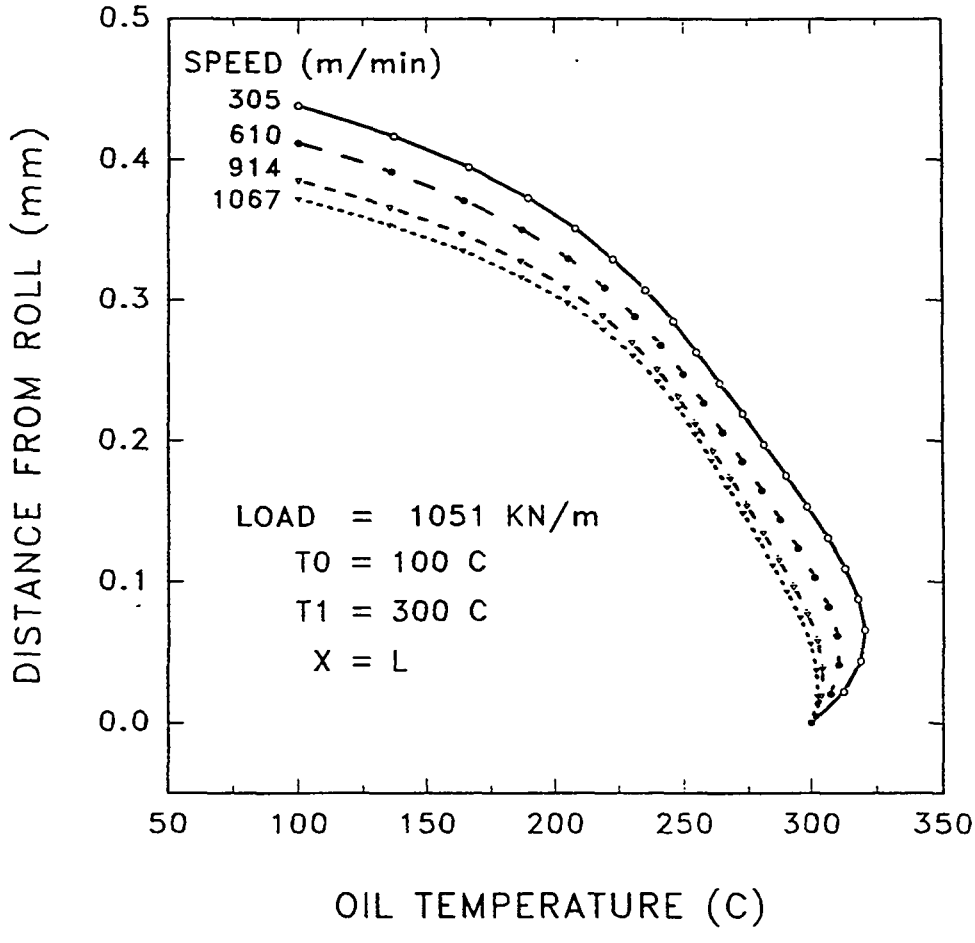

Figure 21c. Lubricant temperature profile at the end of the right-hand sub-channel for the an applied load of 1051 KN/m and various roll speeds (T_0 = 100°C, T_1 = 300°C).

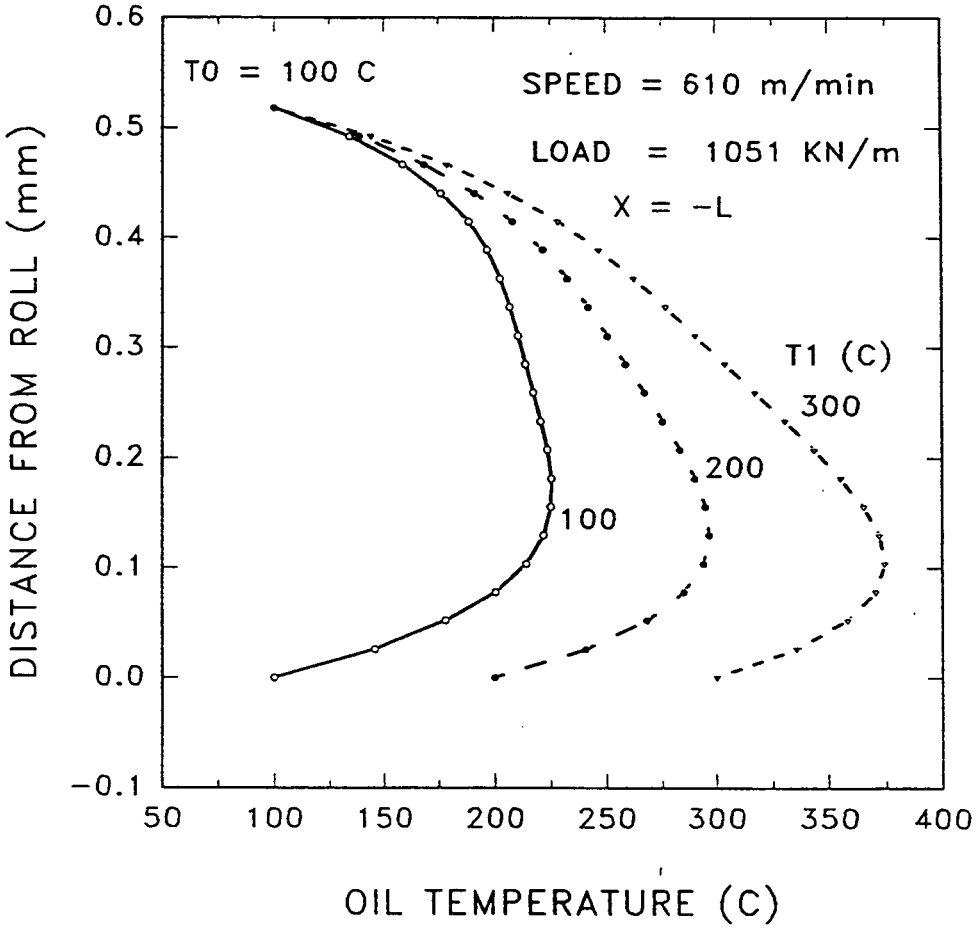

Figure 22a. Lubricant temperature profile at the end of the left-hand sub-channel for the an applied load of 1051 KN/m, and roll speed of 610 m/min and various inner roll surface temperatures (T_0 = 100°C).

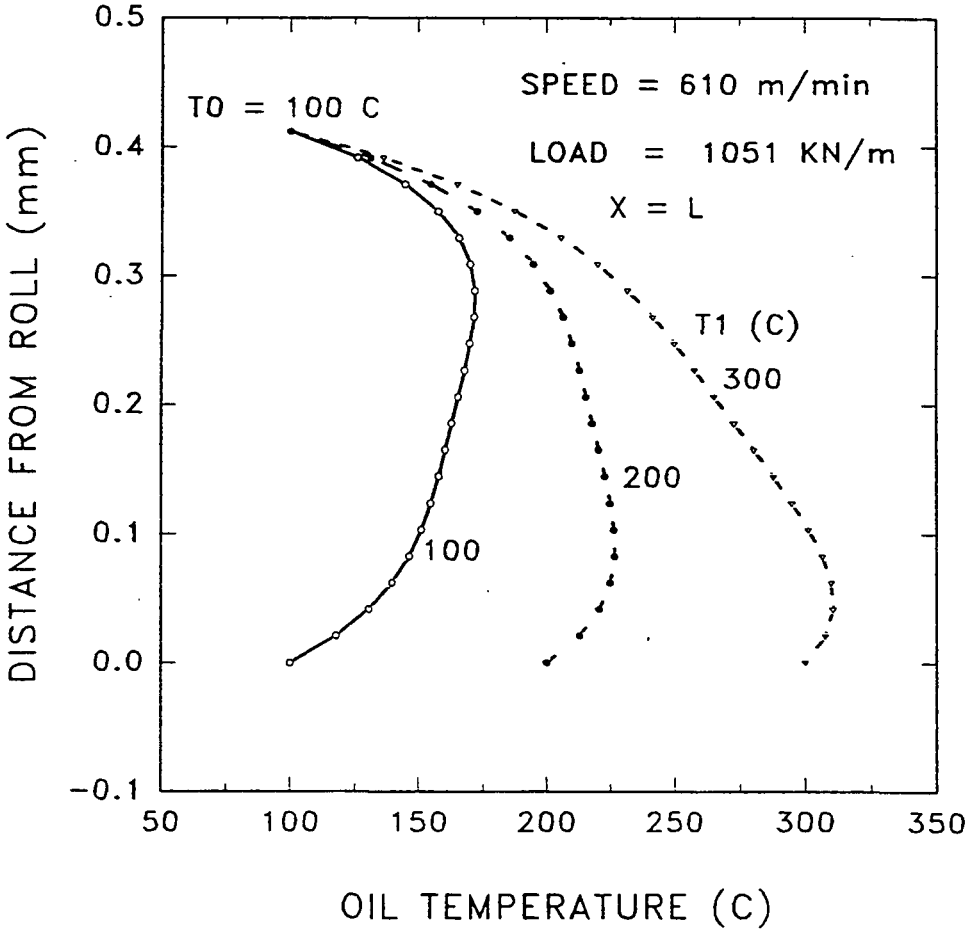

Figure 22b. Lubricant temperature profile at the end of the right-hand sub-channel for the an applied load of 1051 KN/m, and roll speed of 610 m/min and various inner roll surface temperatures (T_0 = 100°C).

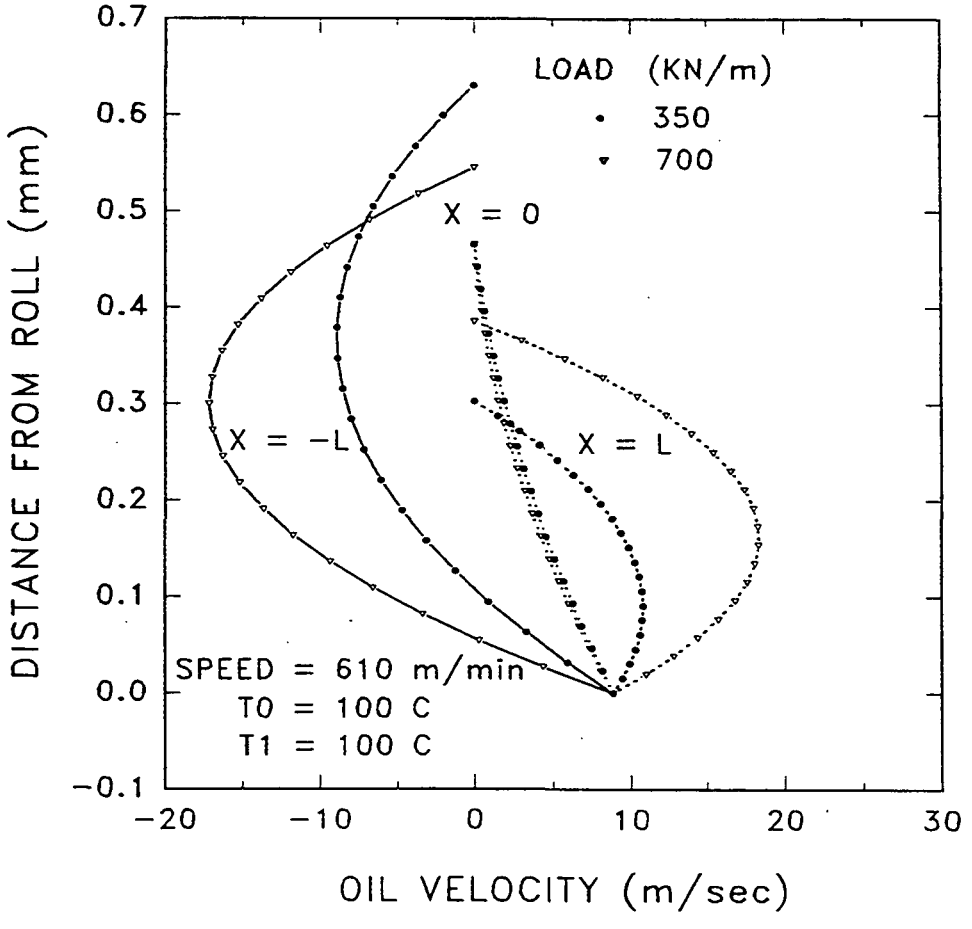

Figure 23a. Lubricant velocity profile at three locations along the left-hand and right-hand sub-channels for the roll speed of 610 m/min, and applied loads of 350 KN/m and 700 KN/m ($T_0 = T_1 = 100°C$).

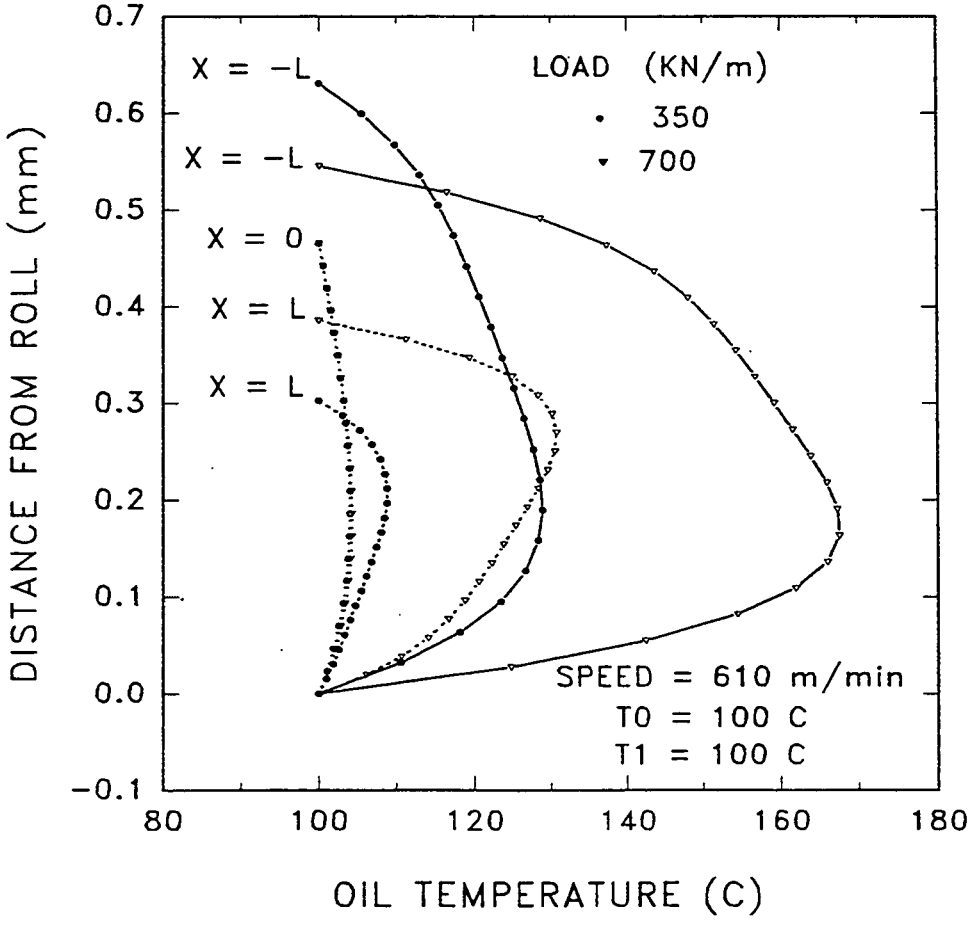

Figure 23b. Lubricant temperature profile at three locations along the right-hand and left-hand sub-channels for the roll speed of 610 m/min and applied loads of 350 KN/m and 700 KN/m ($T_0 = T_1 = 100°C$).

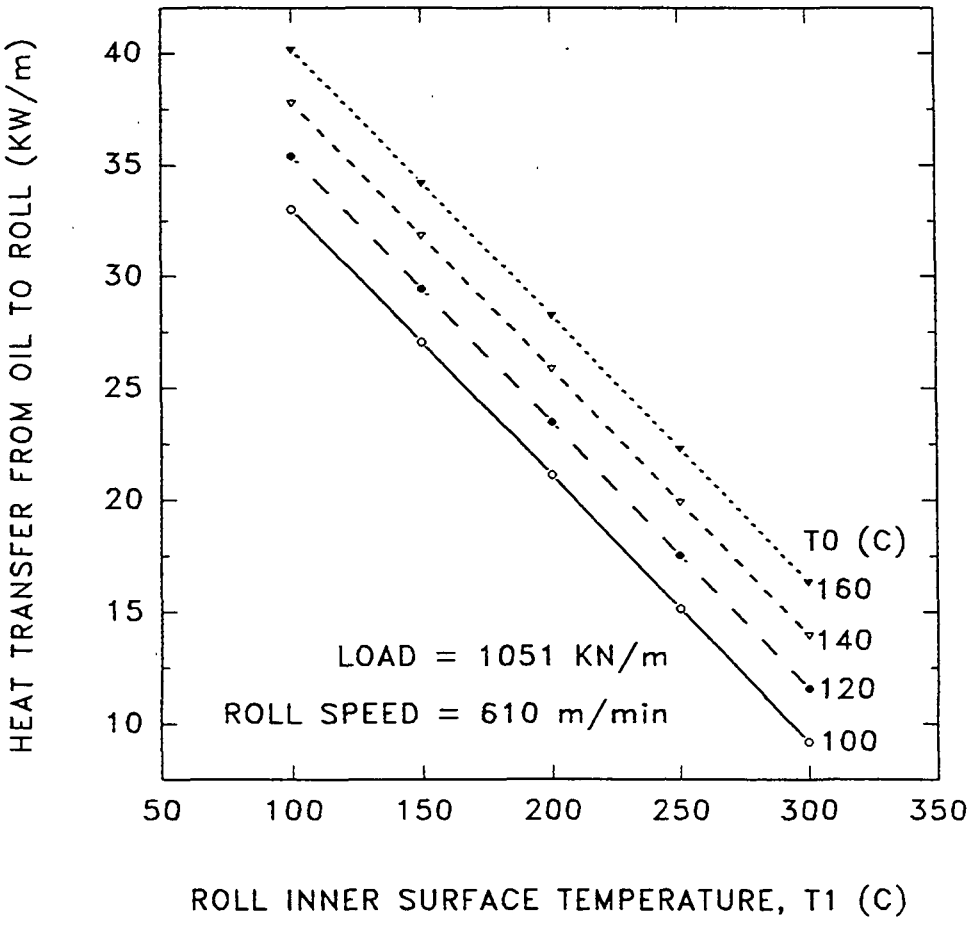

Figure 24a. Heat transfer from oil to roll as a function of roll inner surface temperature (load =1051 KN/m, roll speed = 610 m/min).

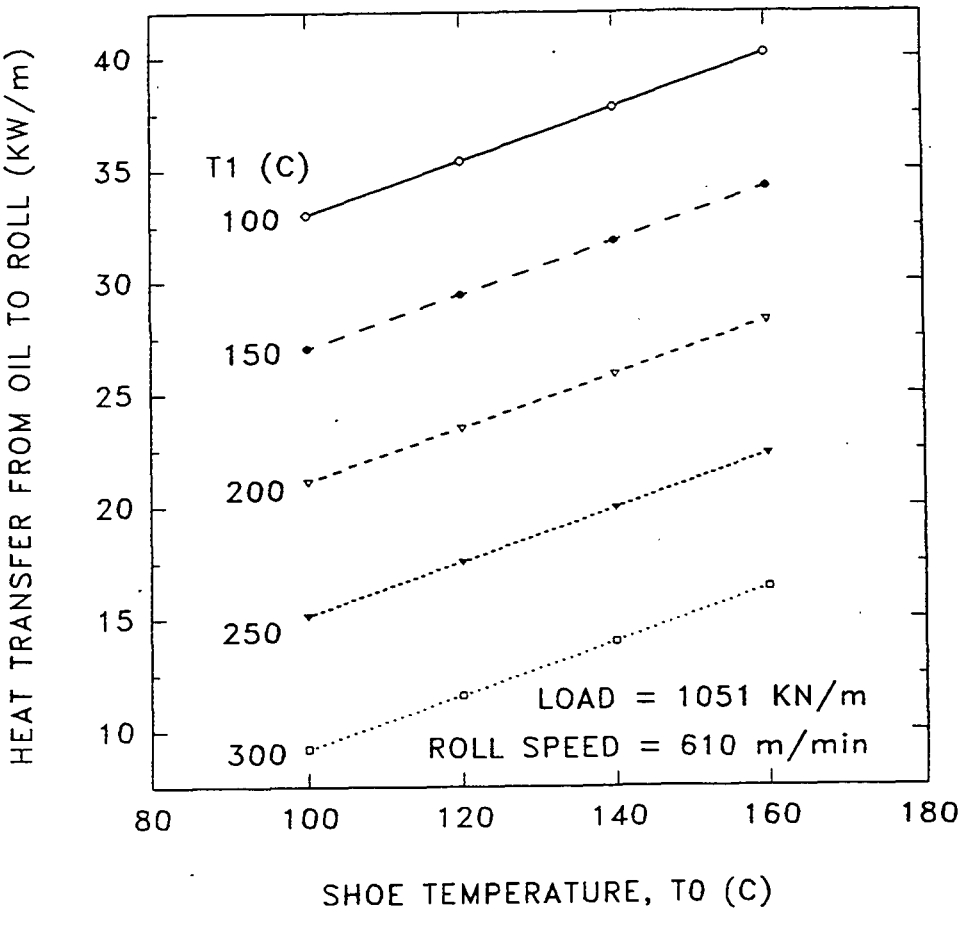

Figure 24b. Heat transfer from oil to roll as a function of shoe temperature (load =1051 KN/m, roll speed = 610 m/min).

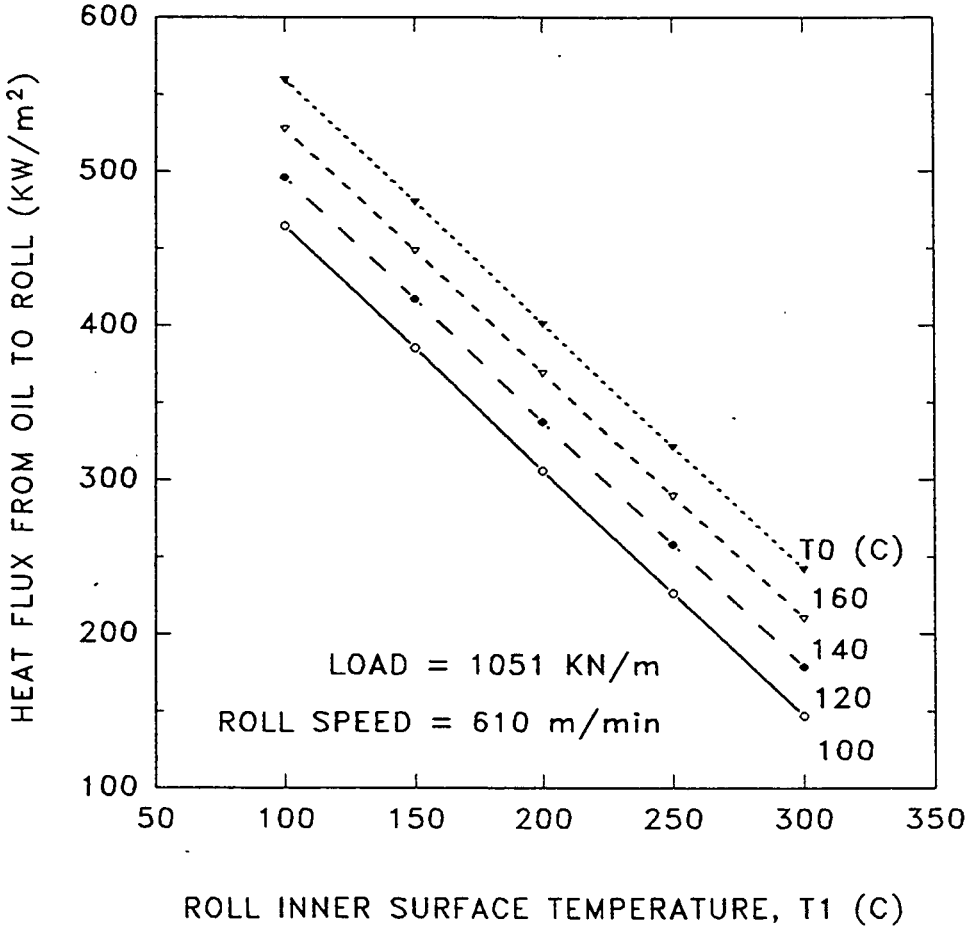

Figure 24c. Heat flux from oil to roll as a function of roll inner surface temperature (load =1051 KN/m, roll speed = 610 m/min).

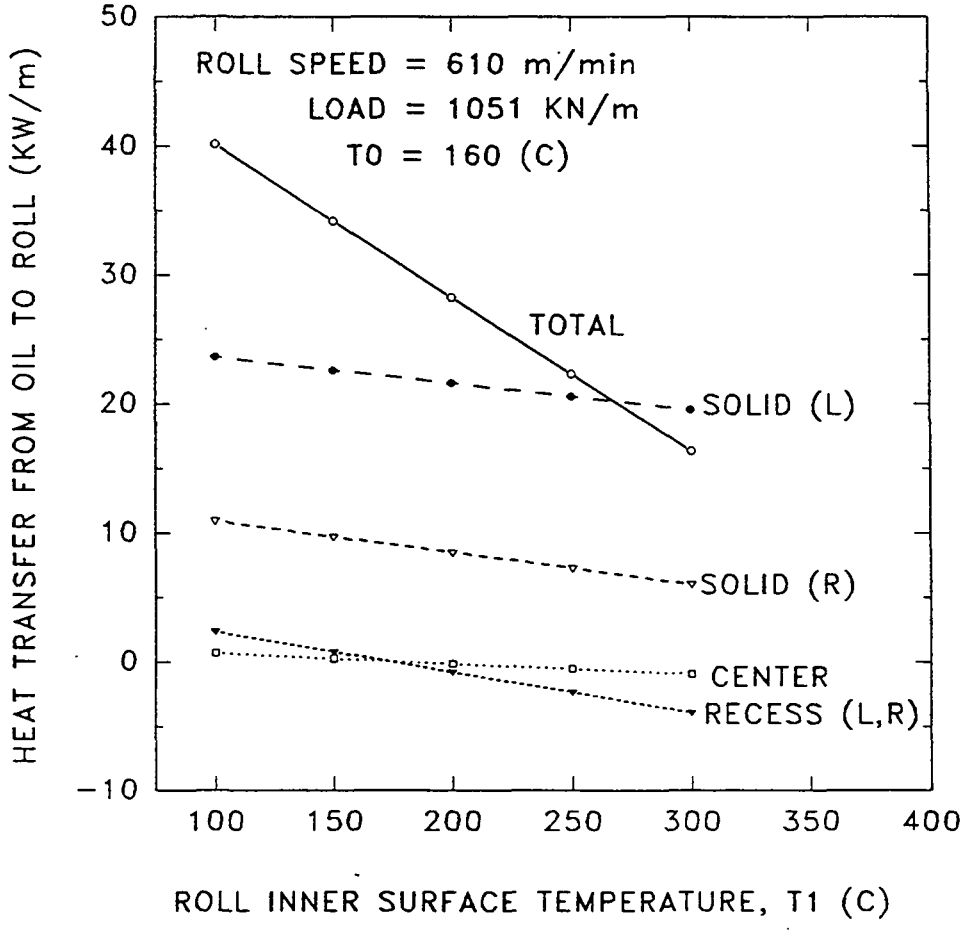

Figure 25a. Contribution of each region of the channel to the net heat transfer from oil to roll (load =1051 KN/m, roll speed = 610 m/min).

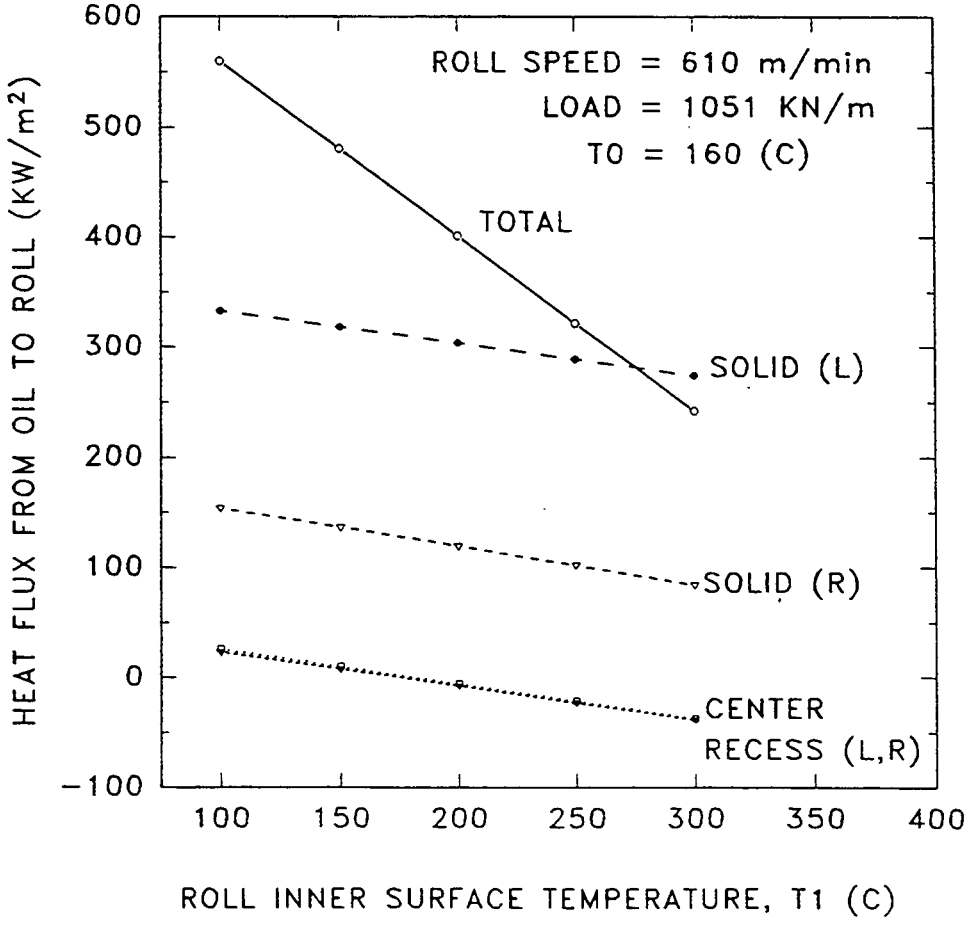

Figure 25b. Contribution of each region of the channel to the net heat flux from oil to roll (load =1051 KN/m, roll speed = 610 m/min).

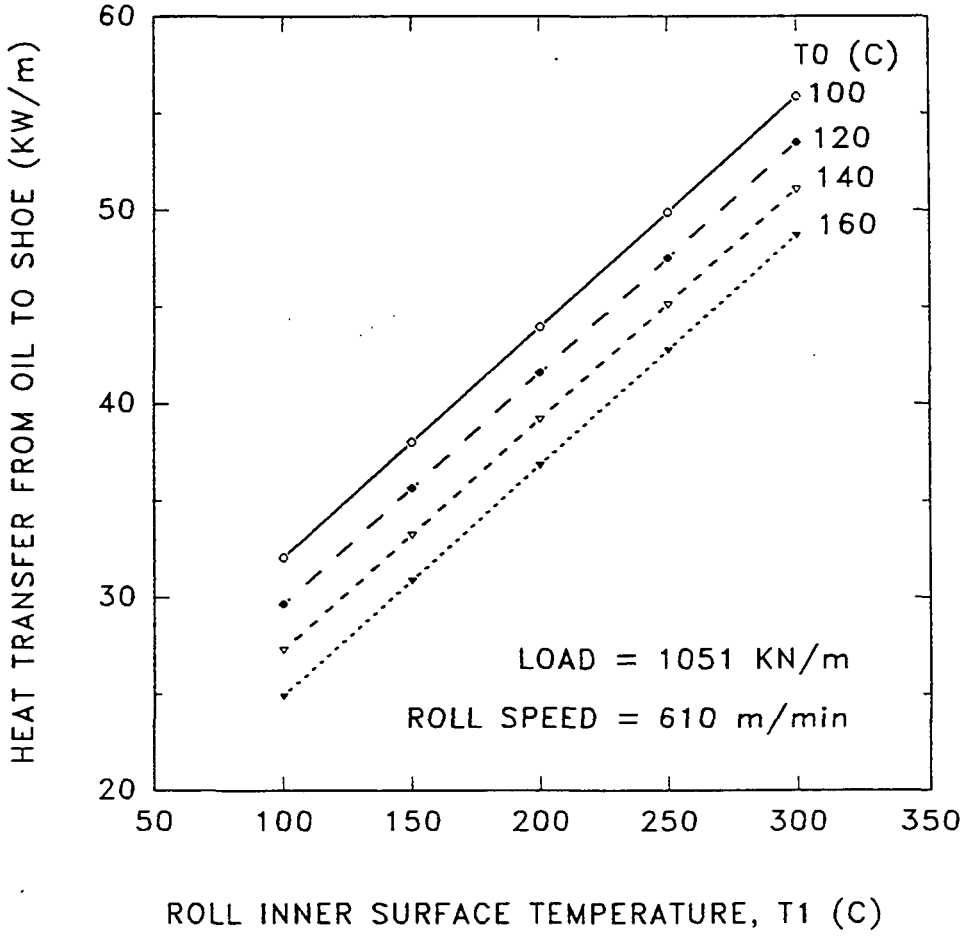

Figure 26a. Heat transfer from oil to shoe as a function of roll inner surface temperature (load =1051 KN/m, roll speed = 610 m/min).

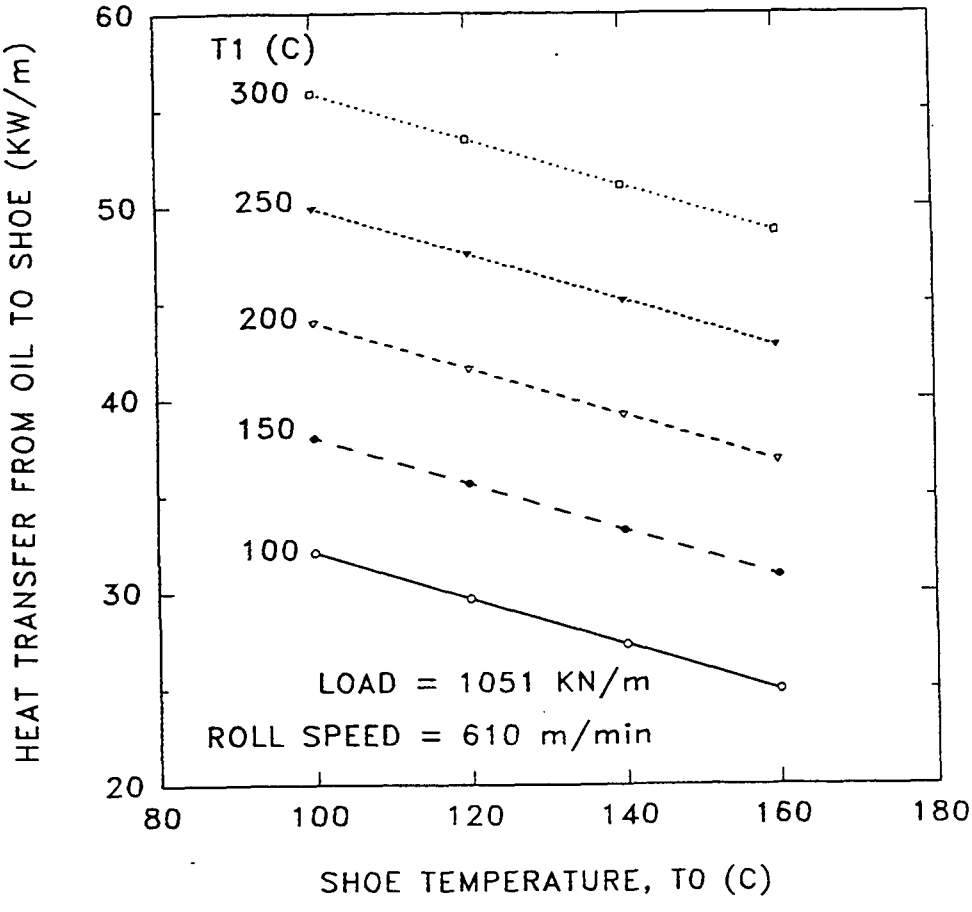

Figure 26b. Heat transfer from oil to shoe as a function of shoe temperature (load =1051 KN/m, roll speed = 610 m/min).

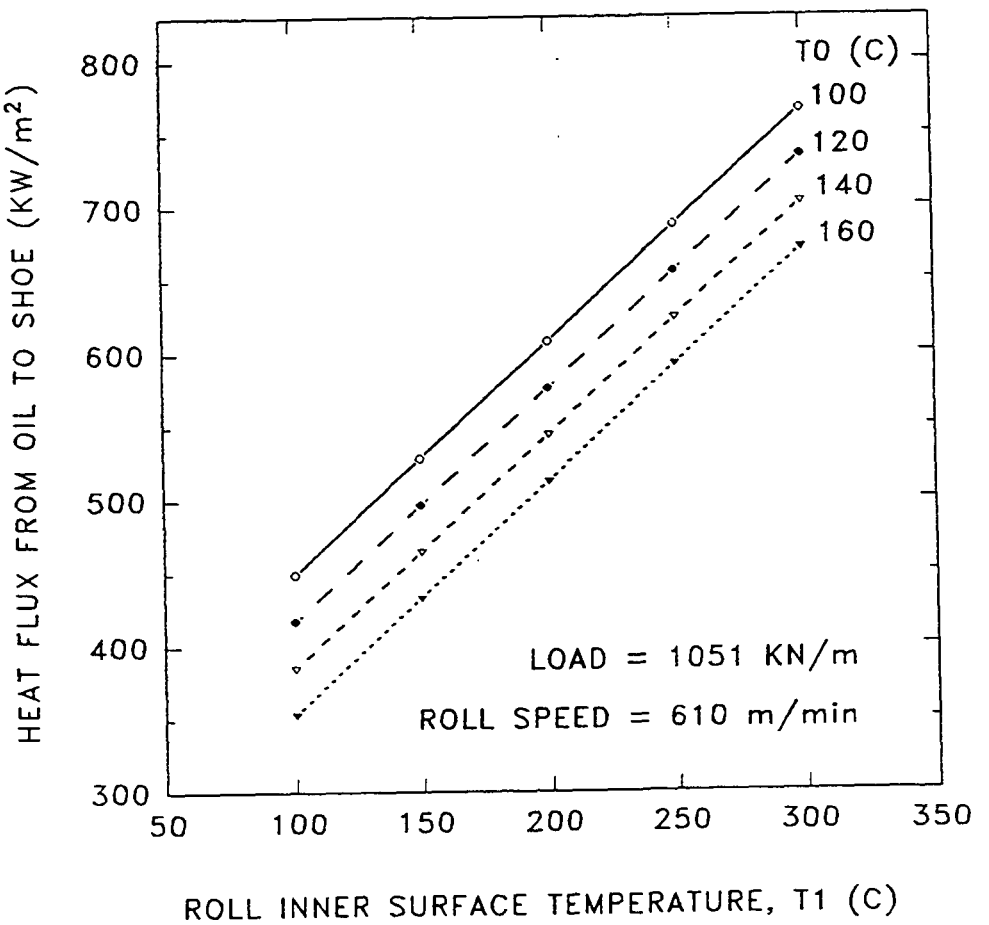

Figure 26c. Heat flux from oil to shoe as a function of roll inner surface temperature (load =1051 KN/m, roll speed = 610 m/min).

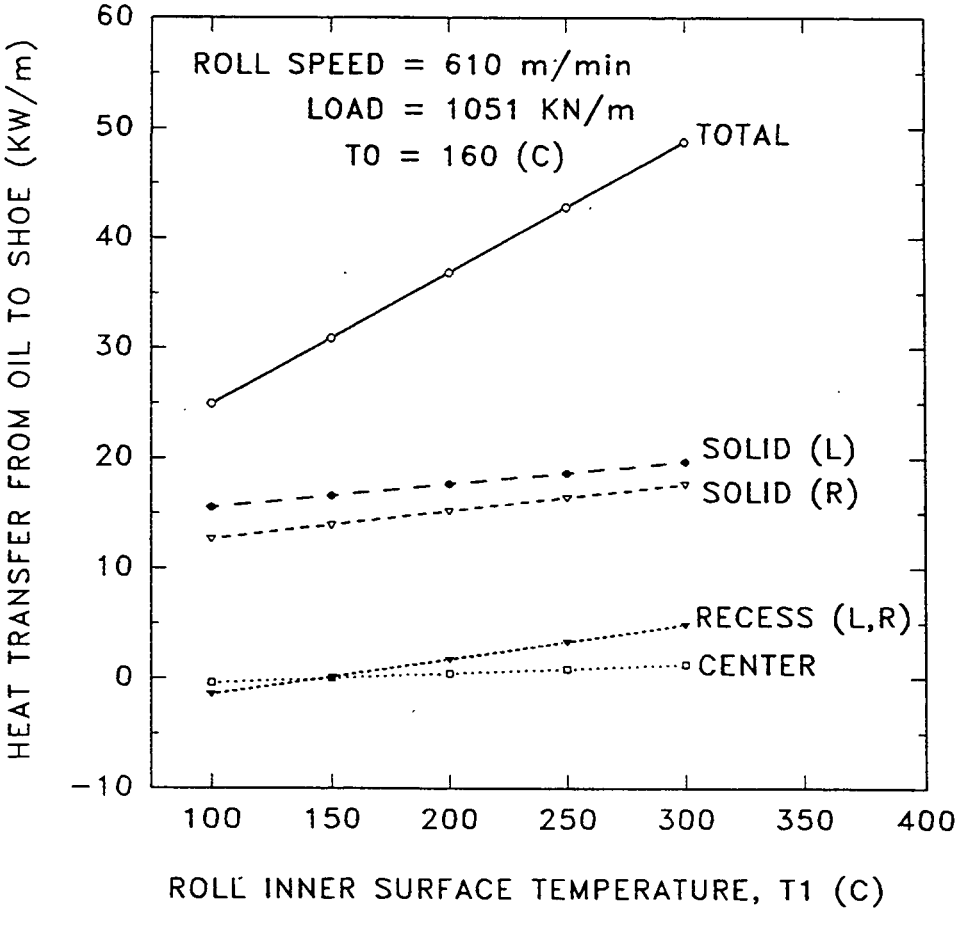

Figure 27a. Contribution of each region of the channel to the net heat transfer from oil to shoe (load =1051 KN/m, roll speed = 610 m/min).

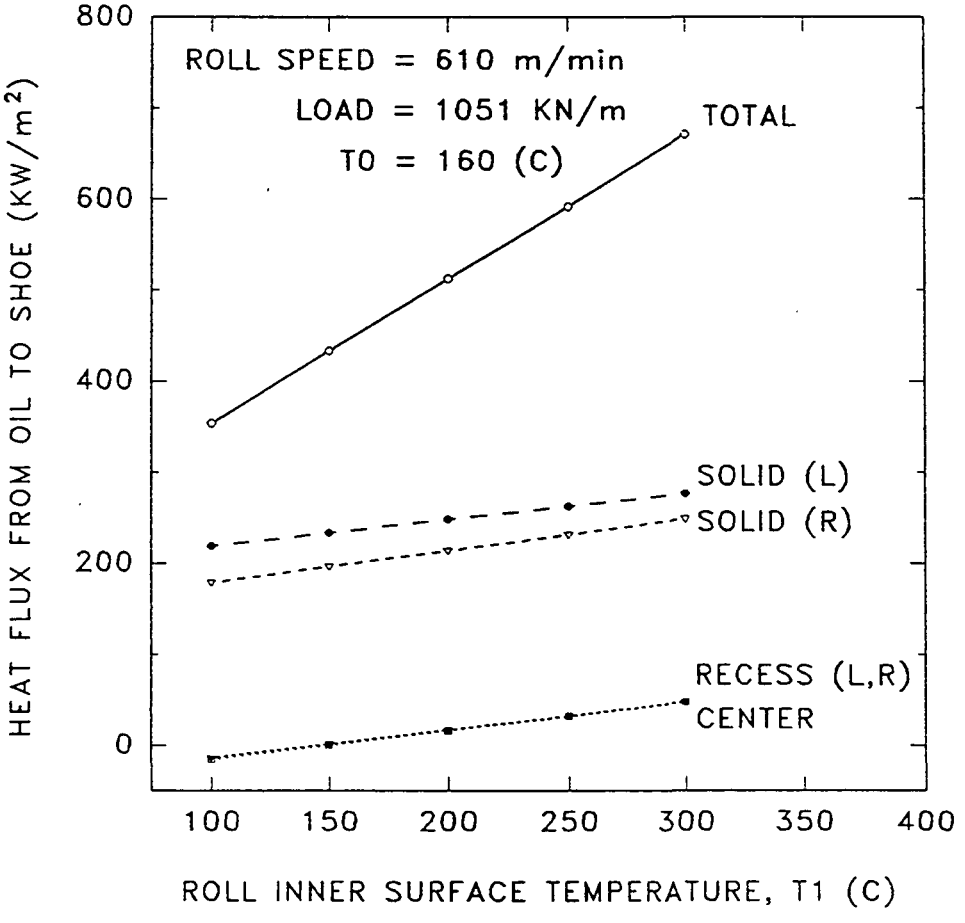

Figure 27b. Contribution of each region of the channel to the net heat flux from oil to shoe (load =1051 KN/m, roll speed = 610 m/min).

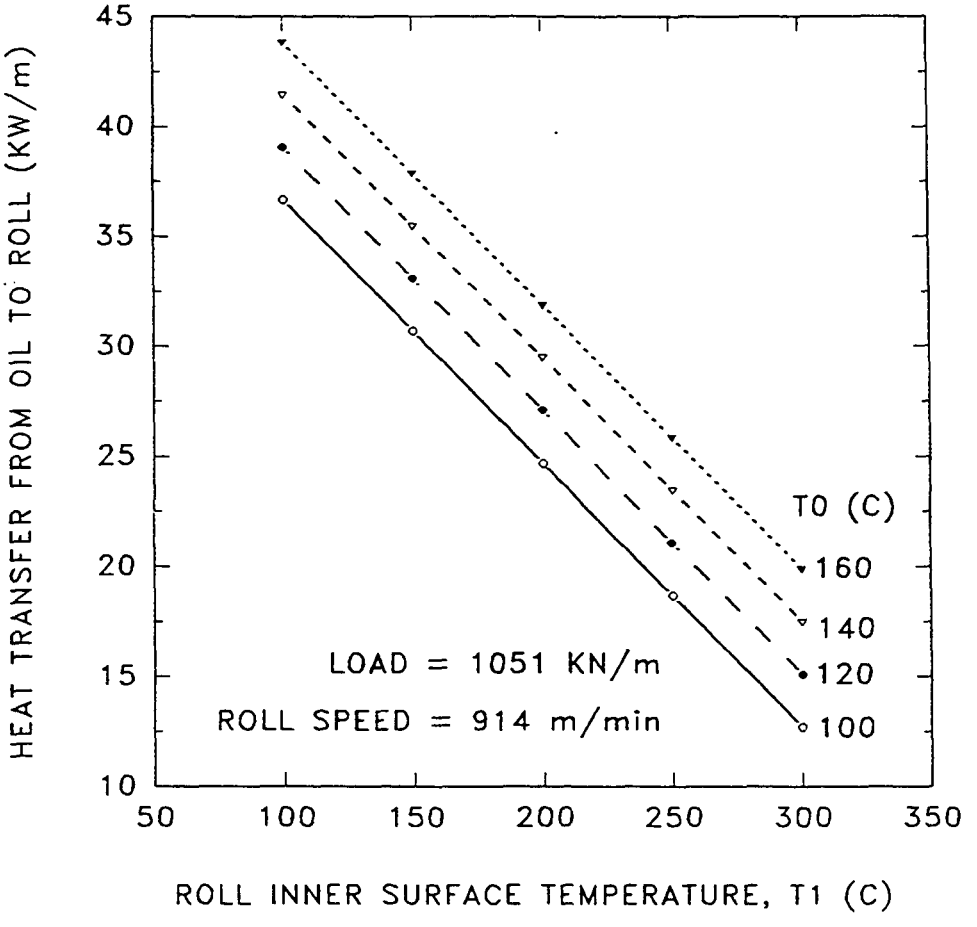

Figure 28. Heat transfer from oil to roll as a function of roll inner surface temperature (load =1051 KN/m, roll speed = 914 m/min).

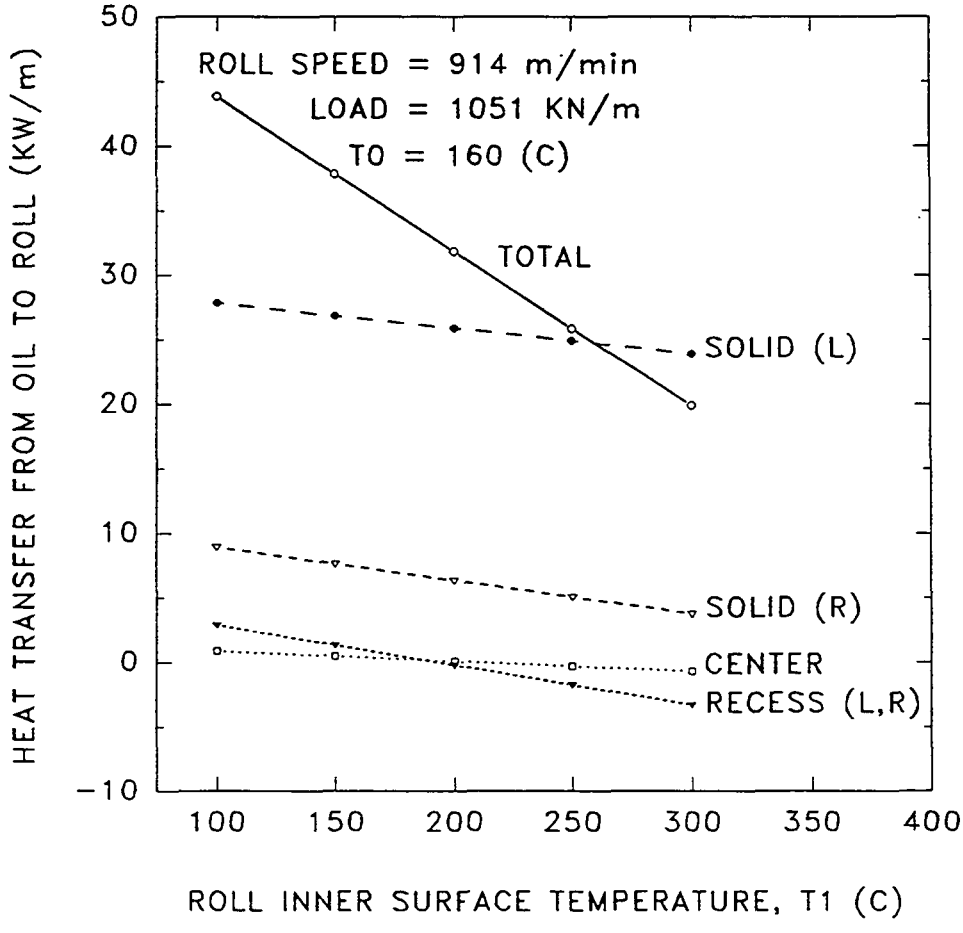

Figure 29a. Contribution of each region of the channel to the net heat transfer from oil to roll (load =1051 KN/m, roll speed = 914 m/min).

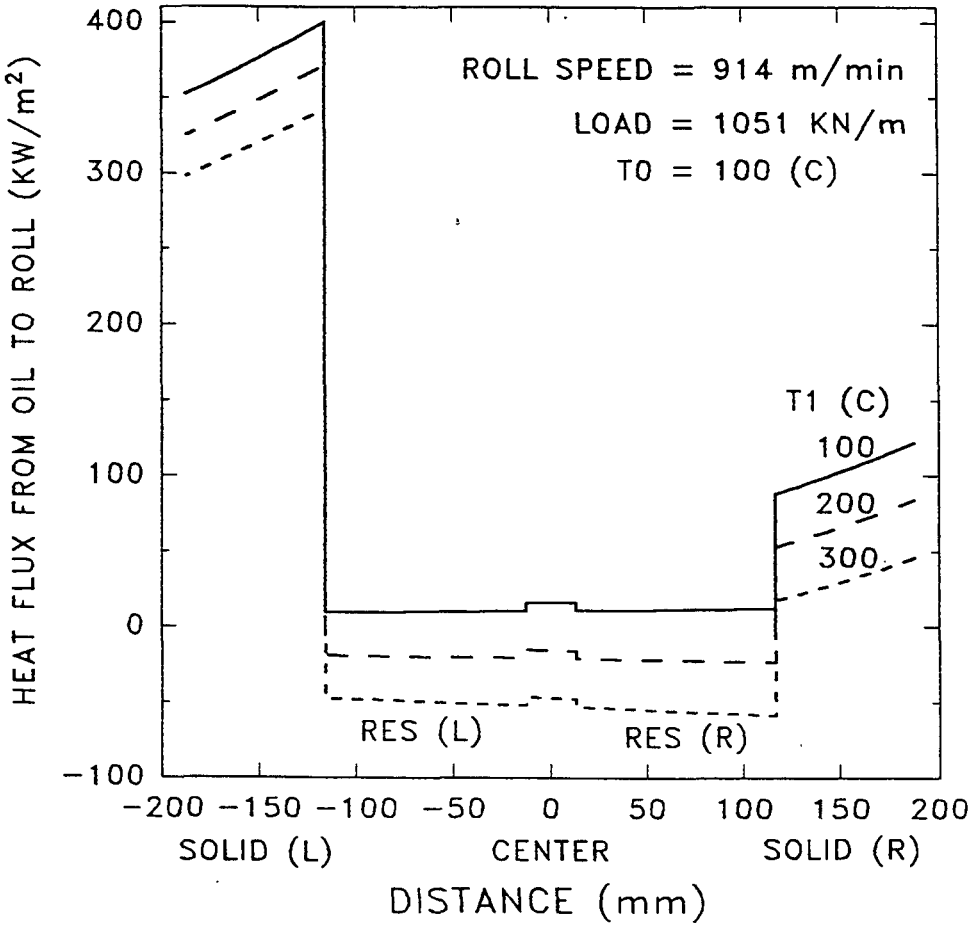

Figure 29b. Heat flux from oil to roll as a function distance from the entrance to each channel for three roll inner surface temperatures (T_0 = 100°C, load =1051 KN/m, roll speed = 914 m/min).

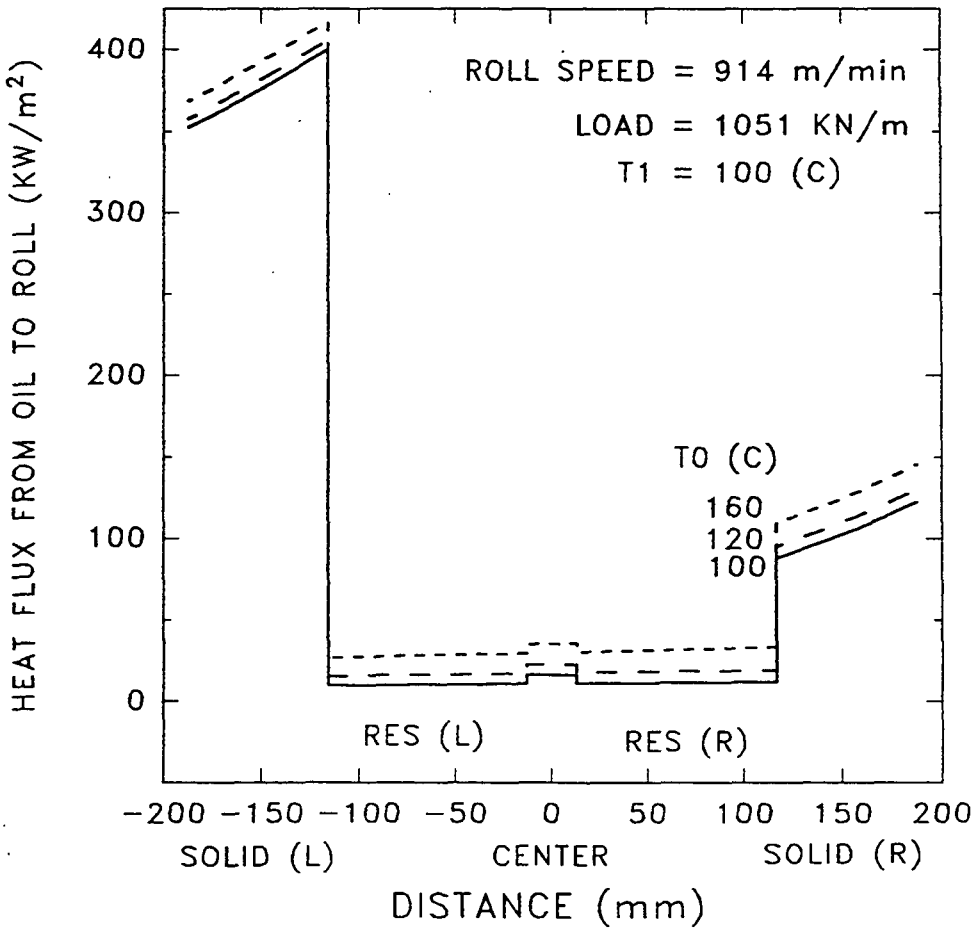

Figure 29c. Heat flux from oil to roll as a function distance from the entrance to each channel for three shoe temperatures (T_1 = 100°C, load =1051 KN/m, roll speed = 914 m/min).

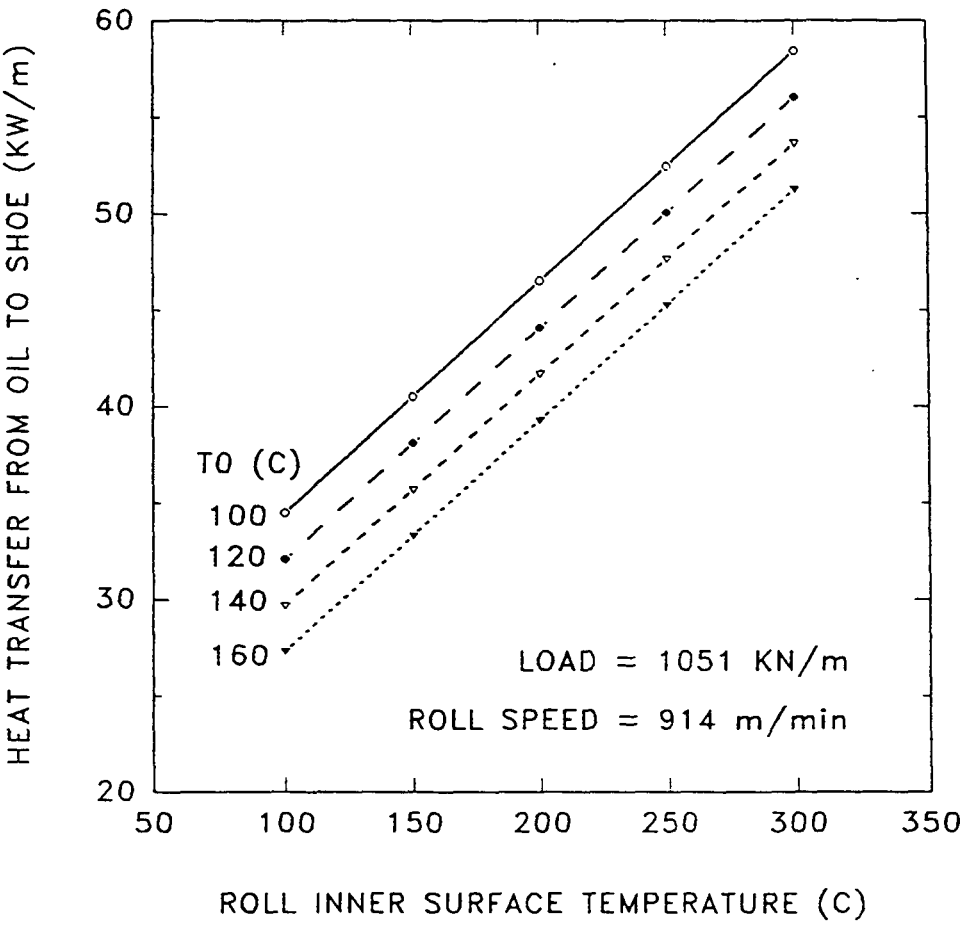

Figure 30. Heat transfer from oil to shoe as a function of roll inner surface temperature (load =1051 KN/m, roll speed = 914 m/min).

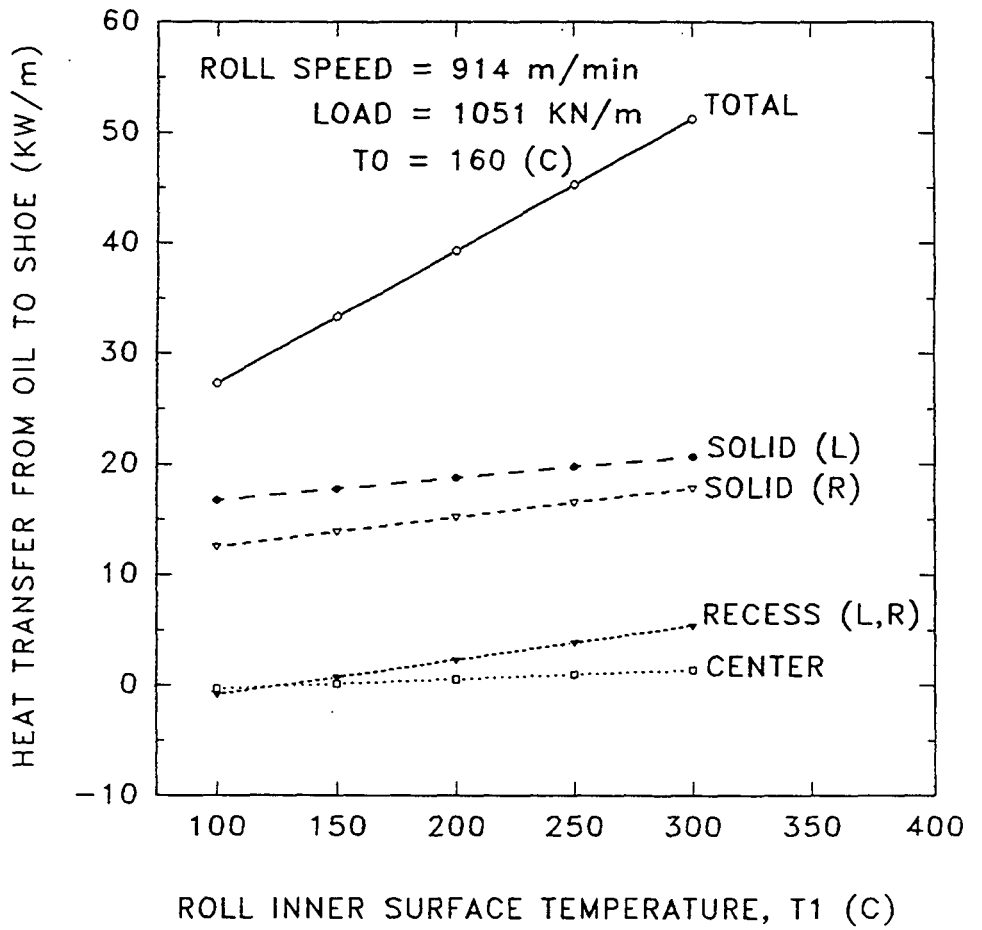

Figure 31a. Contribution of each region of the channel to the net heat transfer from oil to shoe (T_0 = 160°C, load =1051 KN/m, roll speed = 914 m/min).

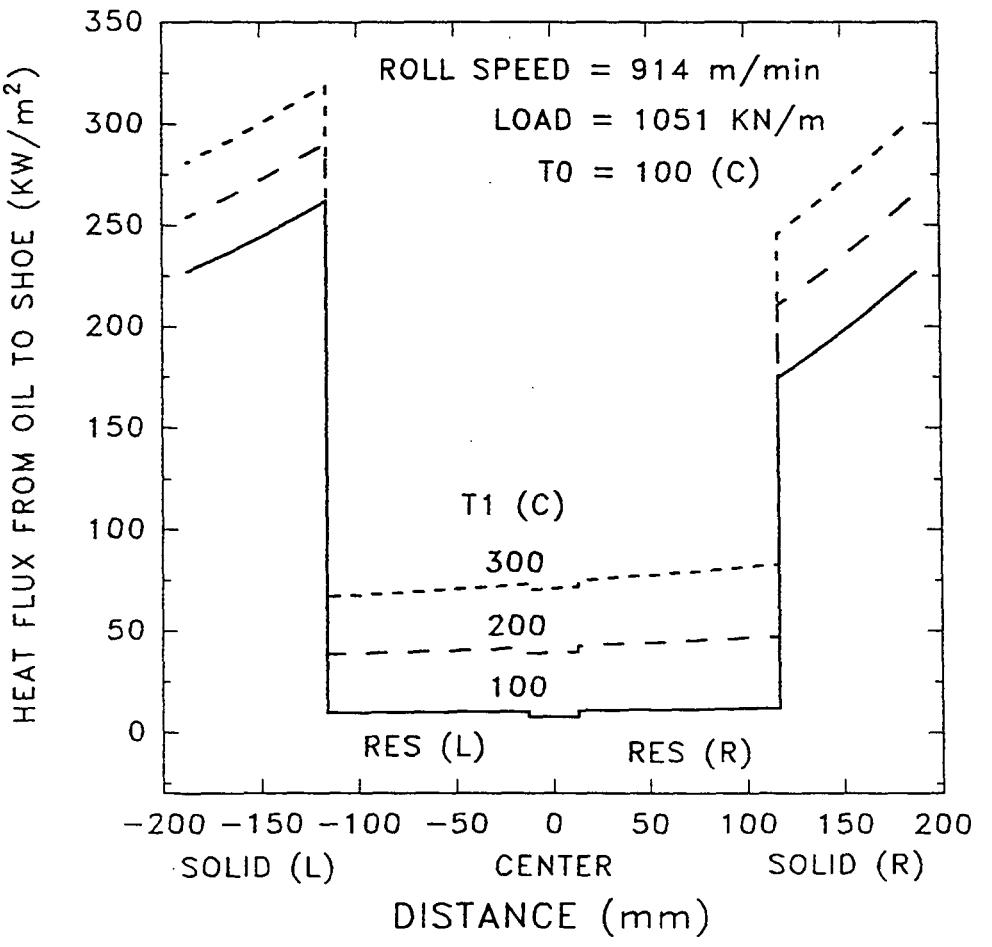

Figure 31b. Heat flux from oil to shoe as a function distance from the entrance to each channel for three roll inner surface temperatures (T_0 = 100°C, load =1051 KN/m, roll speed = 914 m/min).

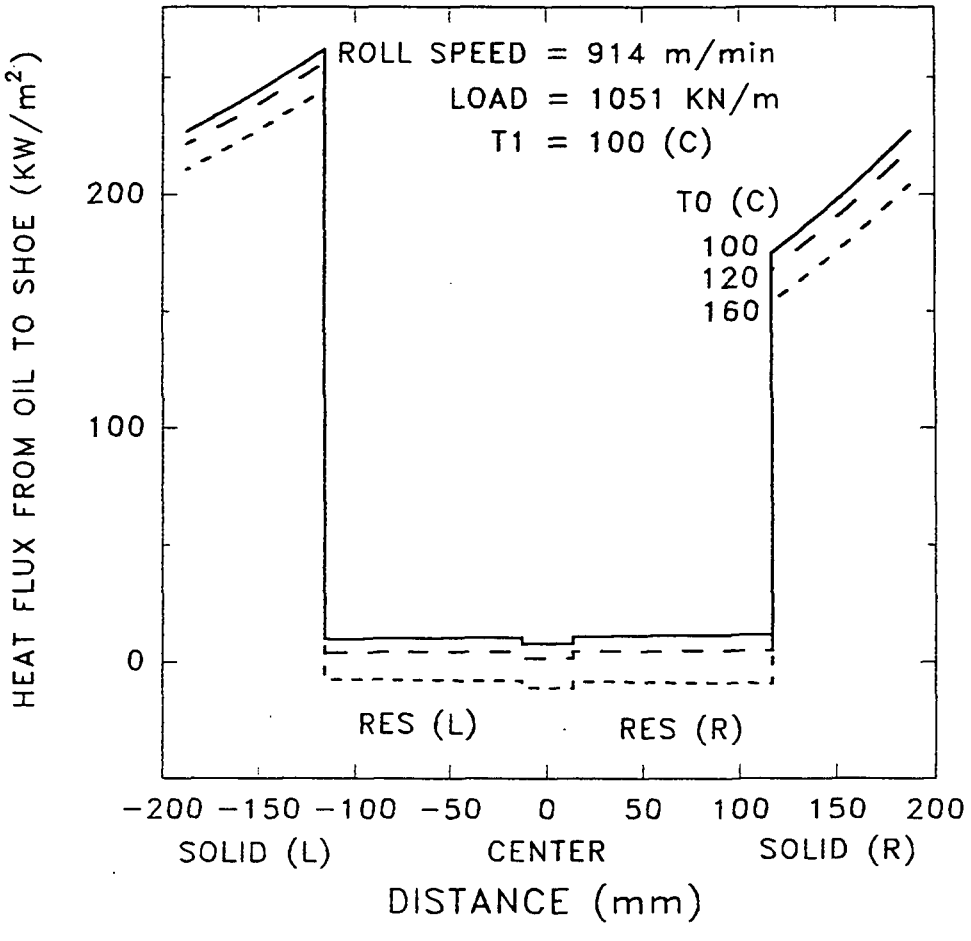

Figure 31c. Heat flux from oil to shoe as a function distance from the entrance to each channel for three shoe surface temperatures (T_1 = 100°C, load =1051 KN/m, roll speed = 914 m/min).

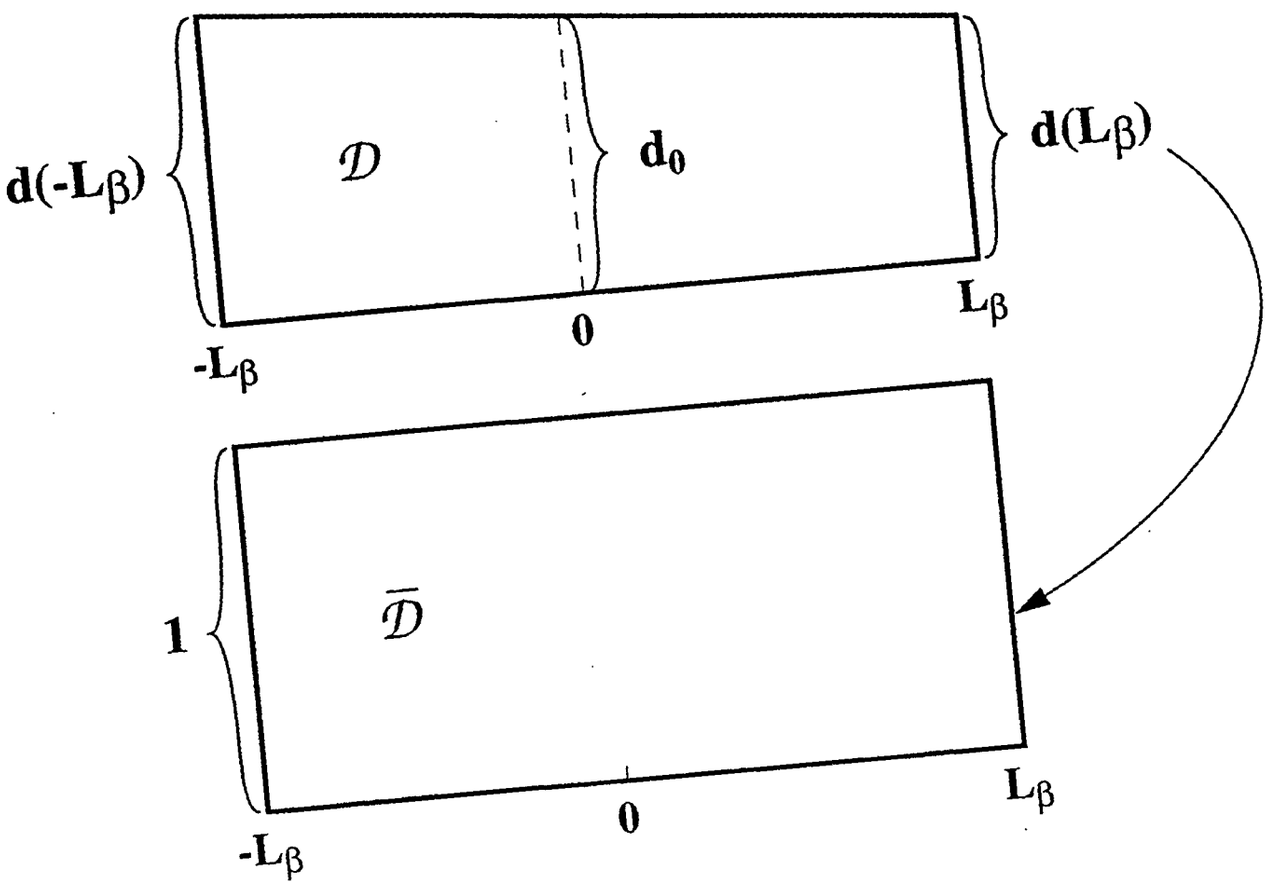

Figure 32a. Mapping of the domain for the heat transfer boundary value problem.

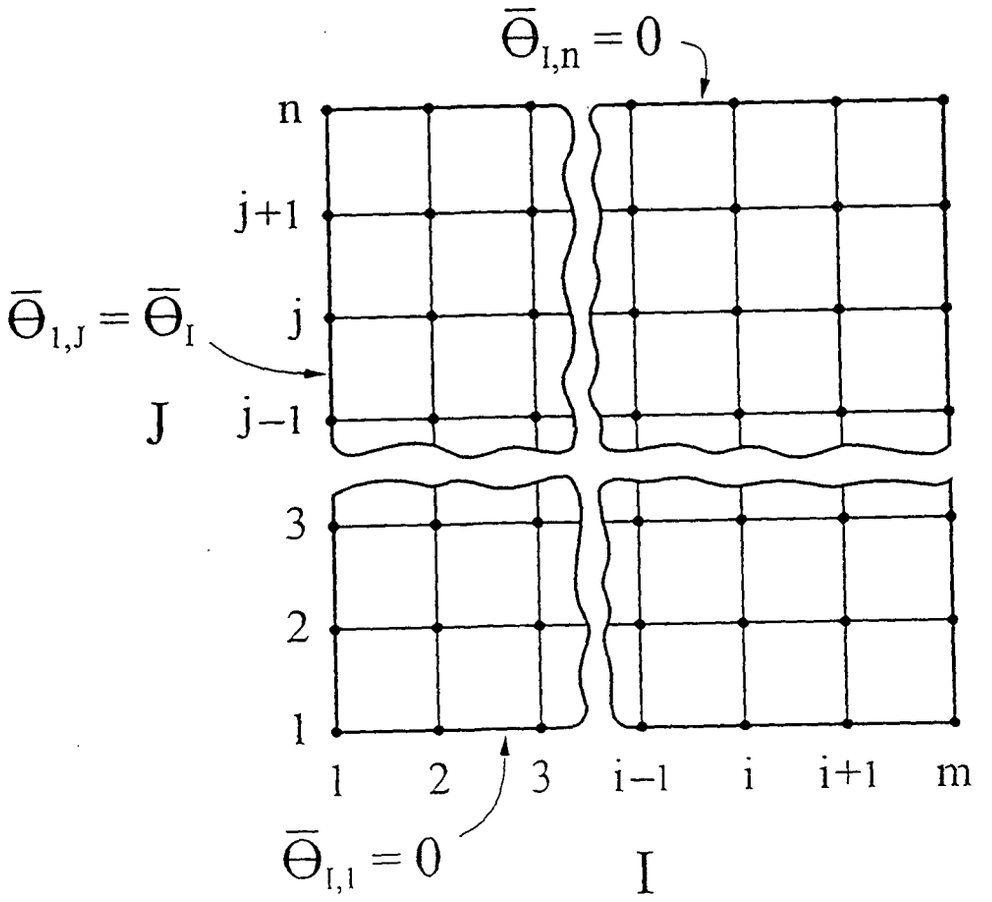

Figure 32b. Domain for the finite difference approximation.